HISTORICAL BIOLOGY
https://doi.org/10.1080/08912963.2021.1966777

Taylor & Francis
Taylor & Francis Group

An exceptional partial skeleton of a new basal raptor (Aves: Accipitridae) from the late Oligocene Namba formation, South Australia

Ellen K. Mather[a], Michael S. Y. Lee[a,b], Aaron B. Camens[a] and Trevor H. Worthy[a]

[a]College of Science and Engineering, Flinders University, Adelaide, SA, Australia; [b]Earth Sciences Section, South Australian Museum, North Terrace, Adelaide, SA, Australia

ABSTRACT

The Australian pre-Pleistocene fossil record of Accipitridae (eagles, hawks, old-world vultures) comprises one latest Oligocene or early Miocene and one middle Miocene species, each represented by partial bones. Globally, most fossil accipitrids are based on single bones. The recent discovery of an older and considerably more complete accipitrid from late Oligocene sediments in Australia is therefore significant. It is derived from the Pinpa Local Fauna from the Namba Formation at Lake Pinpa, South Australia (~26–24 Ma). The fossil, described as *Archaehierax sylvestris* gen. et sp. nov., represents a raptor that was larger than the black-breasted buzzard *Hamirostra melanosternon* but smaller and more gracile than the wedge-tailed eagle *Aquila audax*. Comprehensive morphological and molecular phylogenetic analyses resolved *Archaehierax* as a basal accipitrid, not closely related to any living subfamily and perhaps the sister taxon to all other accipitrids exclusive of elanines. Relatively short wings similar to species of *Spizaetus* and *Spilornis* suggest it was adapted for flight within enclosed forests. Additional accipitrid fossils from the Namba Formation, a distal femur and a distal humerus, are incomparable with the holotype of *A. sylvestris*; they may represent distinct species or smaller individuals of the new taxon.
lsid:zoobank.org:pub:6A25C569-3E9F-43B8-AAF8-F36CE405C06E

ARTICLE HISTORY
Received 11 June 2021
Accepted 8 August 2021

KEYWORDS
Lake Pinpa; Accipitriformes; Cenozoic fossil birds; accipitrid evolution; Australia

Introduction

The Accipitridae and kin

The Accipitriformes comprises four extant families and 259 species: the New-World vultures (Cathartidae, seven species), secretary birds (Sagittariidae, one species), ospreys (Pandionidae, one species) and the eagles, hawks and Old-World vultures (Accipitridae, ~250 species) (Dickinson and Remsen 2013). The accipitrids are the most widely distributed family in the order, being widespread on every continent except for Antarctica, and play key roles as apex predators and scavengers in many environments.

From the 19th to early 21st century, the Accipitridae were usually placed in Falconiformes with the Falconidae (falcons), Cathartidae, Sagittariidae and Pandionidae (Sharpe 1874; Ridgway 1874; Gadow 1891; Sushkin 1905; Peters 1934; Jollie 1976; Stresemann and Amadon 1979; Lerner and Mindell 2005; Hackett et al. 2008). Molecular data justified recognising Falconidae and Pandionidae as separate families from Accipitridae, though *Pandion* is very closely related to the Accipitridae (Sibley and Ahlquist 1990; Wink and Sauer-Gürth 2004; Lerner and Mindell 2005; Griffiths et al. 2007; Hackett et al. 2008). Accipitriformes was resurrected to include Accipitridae, Pandionidae, Sagittariidae and Cathartidae by Christidis and Boles (2008) and this usage has been followed thereafter (Gill et al. 2010; Dickinson and Remsen 2013). Accipitridae is recognised to include multiple subfamilies, though similarities in plumage and morphology (see Peters 1934; Amadon 1964; Jollie 1976) have obscured relationships and composition which are only recently being revealed by analyses of molecular data (refer to Ferguson-Lees and Christie 2001; Lerner and Mindell 2005; Dickinson and Remsen 2013; Mindell et al. 2018). Here, we use the subfamilies Elaninae, Perninae, Gypaetinae, Aegypiinae, Circaetinae, Harpiinae, Aquilinae, Accipitrinae, Haliaeetinae, and Buteoninae, following Nagy and Tökölyi (2014). We differ from Mindell et al. (2018) in recognising the Haliaeetinae as distinct from the Buteoninae, and Aquilinae from Harpiinae, based on differences in morphology and ecology, and the lack of justification provided by Mindell et al. (2018) for merging them.

Australia has 17 resident breeding accipitrid species in 12 genera, two of which are monotypic and endemic, in five subfamilies (Debus 1998; Christidis and Boles 2008; Dickinson and Remsen 2013).

Pre-Pleistocene Fossil Record of the Accipitridae

The fossil record of Accipitridae begins in the middle Eocene in Europe, although the fragmentary nature of the fossils prohibits definitive identification (Olson 1985; Mlíkovský 2002; Mayr 2017). A further complication is the presence of lineages that resemble Accipitridae, such as the Horusornithidae, thought to be an extinct lineage of Accipitriformes (Mourer-Chauviré 1991), and the Messelasturidae, predators in a lineage now thought to be related to stem-group parrots (Mayr 2006a, 2011). The Eocene raptor *Masillaraptor parvunguis* Mayr, 2006b, represented by several articulated skeletons, was considered to be either an accipitriform or a falconiform when first described (Mayr 2006b), but was later considered to be a falconid (Mayr 2009, 2017).

The Oligocene to Miocene record of accipitrids varies by continent. Africa is extremely poorly represented at the time of writing, with one indeterminate Oligocene fossil from Egypt bearing some

CONTACT Ellen K. Mather math0083@flinders.edu.au College of Science and Engineering, Flinders University, Adelaide, SA 5000, Australia
Supplemental data for this article can be accessed here.

similarity to *Haliaeetus* (Rasmussen et al. 1987); otherwise, African fossils attributable to extant genera are known from the Miocene onwards (Walker and Dyke 2006).

North America has numerous described species of late Oligocene to early Miocene age: four species have been described in the modern genus *Buteo*, (but see Mayr and Perner 2020 for caveats), and nine species in six fossil genera (Brodkorb 1964; Mayr 2009, 2017; Mayr and Perner 2020). Most species are described from a single bone, except for *Palaeoplancus sternbergi* Wetmore, 1933, which is represented by a partial skeleton with axial, pectoral and pelvic limb elements (Wetmore 1933). In contrast, South America has no definitive fossil accipitrids from this time period, possibly due to the dominance of the Cathartidae, Teratornithidae and Phorusrhacidae in the avian predatory and scavenging guilds (Mayr 2017).

Two accipitrids, each based on single bones, are known from Oligocene deposits of Asia: *Buteo circoides* Kurochkin, 1968 and *Venerator* (*Tutor*) *dementjevi* (Kurochkin, 1968). Other indeterminate fossil accipitrids of early Oligocene age are known from Mongolia and of late Oligocene age from Kazakhstan (Kurochkin 1976). Four species of vulturine accipitrids are recorded from middle to late Miocene deposits of China: *Mioaegypius gui* Hou, 1984, *Mioneophron longirostris* Li et al., 2016, *Qiluornis taishanensis* Hou et al., 2000, and *Gansugyps linxiaensis* Zhang et al., 2010, each represented by a partial or near complete skeleton.

Seven fossil accipitrids are known from the early Oligocene to the early Miocene deposits of Europe, six of which are described from single bones: *Palaeohierax gervaisii* (Milne-Edwards, 1863), *Promilio incertus* (Gaillard, 1939), *Aquilavus priscus* (Milne-Edwards, 1863), *Aquilavus depredator* (Milne-Edwards, 1871), *Aquilavus corroyi* (Gaillard, 1939), and *Aquilavus hypogaeus* (Milne-Edwards, 1892). In contrast, *Aviraptor longicrus* Mayr and Hurum, 2020, represented by a complete skeleton, is one of the oldest confirmed accipitrids known from Europe.

The pre-Pleistocene fossil record of the Australian Accipitridae is quite poor (Baird 1991; Vickers-Rich 1991). At the time of writing, Australia has two described pre-Pleistocene accipitrids, the late Oligocene to early Miocene *Pengana robertbolesi* Boles, 1993 from the Riversleigh deposits in Queensland, and the middle Miocene *Aquila bullockensis* Gaff and Boles , 2010 from the Bullock Creek Site in the Northern Territory (Worthy and Nguyen 2020).

The global fossil record, and molecular divergence dating, suggest that by the early Miocene, about 20 Ma, all extant subfamilies of the Accipitridae had evolved (Walker and Dyke 2006; Zhang et al. 2012; Nagy and Tökölyi 2014; Mindell et al. 2018).

The Namba Formation

The vast Kati Thanda–Lake Eyre catchment is approximately 1.2 million km^2, extending over much of mid-central to north-eastern inland Australia. Sedimentary deposition in the central/southern Australian section of the basin occurred in three major phases; the first phase resulted in the Late Palaeocene – Middle Eocene Eyre Formation, which is comprised of sandstone and carbonaceous conglomerates and clasts; the second phase resulted in the Late Oligocene – early Miocene Etadunna, Namba, Doonbarra and Cadelga Formations, which are comprised of clays, silts, fine sand, and carbonates; and the third phase saw the Pliocene – Quaternary Wipajiri, Tirari, Kutjitara, Katipiri, Eurinilla, Millyera Coomb Spring and Coonarbine Formations deposited, which are comprised of a variety of sediments including cobbles, sands and clays from fluvial or lacustrine deposition (Drexel and Preiss 1995; Alley 1998).

Our focus is the Namba Formation, located in the Callabonna Sub-basin of the Lake Eyre Basin, in South Australia to the east of the Flinders Ranges (Alley 1998; see Figure 1). This is sometimes referred to as the Tarkarooloo Basin (see Woodburne et al. 1994) or the Frome Sub-basin (see Megirian et al. 2010). The age of this formation is correlated with that of the Etadunna Formation, in the

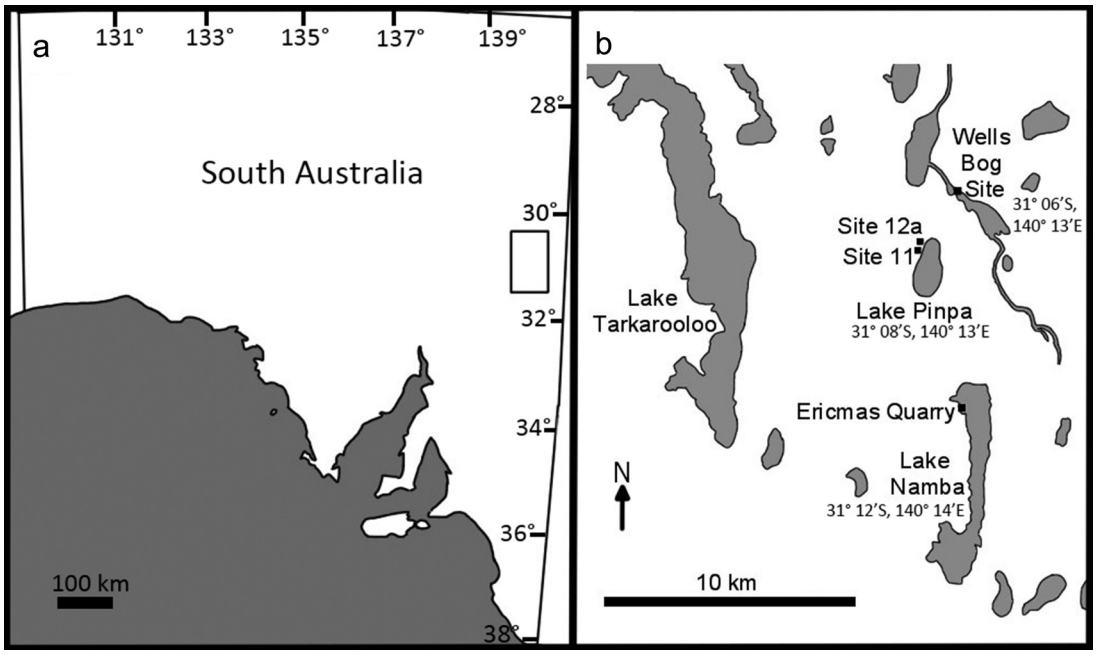

Figure 1. (A) Map of South Australia with general location of Frome Sub-Basin fossil sites marked with a rectangle, (B) detailed map of the study sites in the Frome Sub-Basin. Lake Pinpa Sites 11 and 12, Ericmas Quarry, and Wells Bog Site located by black squares.

Tirari Sub-basin of the Lake Eyre Basin (Alley 1998). The Namba Formation contains three primary Local Faunas (LFs): the Pinpa LF, the Ericmas LF, and the Tarkarooloo LF (Callen and Tedford 1976; Rich and Archer 1979; Rich et al. 1991; Thorn et al. 2021). The Pinpa LF derives from beds of olive and orange mottled clay and white dolomitic mudstone stained with manganese at the top of the lower member of the Namba Formation, which crops out at Lake Pinpa and Billeroo Creek (Tedford et al. 1977; Rich et al. 1991; Thorn et al. 2021). The Ericmas LF derives from fluvial sands deposited in channels cut into the lacustrine units of the Namba Formation, so is younger than the Pinpa LF, and derives from Ericmas Quarry and South Prospect Quarries at Lake Namba a few kilometres south of Lake Pinpa (Tedford et al. 1977; Rich et al. 1991). There is much overlap of species composition between Pinpa and Ericmas LFs suggesting broad similarity in age. While Rich et al. (1991) recognised the Ericmas LF to occur at Lake Pinpa, recent work by THW and ABC recognises only one local fauna from Lake Pinpa and restricts the Ericmas LF to that derived from Ericmas and South Prospect quarries at nearby Lake Namba (Thorn et al. 2021). The Tarkarooloo LF derives from fluvial sands in Tom O's Quarry by Lake Tarkarooloo about 10 kilometres west of Lake Pinpa, but the temporal relationship to the Ericmas LF is unknown, though co-occurrence of some species suggests a broadly similar age (Rich et al. 1991).

The accepted age of the Namba and Etadunna Formations has varied (see Pledge 2016). The Etadunna Formation, and therefore by proxy the Namba Formation, was initially considered to be of Oligocene age when it was first identified (Stirton et al. 1961). Subsequent analysis of the Pinpa and Ericmas LFs of the Namba Formation considered their likely age to be middle Miocene (12–16 Ma) (e.g., Tedford et al. 1977; Woodburne et al. 1985) based on the identification of grass pollen in the basal Namba Formation in Wooltana-1 bore that thereby indicated the presence of extensive grasslands (Callen and Tedford 1976). However, later studies of the same pollen slides determined that grass pollen was exceedingly rare and that of Restionaceae or sedges, which occur wherever wetlands are present, was common along with a host of rainforest taxa (Martin 1990). Therefore, Martin (1990) interpreted the palaeoenvironment as a rainforest surrounding swamps and via correlation with floras elsewhere, inferred a late Oligocene – early Miocene age for the basal Namba Formation.

Woodburne et al. (1994) detailed the biostratigraphy and revised the age of the Etadunna Formation, using four lines of evidence: 1, the presence of Oligocene age (28–24 Ma) foraminiferal fauna in the Etadunna Formation (Lindsay 1987); 2, a reported Rb-Sr age of 25 Ma on an authigenic illite (Norrish and Pickering 1983); 3, the presence of land mammal fossils consistent with those of known Oligocene age; and 4, the magnetostratigraphic record, to conclude that a late Oligocene age for the Etadunna Formation was most likely. As Woodburne et al. (1994) determined that the Pinpa LF correlated with the most basal Zone A 'Wynyardiid' Fauna of the Etadunna Formation, a late Oligocene age was also inferred for it. Woodburne et al. (1994) did not cite Martin (1990) and were apparently unaware of it, as the pollen data provided compelling evidence to support their inferred late Oligocene age. This work was accepted by Megirian et al. (2010) who established a comprehensive land mammal biostratigraphy and advocated a late Oligocene age (28–24 Ma) for the Namba Formation. Some of the ages accepted by Megirian et al. (2010) have been robustly confirmed by direct dating of sites from Faunal Zones B and C at Riversleigh, northwest Queensland, to the early and middle Miocene, respectively (Woodhead et al. 2016), supporting the prior correlation of Faunal Zone B sites with the Kutjamarpu LF (Wipajiri Fm) from Lake Ngapakaldi, Lake Eyre Basin on biochronological grounds; the Kutjamarpu LF is slightly younger than the uppermost Etadunna local fauna – the Ngama LF – on biochronological grounds (Megirian et al. 2010). Therefore, we use the age range of 26–24 Ma advocated by Woodhead et al. (2016) for the Pinpa + Ericmas Local Faunas.

Aquatic or semiaquatic vertebrates are common in both the Pinpa and Ericmas LFs in the Namba Formation, including fish, turtles, crocodilians, and dolphins (Tedford et al. 1977; Fordyce 1983; Rich et al. 1991), revealing the presence of a permanent lake in the basin during this time period. The dolomitic layers at the site suggest periods of time when sections of the lake would seasonally dry out (Callen 1977). The afore-mentioned pollen record from the Namba Formation reveals that the depositional environment was dominated by a mix of rainforest and temperate forest surrounding sedge-lined lakes in the late Oligocene to early Miocene when the Pinpa LF was present (Martin 1990). The range in habitats resulted in a diverse vertebrate fauna inhabiting this area in the late Oligocene, resulting in a fossil fauna that is a key snapshot into our understanding of the evolution of Australian animals.

The Pinpa LF, found at Lake Pinpa and Wells Bog Site at Billeroo Creek (Rich et al. 1991; Thorn et al. 2021) (Figure 1), is extremely diverse, comprising fish and both aquatic and terrestrial reptiles, mammals, and birds (Rich et al. 1991). Reptiles are represented by an indeterminate species of chelid turtle (*Emydura* sp.), an unnamed species of meiolaniid turtle (see Rich et al. 1991), the crocodilian *Australosuchus clarkae* Willis and Molnar, 1991 (See Willis 1997), and an ergerniine skink *Proegernia mikebulli* Thorn et al., 2021.

The mammals of the Pinpa LF are well-documented, see Rich et al. (1991) or subsequently described; Monotremata: Ornithorhynchidae, *Obdurodon insignis* Woodburne and Tedford, 1975. Marsupialia, Vombatiformes: Phascolarctidae, *Madakoala devisi* Woodburne et al., 1987a; Ilariidae, *Ilaria illumidens* Tedford and Woodburne, 1987; Mukupirnidae, *Mukupirna nambensis* Beck et al., 2020 (=Vombatoidea genus A of Tedford et al. 1977); Diprotodontidae, *Raemeotherium yatkolai* Rich et al., 1978; Wynyardiidae, *Muramura pinpensis* Pledge, 2003. Marsupialia, Phalangeriformes: Pseudocheiridae, *Pildra antiquus* Woodburne et al., 1987b; *Pildra secundus* Woodburne et al. , 1987b (listed as from Ericmas LF, Lake Pinpa); Pilkipildridae, *Pilkipildra handae* Archer, Tedford and Rich, 1987; Miralinidae, *Miralina* sp. cf *M. minor*; Ektopodontidae, *Chunia* sp. cf *C. illuminata*; undetermined Petauridae; undetermined Macropodiformes, Macropodidae/Potoroidae; Placentalia, Cetacea: an unnamed species of extinct rhabdosteid dolphin (Fordyce 1983).

Birds are also abundant in the Pinpa LF, with many semi-aquatic taxa, see Rich et al. (1991), as modified by Boles and Ivison (1999), Worthy (2009, 2011), Boles et al. (2013) and De Pietri et al. (2016). Presbyornithidae, *Wilaru tedfordi* Boles et al., 2013; Megapodiidae, *Ngawupodius minya* Boles and Ivison, 1999 (listed as from the Ericmas LF by Boles and Ivison 1999, but derives from the South end of Lake Pinpa where only deposits preserving the Pinpa LF occur (Thorn et al. 2021), and as a pigeon in Rich et al. [1991, p. 1025]). Anatidae: *Pinpanetta tedfordi* Worthy, 2009; *Pinpanetta vickersrichae* Worthy, 2009; *Pinpanetta fromensis* Worthy, 2009, *Australotadorna alecwilsoni* Worthy, 2009. Phalacrocoracidae: *Nambashag billerooensis* Worthy, 2011; *Nambashag microglaucus* Worthy, 2011. Pelecanidae: *Pelecanus tirarensis* Miller, 1966. Other taxa include undescribed species of rails (Rallidae), undetermined flamingos (Phoenicopteriformes), grebes (Podicipedidae), and passerines (authors' unpubl. data).

From the dolomitic beds of the Namba Formation exposed at Site 12 on Lake Pinpa (Figure 1), and hence forming part of the Pinpa LF, a partial skeleton of an accipitrid was recovered in 2016 by a Flinders University expedition, led by THW and ABC. Sixty-three recognisable bones are represented, spanning the tip of the rostrum to the pedal

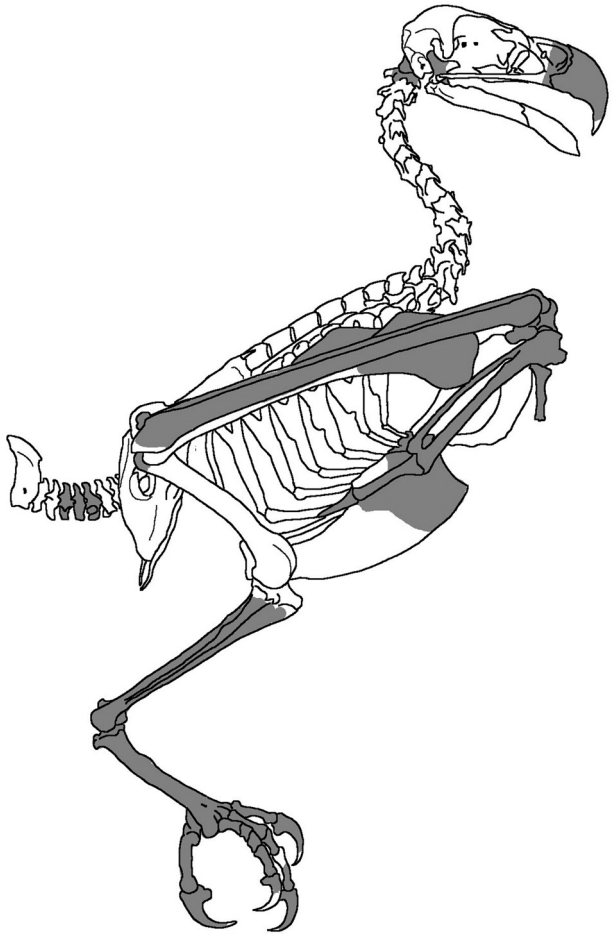

Figure 2. Exemplar accipitriform skeleton, *Pandion haliaetus cristatus*, derived from an illustration in Eyton (1867), showing the bones preserved in the fossil accipitrid specimen SAMA P.54998 shaded in grey. The illustrated taxon and fossil material are not identical in terms of the morphology of individual elements.

digits (Figure 2). The pelvic limb elements are well preserved, except for the femur for which only the caput is preserved. This skeleton represents not only the oldest fossil representative of Accipitridae in Australia but also the most complete (cf. Boles 1993; Gaff and Boles 2010). This relatively complete state is also rare on a global scale, and only observed in a handful of cases, such as the Miocene vultures of China which are near complete (Hou et al. 2000; Zhang et al. 2010; Li et al. 2016), *Palaeoplancus sternbergi* (see Wetmore 1933; Mayr and Perner 2020) and *Aviraptor longicrus* (see Mayr and Hurum 2020). Besides the new skeleton, there are another two accipitrid fossils recognised from the Namba Formation; a distal right humerus, from the dolomitic layers at Site 11, Lake Pinpa (also of the Pinpa LF) and a distal femur from Ericmas Quarry, Lake Namba, of the Ericmas LF. It is the aim of this contribution to formally describe these fossils and determine their phylogenetic relationships in the Accipitridae.

Materials and methods

Abbreviations

Institutions

South Australia Museum, Adelaide, SA, Australia (SAMA); Museums Victoria, Melbourne, VIC, Australia (NMV); Australian National Wildlife Collection, Canberra, ACT, Australia (ANWC); University of Kansas Institute of Biodiversity, Lawrence, KS, USA (KU); Smithsonian Museum of Natural History, Washington DC, USA (USNM); Natural History Museum, London, UK (NHMUK).

Anatomical

Pedal phalanges are identified by the digit first (Roman numeral) and phalanx second (Arabic number), e.g., II.2 is digit II, phalanx 2; cmc, carpometacarpus; cor, coracoid; DW, distal width; L, left; PW, proximal width; R = right; SW, shaft width; tmt, tarsometatarsus. Manus digits are identified akin to the pedal phalanges, e.g., MI.1 is manus digit I, phalanx 1.

Nomenclature

The anatomical nomenclature advocated by Baumel and Witmer (1993) is followed for all bones except for the os carpale radiale, which follows Mayr (2014), and the quadrate, which follows Elzanowski and Zelenkov (2015). Taxonomic nomenclature follows Dickinson and Remsen (2013) and Gill et al. (2020) for composition of Accipitriformes, and Nagy and Tökölyi (2014) for subfamilial composition.

Measurements

Bones were measured with an accuracy of 0.1 mm using digital callipers.

Photography

Photographs were taken using a focus stacking method using a Canon 5DS-r digital camera 50.0 MP with either a Canon EF 100 mm or a 65 mm f2.8 IS USM professional macro lens with multiple images then compiled into a single photo using the program Zerene Stacker. Some fossil specimens were whitened with ammonium chloride powder before imaging (see Feldmann 1989) to retain shape as the primary feature captured rather than variable staining and reflective surfaces.

Comparative material

Skeletons of a broad range of accipitrids and outgroup taxa were loaned from museums and other institutions from Australia and internationally to compare to the fossil as follows.

Extant species (in taxonomic groupings)

Falconidae *Falco berigora* SAMA B55605; *Falco longipennis* SAMA B49055; *Falco peregrinus* SAMA B32515.
Threskiornithidae *Threskiornis spinicollis* AMA B48351.
Ciconiidae *Ciconia ciconia* SAMA B49223, SAMA B11601.
Cathartidae *Coragyps atratus* SAMA B36873.
Sagittariidae *Sagittarius serpentarius* USNM 223836.
Pandionidae *Pandion haliaetus* SAMA B37096, NMV B30256.
Accipitridae Elaninae: *Elanus axillaris* NMV B34037; *Elanus scriptus* NMV B8617, NMV B30263, ANWC 22680; *Gampsonyx swainsonii* USNM 623110; *Chelictinia riocourii* NHMUK S.1904.4.28.3. Perninae: *Elanoides forficatus* USNM 622340; *Chondrohierax uncinatus* USNM 289784; *Aviceda subcristata* ANWC 22665, NMV B19826; *Pernis apivorus* SAMA B59278; *Lophoictinia isura* NMV B18533, ANWC 44373; *Hamirostra melanosternon* ANWC (FALS-41), SAMA B36200. Gypaetinae: *Polyboroides typus* USNM 430434; *Neophron percnopterus* SAMA B11449; *Gypohierax angolensis* USNM 291316; *Gypaetus barbatus*

MNH S.1972.1.59, MNH S.1896.2.16.120, MNH S.1952.3.61. Circaetinae: *Spilornis cheela* USNM 562001; *Terathopius ecaudatus* NMV 18575; *Pithecophaga jefferyi* MNH S.1910.2.11.1a, MNH S.1961.23.1. Aegypiinae: *Necrosyrtes monachus* USNM 620646; *Gyps coprotheres* ANWC 22724; *Gyps fulvus* NMV 18574, NMV B30269; *Aegypius monachus* NMV R553; *Sarcogyps calvus* MNH S.2013.22.1, MNH S.2007.30.1; *Trigonoceps occipitalis* MNH S.1954.30.54; *Torgos tracheliotos* MNH S.1930.3.24.248, MNH S.1952.1.172. Harpiinae: *Harpia harpyja* NHMUK S.1862.3.19, NHMUK S.1909.8.18.1. Aquilinae: *Stephanoaetus coronatus* NHMUK S.1954.30.42, NHMUK S.1862.3.14.19; *Aquila audax* SAMA B46613, NMV B19228; *Aquila chrysaetos* NMV B32659, ANWC 22682 (FALS-123); *Aquila fasciata* (formerly *Hieraaetus fasciatus*) NMV B30575; *Hieraaetus morphnoides* SAMA B47128, NMV B8643, NMV B20224; *Hieraaetus* (=*Harpagornis*) *moorei*, casts of the original type material, NMV P33032 (tibiotarsus), NMV P33031 (pedal phalanx), NMV P33030 (tarsometatarsus), NMV P33029 (femur), NMV P33028 (humerus), NMV P33027 (femur), NMV P33026 (ulna); *Spizaetus tyrannus* KU 35007; *Spizaetus ornatus* KU 72077. Haliaeetinae: *Haliaeetus leucogaster* NMV B8847, SAMA B49459; *Haliaeetus leucocephalus* ANWC 22723 (16,500), NMV B15601; *Haliaeetus albicilla* NMV B34417; *Haliastur indus* ANWC 22719, NMV B13753; *Haliastur sphenurus* NMV B11661, SAMA B33998; *Milvus migrans* SAMA B47130, NMV B20404. Accipitrinae: *Melierax metabates* NHMUK S.1954.30.29; *Kaupifalco monogrammicus* NHMUK S.1869.10.19.28; *Circus assimilis* SAMA B56454, ANWC 22727; *C. approximans* ANWC 22728, ANWC 22729; *C. cyaneus* ANWC 22735; *C. aeruginosus* NMV B12891; *Accipiter fasciatus* NMV B13444, SAMA B36355; *A. cooperii* ANWC 22764, ANWC 22765; *A. striatus* ANWC 22747, NMV B12666; *A. novaehollandiae* NMV B18401; *A. cirrocephalus* NMV B16071, NMV B10346; *A. nisus* NMV B12413, ANWC 22742; *A. gentilis* ANWC 22736, NMV B12927. Buteoninae: *Erythrotriorchis radiatus* NHMUK S.1872.10.22.9; *Geranospiza caerulescens* NHMUK S.1903.12.20.318; *Ictinia mississippiensis* ANWC 22681 (21,655), NMV B13343; *Buteo buteo* SAMA B46558, NMV B24505; *B. nitidus* NMV B13222; *Buteo rufofuscus* NMV B24503; *Buteo lagopus* ANWC 22776 (21694), NMV B24884.

Phylogenetic methods

Morphological analysis

A total of 300 morphological characters were coded for both extant and fossil specimens, from the following elements: cranium, sternum, coracoid, humerus, ulna, carpometacarpus, ossa carpi, ossa digitorum manus, pelvis, femur, tibiotarsus, tarsometatarsus, and pedal phalanges (see SI.1). A total of 154 characters were derived from Migotto (2013, unpublished thesis), two from Elzanowski and Stidham (2010), two from Elzanowski and Zelenkov (2015), six from Gaff and Boles (2010), one from Worthy et al. (2016), three from Mayr (2018) and three from Mayr (2014). The remaining 129 characters were novel traits derived from observations and comparisons between the extant and fossil specimens.

Molecular data

Molecular data from Burleigh et al. (2015) was added to the morphological data to improve estimated relationships between living species (Lerner and Mindell 2005; Nagy and Tökölyi 2014; Burleigh et al. 2015). This allows the fossil taxa to be placed phylogenetically according to the signal in the morphological data, but in the context of a DNA-informed tree for living taxa which better accommodates homoplasy in skeletal morphology (see Holdaway 1994; Griffiths et al. 2007). The following genes, well-sampled in accipitrids, were used: cytochrome b, cytochrome oxidase 1, NADH dehydrogenase 2, 12s RNA, RAG 1, and fibrinogen B beta introns 6 and 7, for an aligned matrix totalling seven gene regions and six loci.

Genomic data for the above gene regions from Burleigh et al. (2015) were used for the following species: *Ciconia ciconia, Coragyps atratus, Sagittarius serpentarius, Pandion haliaetus, Elanus caeruleus, Gampsonyx swainsonii, Elanoides forficatus, Chondrohierax uncinatus, Aviceda subcristata, Pernis apivorus, Lophoictinia isura, Hamirostra melanosternon, Polyboroides typus, Neophron percnopterus, Gypohierax angolensis, Gypaetus barbatus, Spilornis cheela, Terathopius ecaudatus, Pithecophaga jefferyi, Necrosyrtes monachus, Gyps fulvus, Gyps coprotheres, Aegypius monachus, Sarcogyps calvus, Trigonoceps occipitalis, Torgos tracheliotos, Harpia harpyja, Stephanoaetus coronatus, Aquila chrysaetos, Hieraaetus morphnoides, Hieraaetus fasciatus/Aquila fasciata, Hieraaetus moorei, Spizaetus tyrannus, Spizaetus ornatus, Haliaeetus leucogaster, Haliaeetus leucocephalus, Haliaeetus albicilla, Milvus migrans, Melierax metabates, Kaupifalco monogrammicus, Circus aeruginosus, Circus cyaneus, Accipiter cooperii, Accipiter striatus, Accipiter novaehollandiae, Accipiter gentilis, Ictinia mississippiensis, Geranospiza caerulescens, Buteo buteo, Buteo lagopus, Buteo rufofuscus*, and *Platalea leucorodia*. To reduce missing data, genetic data from *Platalea leucorodia* was paired with *Threskiornis spinicollis*, and *Elanus caeruleus* paired with *Elanus scriptus*, as these species pairs consist of closely related taxa (see Campbell and Lapointe 2009 regarding this method).

Phylogenetic analysis

Phylogenetic comparisons were aimed primarily at determining the relationships of the fossil specimen SAMA P.54998. A total of 47 species of Accipitridae, and one species each of Pandionidae, Sagittariidae, Cathartidae, Threskiornithidae, and Ciconiidae were sampled. The non-accipitrid species were selected for the following reasons; Pandionidae, Sagittariidae and Cathartidae are successive sister-taxa to the Accipitridae within the Accipitriformes; the species of Ciconiidae and Threskiornithidae (Ciconiiformes), are examples of bird families outside of Accipitriformes that share similar size and flight morphology, as well as a history of grouping with the Cathartidae in older phylogenies (see Sibley and Ahlquist 1990; Wink 1995).

Both parsimony and Bayesian analyses were used to explore the data. The parsimony analyses of the morphological, molecular, and combined morphological-molecular datasets used PAUP 4.0b10, and heuristic searches. Each search was comprised of 1000 random addition replicates, and enabled TBR branch swapping, with NCHUCK set to 1000. Characters that were inapplicable to a specimen were coded using '-', while missing data were coded as '?'. The taxa *Threskiornis spinicollis, Ciconia ciconia, Coragyps atratus, Sagittarius serpentarius* and *Pandion haliaetus* were all defined as outgroup taxa in all analyses, with *Threskiornis spinicollis* and *Ciconia ciconia* being the most basal outgroups. Once the heuristic searches had generated a set of most parsimonious trees (MPT), a strict consensus tree was created from them. The support for clades on these trees were then assessed using bootstrapping, with 1000 replicates, and majority-rule consensus trees set to conlevel 50 (support shown if >50%) (see SI.3).

For the Bayesian analyses, MrBayes 3.2.7 was used via the CIPRES platform (Miller et al. 2010). The morphological partition used the standard (Lewis) model for discrete data, with correction for non-sampling of invariant characters. The among-character rate variability was modelled using the gamma parameter, with distribution approximated using four categories. The molecular partitioning scheme and substitution models were identified using PartitionFinder (Lanfear et al. 2016), using BIC. The data was

thus treated as three partitions: morphological data (morph); molecular partition 1 (pfinder Molec1), which contains Cyt-B codons 1 and 2, CO1 codons 1 and 2, ND2 codons 1 and 2, 12s, Rag-1 codons 1, 2 and 3, and FGBint67; and molecular partition 2 (pfinder Molec2), which contains Cyt-B codon 3, CO1 codon 3, and ND2 codon 3. The Molec1 and Molec2 partitions each had a GTR model using a Dirichlet prior for the state frequencies. The among-character rates were set to InvGamma, with the gamma distribution approximated as above. All substitution parameters were unlinked across these molecular partitions (see SI.4).

Each analysis entailed four runs, each run comprising four MCMC chains (incrementally heated to 0.1), the number of generations set to 50,000,000, the sample and print frequency set to 5000. Burnin was set to 20% (and confirmed sufficient using PSRF and SDSF values in MrBayes) and the majority-rule consensus tree was obtained from all post-burnin samples. During the MrBayes runs, *Ciconia ciconia* was set as the sole outgroup taxon, due to limitations of MrBayes, but trees were later rerooted so that both *Ciconia ciconia* and *Threskiornis spinicollis* were the most distal outgroup clade. The Bayesian analyses were performed twice: with morphological and molecular branch lengths linked or unlinked.

Ecomorphological analyses

Measurements of selected elements for a sample of extant accipitrids were used to correlate morphology with ecology of living forms and so to retrodict the ecology and feeding strategy of the fossil taxon. Measurements used reflected their availability in the fossil: height of the quadrate; length and proximal width of the carpometacarpus; length, shaft width and distal width of the ulna; length, shaft width, distal width, height of the condylus lateralis, depth of the condylus lateralis, height of the condylus medialis and depth of the condylus medialis of the tibiotarsus; length, shaft width, distal width, and width and height of trochleae metatarsorum 2, 3 and 4 of the tarsometatarsus; length of the first phalanx of pedal digit 1; and the length of the first and second phalanges of pedal digit 2. The fossil species was compared to *Elanus scriptus, Hamirostra melanosternon, Pernis apivorus, Lophoictinia isura, Neophron percnopterus, Aegypius monachus, Gyps coprotheres, Spilornis cheela, Haliaeetus leucogaster, Aquila audax, Hieraaetus morphnoides, Spizaetus tyrannus*, and *Circus assimilis* in Principal Components Analysis (PCA). These species were chosen as they were considered to be either, exemplars of the different hunting strategies of Accipitridae, or were potential analogues for the fossil. The PCA was performed on measurements of the wings and legs: raw, log-transformed, and standardised for size by division by the height of the quadrate in each individual (as this was possible for the fossil). The extant taxa were classed based on their preferred habitat (open, woodland, or forest) as determined from the literature (Brown and Amadon 1968; Ferguson-Lees and Christie 2001).

Widths of the distal femur, distal humerus, proximal humerus and distal tibiotarsus were measured for both extant and fossil specimens so that the relationships between these values could be used to predict the width of the distal humerus and distal femur for SAMA P.58917, and thereby to assess whether size precluded the isolated distal humerus from Site 11 Lake Pinpa and the distal femur from Ericmas Quarry from being the same taxon as SAMA P.58917.

Results

Systematic palaeontology

Class Aves Linnaeus, 1758
Order Accipitriformes Vieillot 1816
Family Accipitridae Vigors, 1824
Subfamily: Archaehieraxinae subfam. nov.

Type genus: *Archaehierax* gen. nov.

Remarks

The fossil is identified as an accipitrid due to the following combination of characters: Skull – Rostrum deep and narrow, with hooked tip and a large, broad nasal aperture; Tibiotarsus – Pons supratendineus ossified, aligned steeply transversely, medially placed, with unbranched canalis tendinosus, and distal condyles much wider than craniocaudally deep; Tarsometatarsus – Robust, with monosulcate hypotarsus, the lateral and medial hypotarsal crests widely separated and trochleae metatarsorum splayed both medially and laterally, and dorsally arched in distal view; Foot – Four digits with raptorial unguals, those of digits 1 and 2 relatively large; Digit IV – phalanges 2 and 3 are very short compared to phalanx 4.

The fossil can be excluded from Falconiformes (Falconidae) and the other families of Accipitriformes (Cathartidae, Sagittariidae, Pandionidae) by the morphology of the tarsometatarsal hypotarsus cristae and sulcus. The cristae are fused or partially fused together to enclose the sulcus in Cathartidae, Sagittariidae, and Pandionidae, while in Falconidae the medial crista is connected to the shaft by a ridge that extends two-thirds of its length, features that are absent in the fossil.

Diagnosis

Accipitrids in which the following autapomorphic features are found: the pila medialis of the sternum dorsally separates two deep pneumatic fossae, the humerus has the caput humeri only slightly elevated proximally past the tuberculum ventralis, the tip of the processus procoracoideus of the coracoid sharply curves inwards ventrally towards the medial face of the bone, the tibiotarsus has the lateral/distal retinaculum scar in a deep fossa, the tarsometatarsus is relatively elongate with narrow trochleae metatarsorum that are separated by wide incisurae, and the incisura for the m. flexor hallucis brevis tendon is large, distinct, and extends distal to the fossa metatarsi I. In addition to this, the following features occur: the rostral tip of the rostrum is hooked below the tomial margin at a relatively shallow 30–40° angle, the quadrate has a deep, distinct foramen pneumaticum caudomediale, and the sternum has the apex carinae displaced caudally from the base of the spina externa.,

Genus *Archaehierax* Mather, Lee, Camens and Worthy gen. nov.

Type species: *Archaehierax sylvestris* **sp. nov.**

http://zoobank.org/urn:lsid:zoobank.org:act:8C4B01F2-12CE-46F4-A444-C63B18C90BAE

Etymology

Archaehierax is derived from the Greek words 'archaios', meaning ancient, and 'hierax', meaning hawk. Gender masculine.

Diagnosis

An accipitrid distinguished by the combination of the following features; **Rostrum. (1)** The nares are large and fully open, **(2)** processus maxillopalatini not fused; **Quadrate. (3)** the condylus

pterygoideus projects less medially than the condylus medialis, **(4)** a deep, distinct fossa caudomedialis with a small amount of pneumatism; **Sternum. (5)** The apex carinae is displaced caudally from the base of the spina externa, **(6)** the medial crista on the carina does not extend to the spina externa; **(7)** The pila medialis on the dorsal face separates two deep fossae (autapomorphy); **Humerus. (8)** The caput humeri is only slightly elevated proximally past the tuberculum ventralis (autapomorphy); **Os carpale ulnare. (9)** Deepened depression on ulnaris face; **Tarsometatarsus. (10)** The trochleae metatarsorum are splayed and separated by wide incisurae, especially laterally, with the individual trochleae themselves quite narrow in width (autapomorphy); **(11)** The incisura for the m. flexor hallucis brevis tendon is large, distinct, and extends distal to the fossa metatarsi I (autapomorphy); **Phalanx IV.4. (12)** The distal articular end that articulates with phalanx IV.5, is considerably wider than the shaft.

Type Locality/Stratigraphy/Age

31° 07.499′ S; 140° 12.755′ E. Site 12a, Lake Pinpa, Frome Downs Station, Callabonna Sub-Basin, S.A. Dolomite bed of Namba Formation, Pinpa LF, late Oligocene, 26–24 Ma.

Archaehierax sylvestris *Mather, Lee, Camens and Worthy gen. et sp. nov. (Figures 3-10)*

http://zoobank.org/urn:lsid:zoobank.org:act:092140CA-E937-43B3-B3F1-7127C97094F4

Holotype

SAMA P.54998, 63 elements and associated fragments of a single skeleton (see Figure 2) as follows:

Fragments of mandible; rostral majority of rostrum; R pterygoid; L quadratojugal; L quadrate; ceratohyal; atlas vertebra; axis vertebra; partial cervical vertebra #3; caudal vertebrae x3 (position in tail indeterminate); cranial part sternum; LR scapulae; cranial and sternal parts LR coracoids; proximal LR humeri; L and distal R ulna; L and distal R radius; L carpometacarpus; LR os carpi ulnare; L os carpi radiale; R manual phalanges, proximal fragment MI.1, proximal fragment MII.1 and MII.2; L manual phalanges MI.1, MII.2 with distal end eroded, and MIII.1; LR proximal femur fragments; R tibiotarsus reconstructed in two parts; L tibiotarsus; fragmented LR fibulae; LR tarsometatarsi; LR ossa metatarsalia; pedal phalanges: RI.1, RII.1, RII.2, RIII.1, RIII.2, RIII.3 (partial), RIII.4, LI.1, LI.2 (fragmented), LII.1, LII.2, LIII.1, LIII.2, LIII.3 (partial), LIII.4, LIV.1, LIV.2, LIV.3, LIV.4, LIV.5. The skeleton was found eroding out on the surface with surviving elements recovered in a semi-articulated state from within dolomitic clays (equivalent to layer 5 of Thorn et al. 2021), with most large elements fractured into many roughly articulated pieces, presumably by expansion and contraction associated with the wetting and drying of the clays. The fragments for each element were, where possible, separated, cleaned and reassembled by THW.

Measurements (mm)

See Appendix 1 Table S1.

Etymology

The species name 'sylvestris' is derived from the Greek world 'sylvas', meaning forest, and the Latin suffix '-estris', meaning 'belonging to'.

Type locality/Stratigraphy and age

As per genus.

Diagnosis

As for genus.

Descriptions

Rostrum maxillare (Figure 3(A, B)).

The rostral section of the rostrum maxillare is preserved in reasonably good condition. Morphology of its rostral tip, tomial margin, rostral margin of the nares, and the palatines is visible.

The rostrum has a preserved length of 32.6 mm from the rostral tip to the posterior base of the nares, and a preserved depth of 17.3 mm from the tomial margin to the dorsal side of the rostrum taken at the rostral end of the nares. **(Trait 1)** The rostral tip of the rostrum is hooked, descending below the tomial margin at a 30–40° angle. **(2)** The lateral tomial margin (Figure 3A: CT), positioned distal to the nares, is ventrally convex. **(3)** The nasal aperture (Figure 3A: N) is large (height 8.7 mm) and fully open as in most accipitrids, spanning just over half the rostrum depth. **(4)** The ossified section rostral to the incisura ventromedialis is of small to moderate size (10.1 mm preserved length) relative to the total length of the rostrum. **(5)** In ventral aspect, an incisura ventromedialis (Figure 3B: IV) (sensu Livezey and Zusi 2007) is present (sediment filled) extending from where damage destroys it rostrally to the preserved caudal end of the palate; it is narrow and widens caudally, rather than being closed forming a fenestra. The pars maxillaris palatini (Figure 3B: PM) are unfused and diverge slightly caudally, the left being least fragmented although it has broken from the adjacent lateral margin creating a false incision. A small fragment of bone preserved between the pars maxillaris palatini is interpreted as a displaced fragment of the processus maxillopalatinus. **(6)** Damage precludes ascertaining the presence/form of the fenestra ventrolaterale.

Other accipitrid subfamilies differ as follows:

(Trait 1) Compared to the fossil, the tip of the rostrum is much more sharply hooked ventrally in most subfamilies. Only members of Elaninae, Perninae (except *Chondrohierax uncinatus*, which is sharper), Buteoninae, and Gypaetinae have similar or shallower angled tips.

The rostrum maxillare is overall most similar to that of species of Buteoninae (see SI.2 for more detailed differential comparisons).

Quadrate (Figure 3(C, D))

The left quadrate has considerable breakage affecting the lateral side ventrally, the medial side of the processus oticus, and loss of the processus orbitalis. Preservation of morphological detail is best medially. On the processus oticus, only about half of the capitulum squamosum is preserved and the dorsal half of the crista medialis is lost. Of the processus orbitalis, only the well-preserved base remains. Both the condylus pterygoideus and medialis are intact, but the entire condylus lateralis and caudal half of the condylus caudalis are lost.

(Trait 1) The processus oticus (Figure 3D: POt) is short and broad leading up to the capitulum squamosum. **(2)** The capitulum squamosum (Figure 3D: CS), as preserved is relatively small, and has a tuberculum subcapitulare forming a distinct hook projecting ventrally on its cranial margin. **(3)** The processus orbitalis (Figure 3C: POr) is dorsomedially oriented. **(4)** The processus is set entirely in the ventral half of the quadrate, creating a gentle, shallow sloping arc between the base of the processus and the

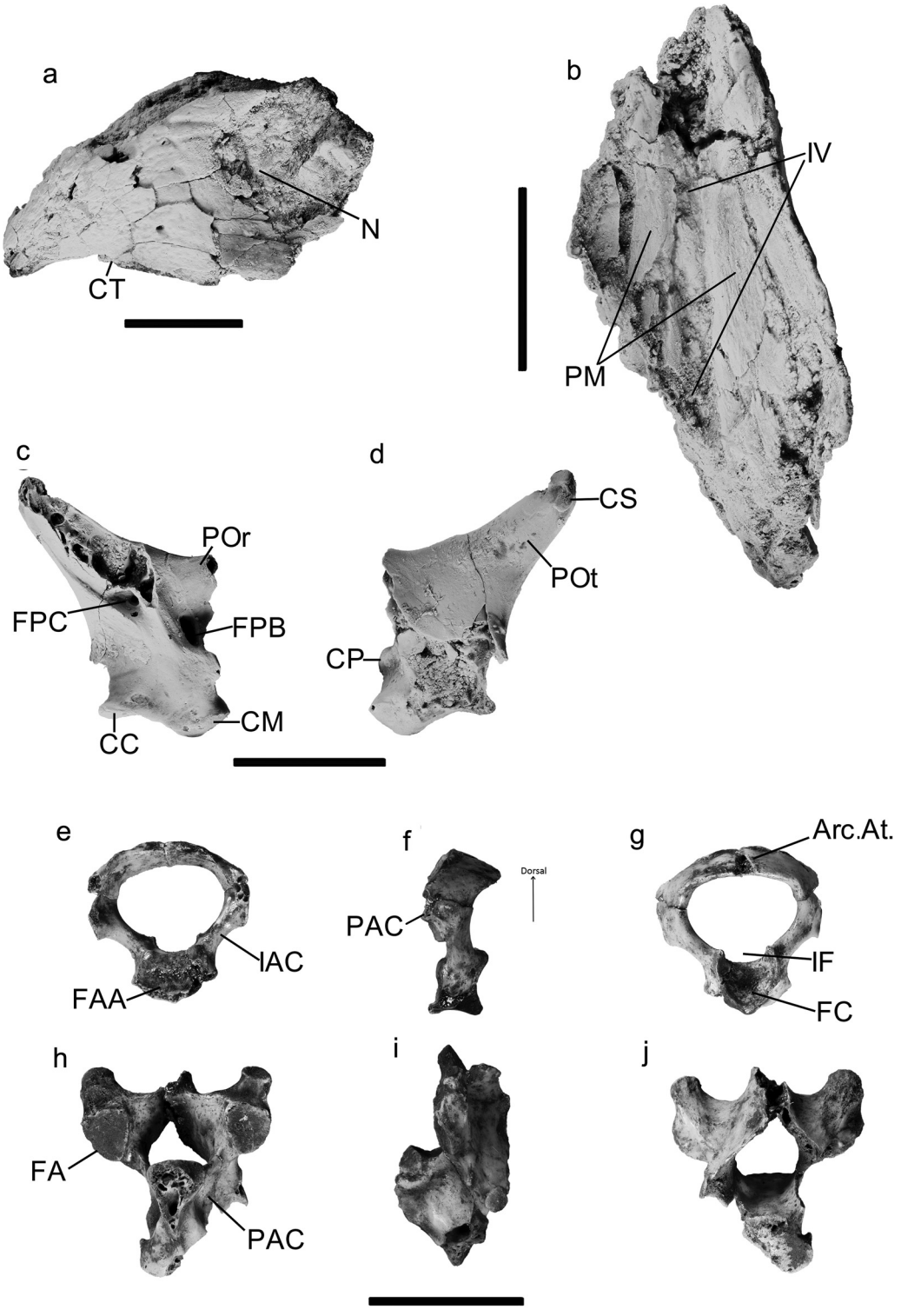

Figure 3. *Archaehierax sylvestris* gen. et. sp. nov. SAMA P.54998 rostrum in lateral (A) and ventral (B) view; quadrate in medial (C) and lateral (D) view; atlas vertebra in caudal (E), lateral (F) and cranial (G) view; and axis vertebra in caudal (H), lateral (I) and cranial (J) view. Specimens in A-D are coated in ammonium chloride. Abbreviations: Arc. At., arcus atlantis; CC, condylus caudalis; CM, condylus medialis; CP, condylus pterygoideus; CS, capitulum squamosum; CT, crista tomialis; FA, facies articularis; FAA, facies articularis axialis; FC, fossa condyloidea; FPB, fossa pneumaticum basiorbitale; FPC, fossa/depressio pneumaticum caudomediale; IAC, incisura caudalis arcus; IF, incisura fossae; IV, incisura ventromedialis; N, nasale; PAC, processus articularis caudalis; PM, pars maxillaris palatini; POr, processus orbitalis; POt, processus oticus. Scale bars are 10 mm.

capitulum. **(5)** A large and deep foramen pneumaticum basiorbitale (Figure 3C: FPB) is present between the processus orbitalis and the condylus pterygoideus. **(6)** Breakage prohibits assessing the status of the foramen rostromediale. **(7)** The ventral section of the crista medialis is preserved and is quite broad and flat with no projecting ridge. **(8)** A thin, distinct sulcus runs along the ventral margin of the crista to connect to the foramen pneumaticum caudomediale. **(9)** A distinct, deep foramen pneumaticum caudomediale (Figure 3C:

FPC) is present just medial of the ventral-most point of the crista medialis. **(10)** The condylus pterygoideus (Figure 3D: CP) is distinct, high-set and well separated from the condylus medialis. **(11)** The condylus medialis (Figure 3C: CM) is well preserved, showing a large (4.0 mm wide by 2.8 mm deep), semi-ovular facet, with a pointed medial margin that extends further medially than the condylus pterygoideus. **(12)** The portion of the condylus caudalis (Figure 3C: CC) preserved indicates a facet of a similar size to the condylus medialis, with a semicircular shape.

Other accipitrid subfamilies differ as follows (variable characters excluded):

(Trait 8) The sulcus running along the ventral crista is broad and indistinct in all other taxa except in species of *Milvus* and *Haliaeetus* (Haliaeetinae) where it is narrow and indistinct. **(9)** The fossa caudomediale is practically absent in the subfamilies Circaetinae and Aegypiinae, as well as the species in *Hamirostra, Lophoictinia* (Perninae), *Neophron* (Gypaetinae), and *Haliaeetus* (Haliaeetinae); shallow in Aquilinae and species of *Elanoides, Chondrohierax* (Perninae), *Polyboroides* and *Gypohierax* (Gypaetinae); and deep in Elaninae, Accipitrinae and Buteoninae, as well as species in *Pernis* (Perninae). The depressio was indistinctly shaped (i.e. a gradually deepened area rather than a defined pit) in all species, and apneumatic in all species except in *Pernis* and *Haliaeetus*.

The quadrate is overall most similar to that of species of Aegypiinae (see SI.2 for more detailed differential comparisons).

Vertebrae (Figure 3E-J)

The atlas vertebra of SAMA P.54998 is 10.7 mm wide by 10.7 mm high (from the proximal margin of arcus atlantis to the distal margin of fossa condyloidea). **(Trait 1)** The arcus atlantis (Figure 3G: Arc. At.) forms a low, flat arch, which dorsally has a maximum proximodistal width of 3.2 mm at the centre, overhanging the fossa condyloidea cranially. **(2)** The incisura fossae (Figure 3G: IF) is shallow and broad, forming a semicircular shape in cranial aspect. **(3)** The fossa condyloidea (Figure 3G: FC) is 4.3 mm wide by 4.2 mm long. **(4)** The dorsolateral eminences of the fossa condyloidea are small. **(5)** The ventral margin of the fossa forms a rounded point in cranial aspect and is prominent cranially in lateral aspect. **(6)** The zygopophyses caudales are badly worn and difficult to assess, but what is preserved indicates they were distinct and caudally projected from the rest of the arcus atlantis. **(7)** The incisurae caudales arcus (Figure 3E: IAC) are very shallow. **(8)** The facies articularis axialis (Figure 3E: FAA) is 5.7 mm wide by approximately 3.8 mm long. **(9)** The rest of the distal corpus atlantis is worn away and cannot be assessed, but what is present suggests that few additional structures were present, and that there was some asymmetry in the shape of the lateral fossa condyloidea.

The axis vertebra is quite fragmented, with most of the neural spine, facies articularis atlantica, dens, facies articularis caudalis, processus ventralis and the area of incisurae caudales arcus broken away. Its width is 12.7 mm across the processus articulares caudales and mid-line length of the corpus vertebra is 8 mm. The facies articularis on zygopophyses caudales are 3.1 mm wide by 3.8–4.1 mm long. **(10)** A short but caudally prominent projection is present dorsal to each facet (Figure 3H: FA), measuring 2–2.5 mm in width. **(11)** There is no evidence of a bridge enclosing the incisurae caudales arcus (Figure 3F, H: PAC).

The three known caudal vertebrae are too broken to identify their position in the caudal series.

The vertebrae are overall most similar to that of species of Elaninae (see SI.2 for more detailed differential comparisons).

Sternum (Figure 4(A, B, C))

The cranial section of the sternum of SAMA P.54998 is preserved, retaining the structure of the spina externa, pila carinae, crista medialis carinae, apex carinae, the left sulcus articularis coracoideus, and the left labrum internum. It is characterised by:

(Trait 1) A spina interna is absent; a small notch exists in its place. **(2)** The spina externa (Figure 4B: SE) is 6.4 mm wide at its base, 4.7 mm wide at its blunt tip and 4.2 mm long. In cranial view, the spina externa is triangular as a medial crista forming a lobe projecting 3.6 mm ventrally. The base of the spina externa is broader than the apex carinae (4.0 mm). **(3)** The crista medialis carinae (Figure 4A: CMC) is short, extending dorsally from the apex carinae to mid-height of the pila carinae with a low profile in lateral view. More dorsad, the pila carinae is smooth to the base of the spina externa. **(4)** The pila carinae (Figure 4A: PC) is robust for its size, measuring 5.2 mm at mid-depth. It is 23.3 mm long from the ventral margin of the carina sterni to where the pila carinae meets the spina externa. **(5)** The apex carinae (Figure 4A: AC) at 4.0 mm wide, is noticeably expanded from the width of the pila carinae immediately dorsal to it (3.0). **(6)** The apex carinae is rounded, with no hooked projection extending cranially. **(7)** The maximum carina depth below the sternal basin is roughly equivalent to basin depth below the costal margin, typical of most accipitrids except for certain vulture species (Aegypiinae). **(8)** The apex carinae is set well caudally [assuming the junction of the carina with the pars cardiaca is aligned horizontally] from the base of the spina externa. **(9)** There are no small, dispersed pneumatic foramina present dorsally in the body of the sternum. **(10)** The small part of the carina sterni preserved narrows caudally from the pila carinae. **(11)** The left sulcus articularis coracoideus (Figure 4B: SAC) is 4.3 mm dorsoventrally deep, and extends to the midline of the sternum, directly dorsal to the spina externa, where it does not overlap the right sulcus. **(12)** The left labrum internum (Figure 4A: LI) is maximally 4.2 mm deep and 2.8 mm wide in dorsal view as preserved. **(13)** A pila medialis (Figure 4C: PM), 2.1 mm wide, on the dorsal face of the sternum separates two deep, pneumatic fossae in the pars cardiaca.

Extant accipitrid subfamilies differ as follows:

(3) The crista medialis extends to the base of the spina externa in members of all subfamilies except Aegypiinae. **(8)** The apex carinae lies directly ventral to the base of the spina externa, or projects more craniad, in species in all subfamilies except for Gypaetinae and Aegypiinae. **(11)** The sulci articularis coracoidei overlap in all species except for *Gampsonyx swainsonii* (Elaninae) and *Sarcogyps calvus* (Aegypiinae). **(13)** No species in any subfamily has a distinct pila medialis separating pneumatic fossae in the pars cardiaca, which is thus an autapomorphy suggesting subfamilial distinction for the new species.

The sternum is overall most similar to that of species of Aegypiinae (see SI.2 for more detailed differential comparisons).

Coracoid (Figure 4(F, G, H, I))

The well-preserved left and right omal ends and fragments of both sternal ends of the coracoids of SAMA P.54998 were recovered. They reveal the following:

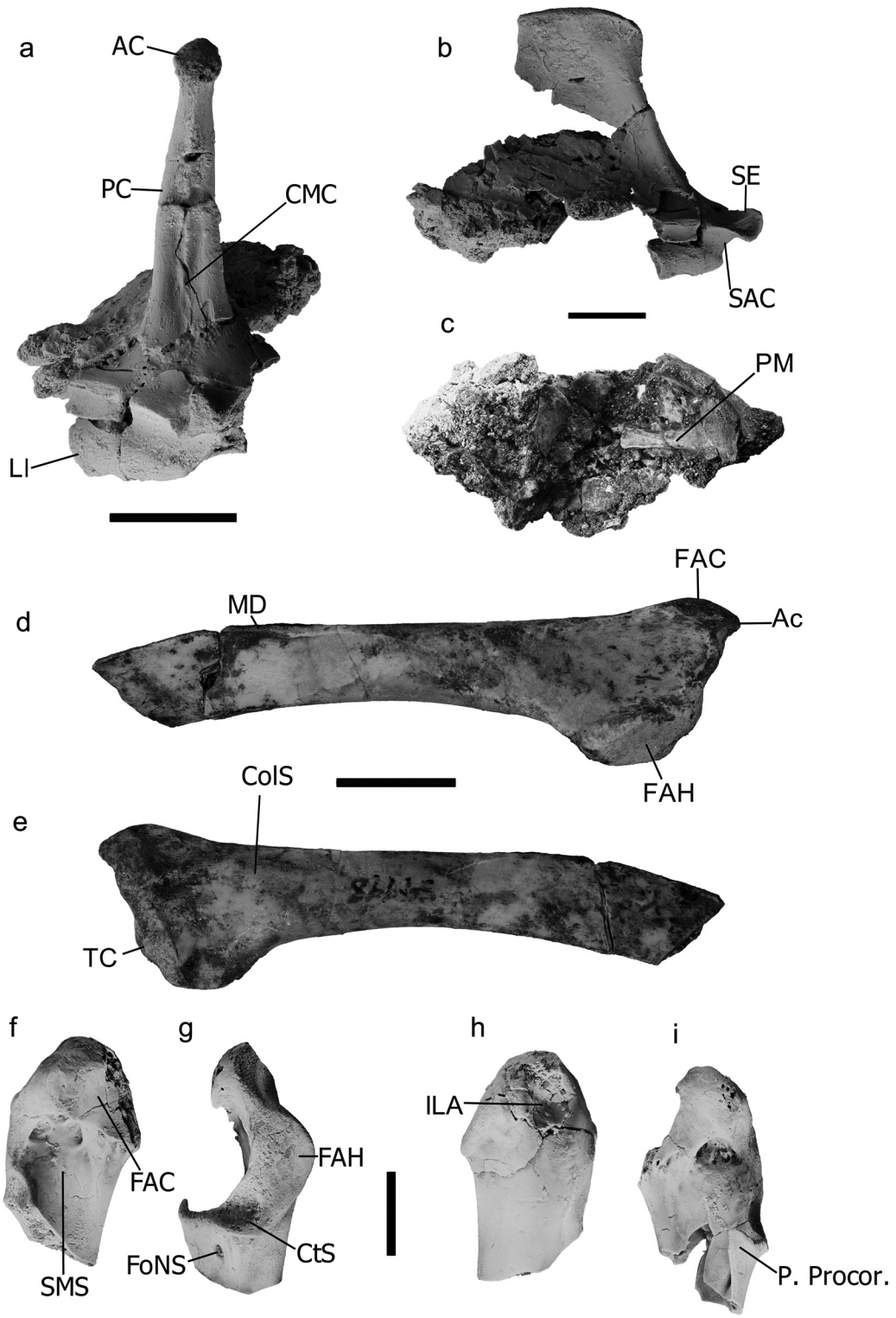

Figure 4. *Archaehierax sylvestris* gen. et. sp. nov. SAMA P.54998 partial sternum in cranial (A), left lateral (B) and dorsal (C) view; right scapula in lateral (D) and medial (E) view; omal fragments of the left coracoid in medial (F) and lateral (H) view and of the right coracoid in dorsal (G) and medial (I) view. Specimens in A, B, and F-I are coated in ammonium chloride. Abbreviations: AC, apex carina; Ac, acromion; CMC, crista medialis carinae; CtS, cotyla scapularis; ColS, collum scapulae; FAC, facies articularis clavicularis; FAH, facies articularis humeralis; FoNS, foramen nervi supracoracoidei; ILA, impressio ligamenti acrocoracohumeralis; LI, labrum internum; MD, margo dorsalis; PC, pila carinae; PM, pila medialis; P. Procor., processus procoracoideus; SAC, sulcus articularis coracoideus; SE, spina externa; SMS, sulcus m. supracoracoidei; TC, tuberculum coracoideum. Scale bars are 10 mm.

(Trait 1) A foramen nervi supracoracoidei (Figure 4G: FoNS) is present and located adjacent to the shaft rather than near the medial margin of the processus procoracoideus; **(2)** The foramen lacks an opening into the corpus; and **(3)** it is small, about 1 mm in width, and positioned just sternal of the cotyla scapularis. **(4)** A large (6 mm wide) pneumatic foramen is present in the

sulcus m. supracoracoidei (Figure 4F: SMS). The width of the sulcus is approximately 14.5 mm from the ventrosternal corner of the facies articularis clavicularis to the facies articularis humeralis, and 12.8 mm from the medial margin to the laterodorsal margin immediately cranial to the cotyla scapularis. **(5)** The facies articularis clavicularis (Figure 4F: FAC) is large, broad, and clearly delineated sternally by a crista that dorsally overhangs the aforementioned foramen, and ventrally is a low non-overhanging crista. The sternal margin of this facet is straight with no notch nor dorsal or ventral projections directed sternally. **(6)** The cotyla scapularis (Figure 4G: CtS), preserved on the right omal fragment, is deep and large (6.7 mm wide by 5.7 mm long) in relation to the processus procoracoideus and triangular shaped. **(7)** The facies articularis humeralis (Figure 4G: FAH) is 7.7 mm wide and 12.8 mm long. **(8)** The impressio lig. acrocoracohumeralis (Figure 4H: ILA), best seen on the left specimen, forms a distinct sulcus ~7 mm wide by 18.1 mm long on the processus acrocoracoideus, although this may be exaggerated by damage to the fossil. **(9)** The processus procoracoideus (Figure 4I: P. Procor.) forms a short projection medially, barely as long again as the cotyla scapularis width, with its tip sharply angling ventrally towards the medial face to partly enclose the triosseal canal. **(10)** The best preserved sternal-end fragment shows that the angulus medialis is acute, forming a 30–45° angle. **(11)** The medial side of the facies articularis sternalis is 6.5 mm wide at its broadest point, and shallow, with little deepening towards the dorsal margin.

Extant accipitrid subfamilies differ as follows:

(Trait 5) The sternal margin of the facies articularis clavicularis does not form a crest overhanging the sulcus supracoracoideus in Elaninae, Perninae (except *Chondrohierax uncinatus*), Gypaetinae (except *Polyboroides typus*), Aegypiinae, Haliaeetinae, Accipitrinae, and Buteoninae. **(8)** The impressio lig. acrocoracohumeralis is shallow in Elaninae, Perninae, Gypaetinae, Accipitrinae, and Buteoninae. **(9)** In all subfamilies, the processus procoracoideus does not, or barely, angles ventrally towards the medial face.

The coracoid is overall most similar to that of species of Aegypiinae, Accipitrinae and Buteoninae (see SI.2 for more detailed differential comparisons).

Scapula (Figure 4(D,E))

Both the left and right scapulae of *Archaehierax sylvestris* gen. et. sp. nov. are almost complete, lacking only the distal third or less of the corpus scapulae. In total, the preserved craniocaudal length of the scapulae is 56.8 mm (left) and 53.3 mm (right).

The proximal dorsoventral width of the scapula is 14.4 mm from the acromion to the ventral side of the facies articularis humeralis. **(1)** The tuberculum coracoideum (Figure 4E: TC) is low and barely cranially prominent dorsal of the facies articularis humeralis. **(2)** The acromion (Figure 4D: Ac) has a distinct cranio-laterally oriented crista lig. acrocoracoacromiali dorsally, and a robust rounded medial prominence. **(3)** There are no pneumatic foramina or fossae present in the acromion cranially, **(4)** nor on the lateral or medial facies between the acromion and the facies articularis humeralis. **(5)** The facies articularis humeralis (Figure 4D: FAH) is quite large and broad, measuring 6.3 mm dorsoventrally by 10.8 mm craniocaudally on the left specimen; 6.3 mm by 10.4 mm on the right. **(6)** The acromion barely projects proximally/cranially of the tuberculum coracoideum. **(7)** Minimum dorsoventral depth of the collum scapulae (Figure 4E: ColS) is 6.3 mm. **(8)** While the extremitas caudalis is broken off, the corpus scapulae is elongate and moderately narrow, **(9)** but it greatly increases in depth caudal to the margo dorsalis ridge (Figure 4D: MD), attaining a maximum dorsoventral depth of 8.1 mm. **(10)** The lateral face dorsal to and immediately posterior to the facies articularis humeralis is flat. **(11)** The ligamental attachment on the margo dorsalis has a very small prominence and is not elevated dorsally above the rest of the margo dorsalis.

Extant accipitrid subfamilies differ as follows:

(Trait 6) The acromion strongly projects cranially in all species except in pernines (*Chondrohierax uncinatus, Pernis apivorus, Aviceda subcristata*), and *Ictinia mississippiensis* (Buteoninae).

The scapula is overall most similar to that of species of Elaninae (see SI.2 for more detailed differential comparisons).

Humerus (Figure 5).

The humeri are poorly preserved in SAMA P.54998. Only the caput humeri, crus dorsale fossae, fossa pneumotricipitalis, and the incisura capitis of the proximal end of the right humerus is preserved. The left humerus is more complete, preserving about 60mm of proximodistal length of the proximal end including the caput humeri, crus dorsale fossae, fossa pneumotricipitalis, incisura capitis, sulcus lig. transversus, facies bicipitalis, crista deltopectoralis, and some of the proximal shaft. However, there is also significant breakage and fracturing of the bone surface in this specimen, which has resulted in the loss of the tuberculum dorsale, the ventral margin of the crista bicipitalis, tuberculum ventrale, and sulcus n. coracobrachialis. These specimens reveal the following:

(1) The incisura capitis (Figure 5A: IC), as best observed in the left humerus, is shallow and lacks secondary deepening. **(2)** There is no visible ligamental scar in the distal incisura capitis. **(3)** The caput humeri (Figure 5A: CH) is quite flattened, projecting proximal to the incisura capitis only a few millimetres. **(4)** The fossa pneumotricipitalis (Figure 5A: FP) was large and deep, although breakage precludes assessing its former width. The better-preserved left specimen shows it was minimally 7.7 mm wide. **(5)** The crus dorsale fossae (Figure 5A: CDF) is broad, measuring 4.0 mm wide, and is caudally convex. **(6)** The sulcus lig. transversus (Figure 5C: SLT), best seen in the left humerus, is shallow but well defined, and seems continuous between the ventral and dorsal sections. Ventrally, the sulcus is deep and round, measuring 6.3 mm wide by 4.5 mm long cranial to the incisura capitis. The crista deltopectoralis (Figure 5B: CrD), while quite fractured, is preserved in its entirety in the left specimen. Preserved length is 42.7 mm from the assumed position of the tuberculum dorsale to its distal end. **(7)** The profile of the proximal section of the dorsal margin of the crista between its origin near the tuberculum dorsale and the angulus cristae of the crista deltopectoralis is flat in a ventro-cranial view. **(8)** The angulus cristae of the crista deltopectoralis is very prominent and distinctly triangular in dorsal view. **(9)** Distally, the crista deltopectoralis, while fractured, projected mainly cranially (shaft margin visible proximal to the distal point of crista).

Extant accipitrid subfamilies differ as follows:

(Trait 1) In all subfamilies except Aegypiinae and *Spilornis cheela* in Circaetinae, species have a deep incisura capitis; **(3)** The caput humeri is more elevated proximal to the incisura capitis and tuberculum ventrale, ranging from a moderate (Elaninae) to a large proximal projection (all other subfamilies) so a low flattened caput is identified as an autapomorphy of the species.

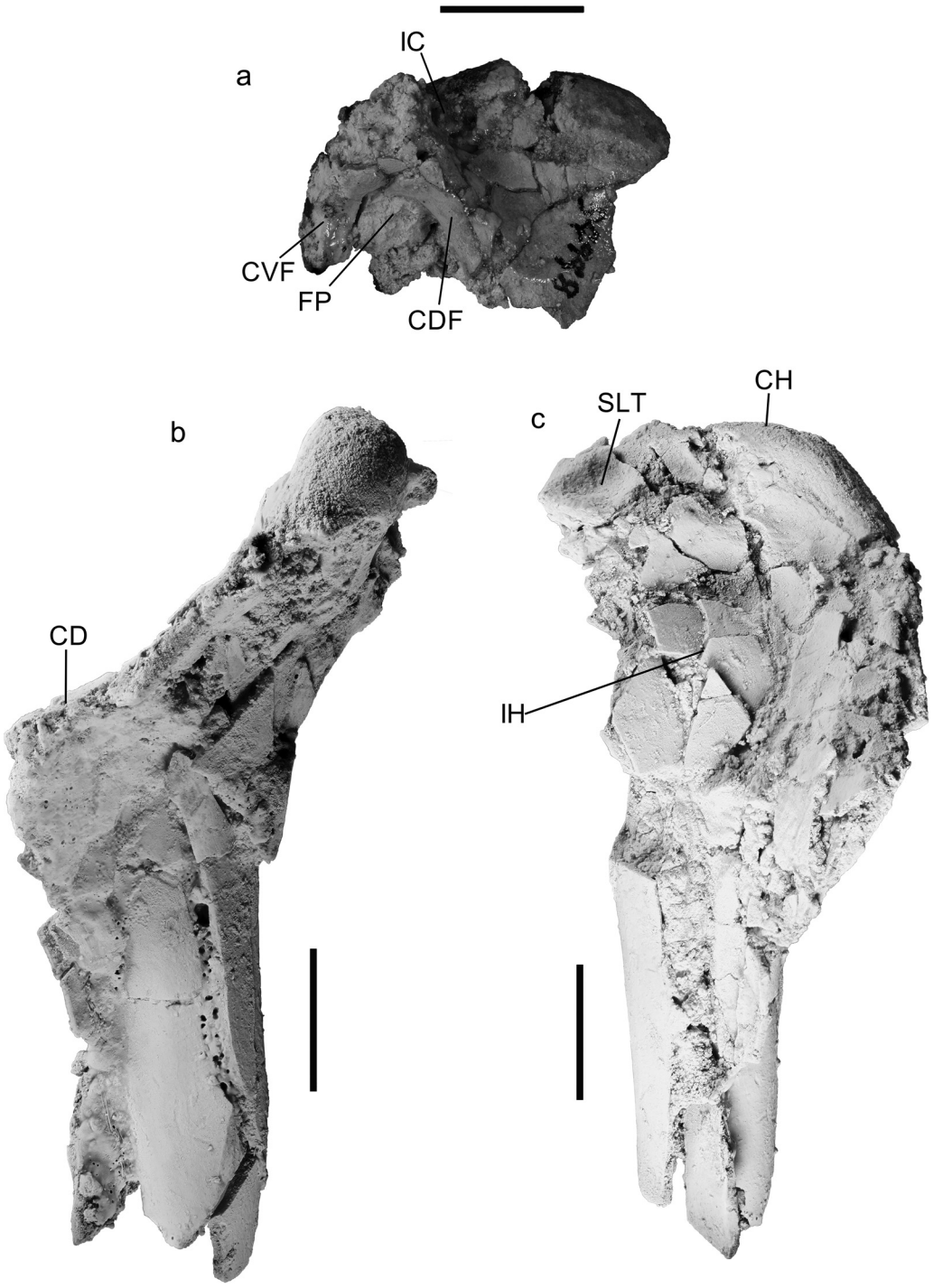

Figure 5. Proximal humerus fragments of *Archaehierax sylvestris* gen. et. sp. nov. SAMA P.54998: right, in caudal view (A); left, in dorsal (B) and cranial (C) views. Specimens in B and C are coated in ammonium chloride. Abbreviations: CD, crista deltopectoralis; CDF, crus dorsale fossae; CH, caput humeri; CVF, crus ventrale fossae; FP, fossa pneumotricipitalis; IC, incisura capitis; IH, intumescentia humeri; SLT, sulcus ligamenti transversus. Scale bars are 10 mm.

The proximal humerus is overall most similar to that of species of Elaninae, Aegypiinae, Aquilinae, Haliaeetinae and Buteoninae (see SI.2 for more detailed differential comparisons).

Ulna (Figure 6(C, D, E))

SAMA P.54998 preserves a near-complete left ulna, reassembled from fragments, that is only missing the olecranon, parts of the ventral margin of the cotyla ventralis contiguous with the olecranon, and the caudodorsal margin of the cotyla dorsalis. The distal right ulna is also preserved with the condyles mostly intact, with only the ventrocaudal margin of the condylus dorsalis and condylus ventralis worn away. They reveal the following features:

(1) The ulna is largely straight in dorsal and ventral view, with only very slight caudal curvature towards the proximal and distal ends. The processus cotylaris dorsalis projects distally of the cotyla ventralis (Figure 6E: PCD), is 5.8 mm wide, and **(2)** is quadrangular in shape with a flattened dorsal tip between parallel equal-length

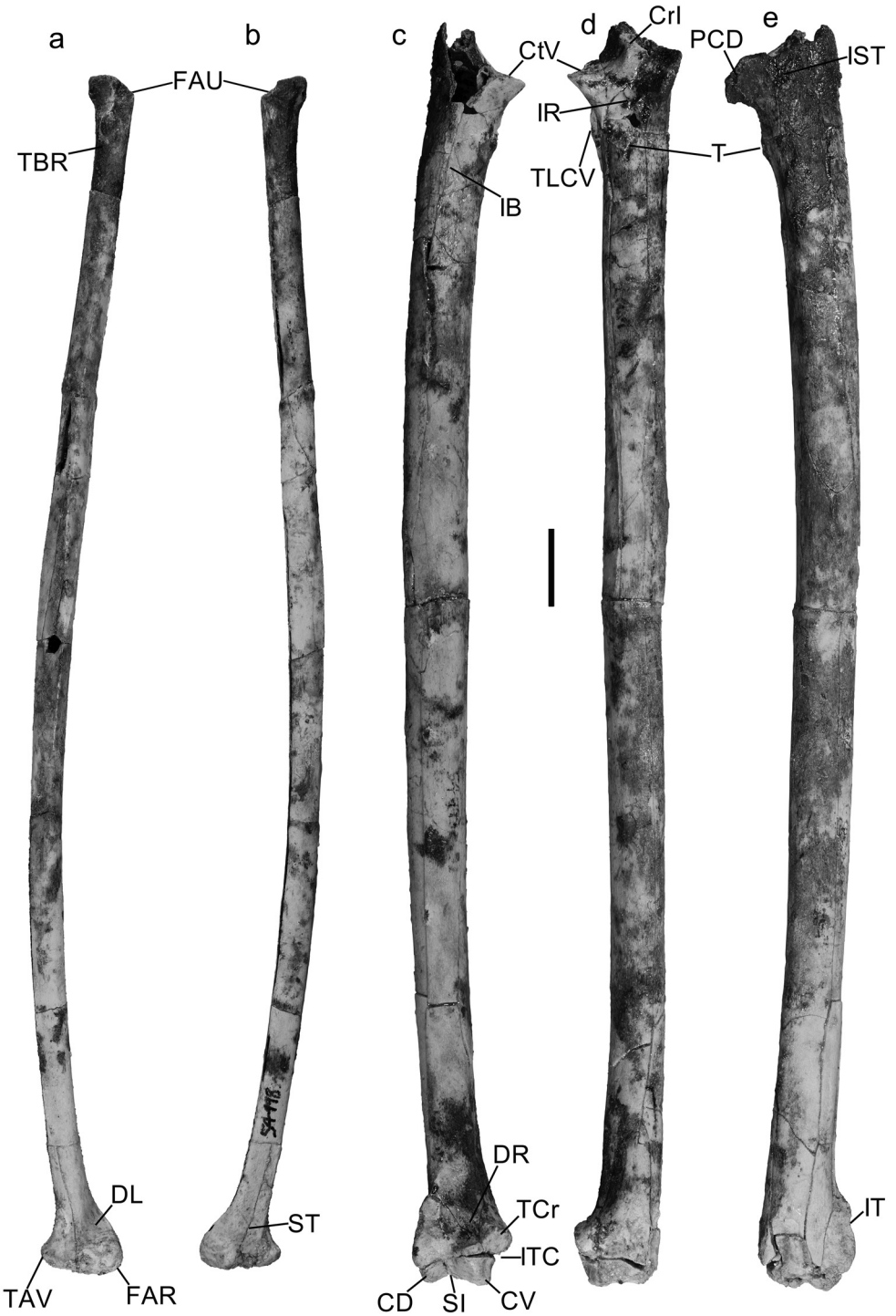

Figure 6. *Archaehierax sylvestris* gen. et. sp. nov. SAMA P.54998 left radius in ventral (A) and dorsal (B) view, and left ulna in ventral (C), cranial (D) and caudal (E) view. Abbreviations: CD, condylus dorsalis; CrI, crista intercotylaris; CtV, cotyla ventralis; CV, condylus ventralis; DL, depressio ligamentosa; DR, depressio radialis; FAR, facies articularis radiocarpalis; FAU, facies articularis ulnaris; IB, impressio brachialis; IR, incisura radialis; IST, impressio scapulotricipitis; IT, incisura tendinosa; ITC, incisura tuberculum carpalis; PCD, processus cotylaris dorsalis; SI, sulcus intercondylaris; ST, sulcus tendineus; T, tuberculum; TAV, tuberculum aponeurosis ventralis; TBR, tuberculum bicipitale radiale; TCr, tuberculum carpale; TLCV, tuberculum ligamentum collateralis ventralis. Scale bar 10 mm.

proximodorsal and distoventral sides. **(3)** The cotylae are shallow, separating by a moderately proximally protruding crista intercotylaris (Figure 6D: CrI). Breakage precludes assessing if a pneumatic fossa or foramen was present caudal of the cotylaris dorsalis. **(4)** The impressio scapulotricipitis (Figure 6E: IST) is shallow. **(5)** The incisura radialis (Figure 6D: IR), defined by the margin of the cotyla ventralis proximoventrally, the tuberculum cranialis distally, and a ridge descending ventrodistally from the base of the processus cotylaris dorsalis dorsally, is shallow. **(6)** Distal to the incisura radialis two tubercula are present, one on the cranial face is large and round (3.8 mm wide) and distinctly projects from the shaft (Figure 6D, E: T), the other smaller (1.9 mm wide) and flatter positioned adjacent to it on the ventral face. **(7)** The impressio brachialis (Figure 6C: IB) is shallow, with the base flat and not

depressed relative to the shaft and is 12 mm long proximodistally. The midshaft of the left specimen is 7.7 mm craniocaudally wide in dorsal aspect. **(8)** The papillae remigales caudales form low, barely prominent scars, which is typical of most accipitrids. The distal end of the ulna measures 12.9 mm wide (left) and 12.2 mm wide (right) between the cranial point of the tuberculum carpale (Figure 6C: TCr) and the caudal margin of the condylus dorsalis (Figure 6C: CD) in ventral aspect. **(9)** The tuberculum carpale is short and blunt, or rounded, in dorsal and ventral view, **(10)** with a flattened facet directed ventrodistally. **(11)** The incisura tuberculum carpale (Figure 6C: ITC) forms a distinct notch separating the tuberculum carpale and condylus ventralis (Figure 6C: CV) when viewed in dorsal aspect. The condylus dorsalis (left specimen) is 13.5 mm long proximodistally along its caudal margin in ventral aspect, and 9.3 mm deep from the caudal margin to the incisura tendinosa, in caudodorsal view. **(12)** The caudal margin of the condylus dorsalis forms a continuous curve in the proximal half, best visible in either craniodorsal or caudodorsal view, interrupted only by a small notch for the incisura tendinosa (Figure 6E: IT). **(13)** The incisura tendinosa lies between the condylus dorsalis and the condylus ventralis (dorsal aspect), though it does not quite separate the two proximodistally. **(14)** The depressio radialis (Figure 6C: DR) is shallow and not pneumatized. **(15)** The sulcus intercondylaris (Figure 6C: SI) forms a relatively deep v-shape in ventral aspect. **(16)** The condylus ventralis distinctly projects distocranially, and measures 5.7 mm wide (in ventral aspect) by 11.2 mm deep (in cranial aspect).

Extant accipitrid subfamilies differ as follows:

(Trait 1) The proximal shaft is notably curved cranially in elanines, most pernines (except *Aviceda subcristata, Lophoictinia isura* and *Hamirostra melanosternon*), and buteonines (except species of *Circus*).

The ulna is overall most similar to that of species of Circaetinae (see SI.2 for more detailed differential comparisons).

Radius (Figure 6(A, B))

In SAMA P.54998, the left radius is complete, preserving most features of the proximal (cotyla humeralis slightly worn ventrocaudally) and distal ends.

The cotyla humeralis is large, measuring 5.5 mm deep dorsoventrally, and 4.1 mm wide. It shows the following:

A tuberculum bicipitale radiale (Figure 6A: TBR) is located 5.4 mm distal of the facies articularis ulnaris on the dorsal face. The tuberculum has **(1)** a large, deep, non-pneumatic fossa (2.6 mm wide by 3.8 mm proximodistal length) on it, and **(2)** has a distinct profile in cranial view as a low, quadrangular ridge. **(3)** The sulcus tendineus (Figure 6B: ST) is very shallow, barely differentiated from the corpus. **(5)** The tuberculum aponeurosis ventralis (Figure 6A: TAV) projects ventrally at approximately 60–70°, and its tip is rounded. **(6)** The facies articularis radiocarpalis (Figure 6A: FAR) is quite flat in dorsal view, but slightly curves out distally from the tuberculum aponeurosis ventralis to the opposite margin. **(7)** The depressio ligamentosa (Figure 6A: DL) on the ventral face of the distal end is deep but lacks pneumatism. **(8)** The facies articularis ulnaris (Figure 6(A, B): FAU) forms a prominent bulb that projects out ventrally, and which has a deep notch on the proximal margin that gives it a double-peaked appearance.

Extant accipitrid subfamilies differ as follows:

(Trait 1) The fossa associated with the tuberculum bicipitalis is shallow in all species except some pernines e.g., *Elanoides forficatus* (absent) and *Pernis apivorus* (deep). **(5)** The tuberculum aponeurosis ventralis projects at a more abrupt angle in all taxa except *N. percnopterus* (Gypaetinae), species of *Gyps* (Aegypiinae), and *H. morphnoides* and *A. chrysaetos* (Aquilinae). **(7)** The depressio ligamentosa is shallower in Perninae (except *E. forficatus*), Gypaetinae, Circaetinae, Aquilinae, Haliaeetinae, and Buteoninae.

The radius is overall most similar to that of species of Haliaeetinae and Gypaetinae (see SI.2 for more detailed differential comparisons).

Os carpale radiale (Figure 7(G, H))

The left os carpale radiale is complete in SAMA P.54998.

Measurements: proximodistal length 8.6 mm, dorsoventral width 12.3 mm, and depth 5.4 mm.

It has the following features, terminology from Mayr (2014): **(1)** The distoventral projection (Figure 7G: DVP) is small and pointed, oriented at an angle between 45° and 60°. **(2)** The notch for the musculus ulnometacarpalis ventralis (Figure 7H: NMUMV) is distinct, but shallow. **(3)** The facies articularis metacarpalis (Figure 7H: FAM) slightly projects distally from the cranial face in cranial view. **(4)** The sulcus for the musculus extensor carpi radialis (Figure 7H: ECR) is shallow, forming a gentle curve at about a 160° angle between the ventral and dorsal ends. **(5)** A broad, deep fossa covers most of the ventral half of the cranial face (Figure 7H: CVFos), which is open towards the proximo-ventral corner. **(6)** A second smaller and deep fossa is present on the dorsal half of the cranial face (Figure 7H: DVF), and is apneumatic and oriented more craniodorsally. **(7)** The facies articularis radialis (Figure 7G: FARad) is broad (depth ~5.7 mm, dorsoventral width 11.0 mm) and strongly marked on the caudal face. **(8)** The caudal face has a small but deep fossa (Figure 7G: FAUF), set in the facies articularis ulnaris (Figure 7G: FAU) close towards the ventral end. **(9)** The caudal margin of the facies articularis metacarpalis forms a convex continuous curve from the ventral margin to the dorsal margin.

The os carpale radiale is overall most similar to that of species of Elaninae and Buteoninae (see SI.2 for more detailed differential comparisons).

Os carpale ulnare (Figure 7(I, J))

Both the right and left os carpale ulnare are complete in SAMA P.54998. Measurements (mm) right/left: dorsoventral width 12.2/11.8, craniocaudal depth (excluding cranial projection) 4.4/4.6, and proximodistal length 9.9/9.2. They show:

(1) A distinct projection, roughly in the centre of the cranial face (Figure 7J: CrPro), extends well cranially above the margin of the proximal ligament attachment, and lacks a prominent ridge that makes it contiguous with the proximodorsal corner. **(2)** The rest of the cranial face is roughly equal in cranial height towards the crus breve (Figure 7J: CB) and the crus longus (Figure 7J: CrL). **(3)** The proximodorsal corner of the crus longus is distinctly notched by a deepened apneumatic fossa (Figure 7J: PDF). **(4)** The proximal margin of the cranial face has a distinct ligament attachment point (Figure 7J: PLA), projecting slightly proximally above the face and positioned ventrally adjacent to the proximal end of the crus longus. **(5)** The crus breve is slightly shorter (8.7 mm long) in the right specimen, than total length (9.4 mm) from the proximal point of the crus longus to the distal margin, **(6)** and has a flattened, ventral face. **(7)** On the caudal face, a very low projection is present on the proximal margin immediately adjacent to the ventral crus breve (Figure 7I: PVP). **(8)** A distinct, deep impression is present in the caudal surface (Figure 7I: CaD). **(9)** This depression is separated from the rest of the distal face by a distinct but low crista that extends dorsoventrally across the face from the caudal projection

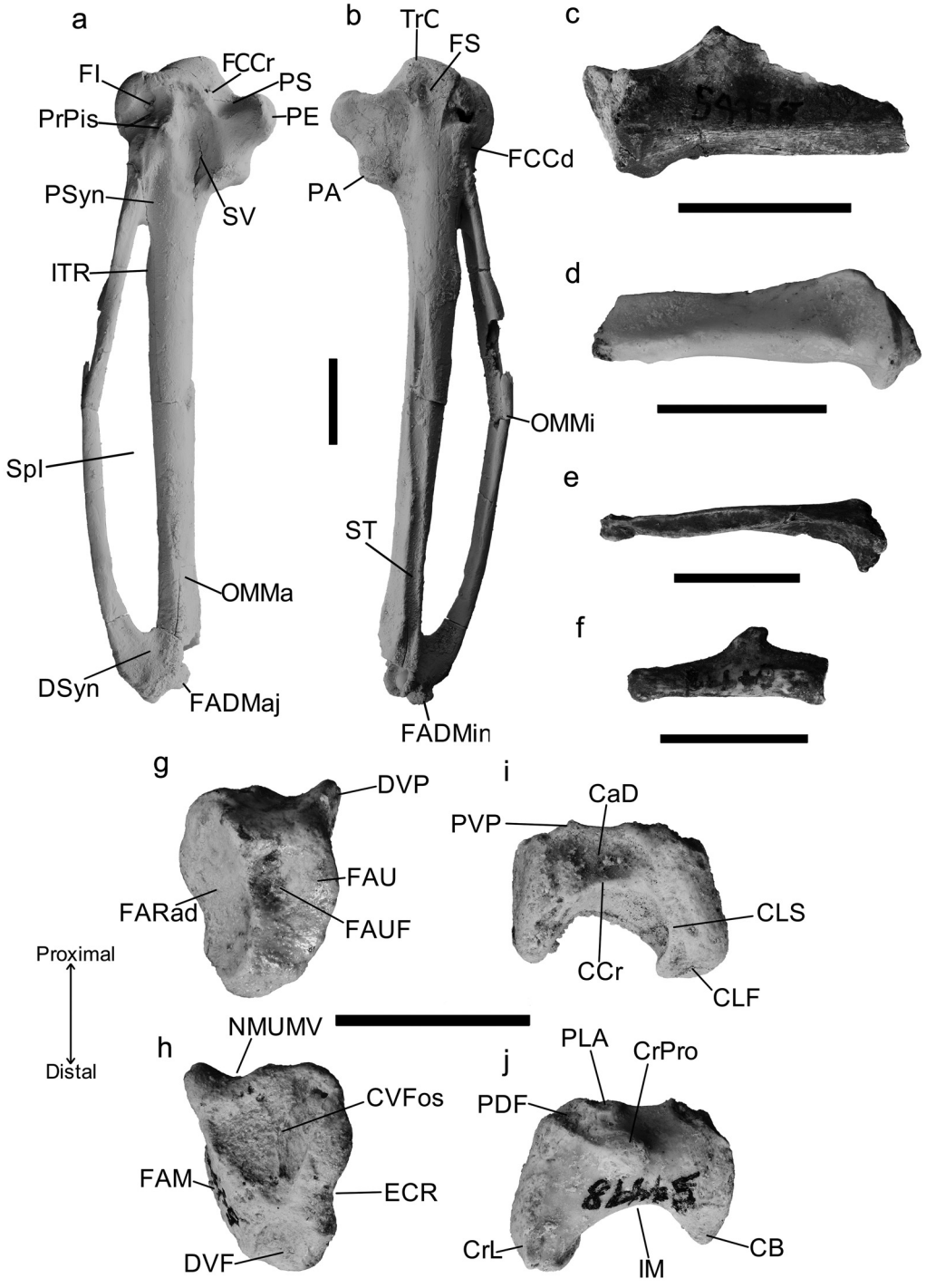

Figure 7. *Archaehierax sylvestris* gen. et. sp. nov. SAMA P.54998 left carpometacarpus in ventral (A) and dorsal (B) view, manual phalanx digiti majoris II.1 broken distally (C), manual phalanx digiti majoris II.2 (D), manual phalanx digiti alularis I.1 (E), manual phalanx digiti minoris III.1 (F), os carpale radiale in caudal (G) and cranial (H) view, and os carpale ulnare in caudal (I) and cranial (J) view. Carpometacarpus coated with ammonium chloride. Abbreviations: CaD, caudal fossa; CB, crus breve; CCr, caudal crista; CrL, crus longus; CLF, crus longus fossa; CLS, crus longus sulcus; CrPro, cranial projection; CVFos, cranial ventral fossa; DSyn, distal synostosis; DVF, dorsal ventral fossa; DVP, distoventral projection; ECR, extensor carpi radialis; FADMaj, facies articularis digitalis major; FADMin, facies articularis digitalis minor; FAM, facies articularis metacarpalis; FARad, facies articularis radialis; FAU, facies articularis ulnaris; FAUF, facies articularis ulnaris fossa; FCCr, fovea carpalis cranialis; FCCd, fovea carpalis caudalis; FI, fossa infratrochlearis; FS, fossa supratrochlearis; IM, incisura metacarpalis; ITR, intermetacarpal tuberosity; NMUMV, notch for musculus ulnometacarpalis ventralis; OMMa, os metacarpale majus; OMMi, os metacarpale minus; PA, processus alularis; PDF, proximodorsal fossa; PE, processus extensorius; PLA, proximal ligament attachment; PrPis, processus pisiformis; PS, proximal sulcus; PSyn, proximal synostosis; PVP, proximoventral projection; SpI, spatium intermetacarpale; ST, sulcus tendineus; SV, sulcus on ventral facies; TrC, trochlea carpalis. Scale bars 10 mm.

(Figure 7I: CCr), connecting to both the crus breve and crus longus. **(10)** The incisura metacarpalis is deep and broadly v-shaped (Figure 7J: IM), with the peak offset towards the crus breve. **(11)** A very shallow sulcus is seen running along

the proximodistal extent of the caudal face of the crus longus (Figure 7I: CLS), **(12)** which terminates in a shallow fossa on the distal point of the crus (Figure 7I: CLF).

Extant accipitrid subfamilies differ as follows:

(Trait 2) The ventral cranial face is higher set cranially than the dorsal cranial face in all subfamilies except Accipitrinae. **(3)** There is no notch on the proximal end of the crus longus in all subfamilies except in the genera *Aquila* (Aquilinae), *Haliaeetus* (Haliaeetinae) and *Buteo* (Buteoninae), which have a shallow notch. **(8)** There is no deepened depression on the caudal face in all subfamilies except Aquilinae, *Aegypius monachus* (Aegypiinae), Accipitrinae, and the genus *Buteo* (Buteoninae). **(9)** There is no raised crista on the caudal face in all subfamilies except in the genus *Buteo* (Buteoninae).

The os carpale ulnare is overall most similar to that of species of Elaninae, Perninae, Gypaetinae and Aquilinae (see SI.2 for more detailed differential comparisons).

Carpometacarpus (Figure 7(A, B))

For SAMA P.54998, the left carpometacarpus is almost complete, missing only the cranial section of the facies articularis digitalis majus.

(1) The fossa infratrochlearis (Figure 7A: FI) is deep and lacks pneumatisation. **(2)** A rounded ridge extending from the processus pisiformis to the trochlear rim separates the fossa infratrochlearis from **(3)** an extremely deep sulcus (Figure 7A: SV) between the processus pisiformis and the processus extensorius. This sulcus is elongate and extends from the trochlea carpalis (Figure 7B: TrC) to adjacent to the processus alularis (Figure 7B: PA). **(4)** The fossa supratrochlearis (Figure 7B: FS), which is caudoventrally positioned on the ventral face of the proximal end, is shallow and lacks pneumatisation. **(5)** There is a shallow sulcus on the ventral face, on the proximal margin at the base of the processus extensorius just distal to the trochlea carpalis (Figure 7A: PS). **(6)** The fovea carpalis cranialis (Figure 7A: FCCr) is shallow and apneumatic. **(7)** The fovea carpalis caudalis (Figure 7B: FCCd) is very shallow and apneumatic. **(8)** The ventral rim of the trochlea carpale projects strongly caudally and distally is short, terminating slightly distal to the level of the processus pisiformis. **(9)** The proximal margin of the processus extensorius (Figure 7A: PE) and the trochlea carpale forms an approximately 120° angle, with the proximal margin slightly upturned proximally. From base to tip, the processus extensorius measures 7.7 mm in craniocaudal width, and is 39% of the 19.6 mm proximal width of the carpometacarpus. **(10)** The proximodorsal margin of the processus extensorius forms a sharp crista that dorsally overhangs the dorsal face of the processus. **(11)** The processus alularis protrudes slightly cranially in a triangular bulge, with a single curved articular facet distally. **(12)** The processus alularis is separated from the caudal surface of the shaft by a small notch on the dorsal face. **(13)** The processus pisiformis (Figure 7A: PrPis) strongly projects ventrally in caudal and cranial view, and is positioned central on the ventral face between the processus extensorius and the caudal margin of the trochlea carpalis. It is separated from the spatium intermetacarpale (Figure 7A: SpI) by a dorsoventral length of 10.5 mm. **(14)** This region of separation between the processus pisiformis and spatium intermetacarpale is occupied by a shallow sulcus that is bound by the os metacarpale minus in its distal half. **(15)** The synostosal region distal to the processus alularis is wider craniocaudally than it is long dorsoventrally. **(16)** The intermetacarpal tuberosity (Figure 7A: ITR), which is the scar for the insertion of the m. extensor metacarpi ulnaris has almost no caudal projection and is positioned well distal of the proximal synostosis (Figure 7A: Psyn). **(17)** The sulcus tendineus (Figure 7B: ST) is primarily located on the dorsal face of the shaft. **(18)** The sulcus tendineus is broad. **(19)** The proximal region of the os metacarpale minus has a distinct groove on the caudal face, which lacks any pneumatisation. **(20)** The os metacarpale minus (Figure 7B: OMMi) is slightly arched caudally when viewed in ventral and dorsal aspect. **(21)** The facies articularis digitalis minor (Figure 7B: FADMin) projects further distally than the preserved facies articularis digitalis major (Figure 7A: FADMaj). **(22)** The length between the distal point of the facies articularis digitalis minor and the spatium intermetacarpale is approximately equal to the width of the spatium. **(23)** The distal synostosis (Figure 7A: DSyn) is very short. **(24)** The os metacarpale majus (Figure 7A: OMMa) has a markedly flattened cranial face and is dorsoventrally deeper than it is craniocaudally wide. **(25)** The sulcus interosseus positioned in the distal synostosis is slightly deepened.

Measurements – see Appendix 1 Table S1; overall, the carpometacarpus has a proximal craniocaudal width that is equivalent to 25% of the total length, which is moderately gracile.

Extant accipitrid subfamilies differ as follows

(Trait 1) The fossa infratrochlearis is shallow, except in Perninae (deep in *Pernis apivorus* and *Chondrohierax uncinatus*, the latter also pneumatic) and Gypaetinae (deep). **(19)** The proximal section of the os metacarpale minus has a shallower groove, except in *P. typus* (Gypaetinae, deep) and *Haliaeetus leucocephalus* (Haliaeetinae, deep), or in Elaninae (flat, ungrooved).

The carpometacarpus is overall most similar to that of species of Buteoninae (see SI.2 for more detailed differential comparisons).

Manus (Figure 7C, D, E, F)

The manus bones are moderately well-preserved in SAMA P.54998, with a mostly intact left phalanx digiti alulae (L MI.1), complete left phalanx digiti minoris (L MIII.1) and left phalanx digiti majoris 2 (L MII.2), and a mostly intact R MI.1, partial R MII.1 and fragment of the R MII.2.

(1) The proximal L MI.1 has a dorsoventral width of 6.6 mm and a craniocaudal depth of 6.5 mm, and from proximal view is triangular. **(2)** The cranial margin is tapered into a thin crista that continues along the length of the preserved bone. **(3)** A small tuberculum is present on the caudal margin of the ventral face, close to the proximal end. **(4)** The dorsal margin and face of the proximal end is much more protruding than the ventral margin and face and has two ligament attachment points on its dorsal surface. **(5)** The width of the bone narrows distally. **(6)** The L MIII.1 is 14.2 mm long and has a prominent caudal projection slightly less than halfway distally along its length, the tip of which is oriented caudoproximally. **(7)** Both the dorsal and ventral face lack any sort of depression or sulcus. Only the proximal end of the MII.1 is preserved, which is 8.3 mm wide by 6.9 mm deep. **(8)** The caudal margin projects caudally into a thin crista, and a deep depression is visible just distal of the projecting point. The left MII.2 is 24.1 mm long and proximally has a dorsoventral height of 5.8 mm and a craniocaudal depth of 4.8 mm. **(9)** The caudal margin forms a thin crista. **(10)** The proximal quarter of the cranial margin is also flattened, but then

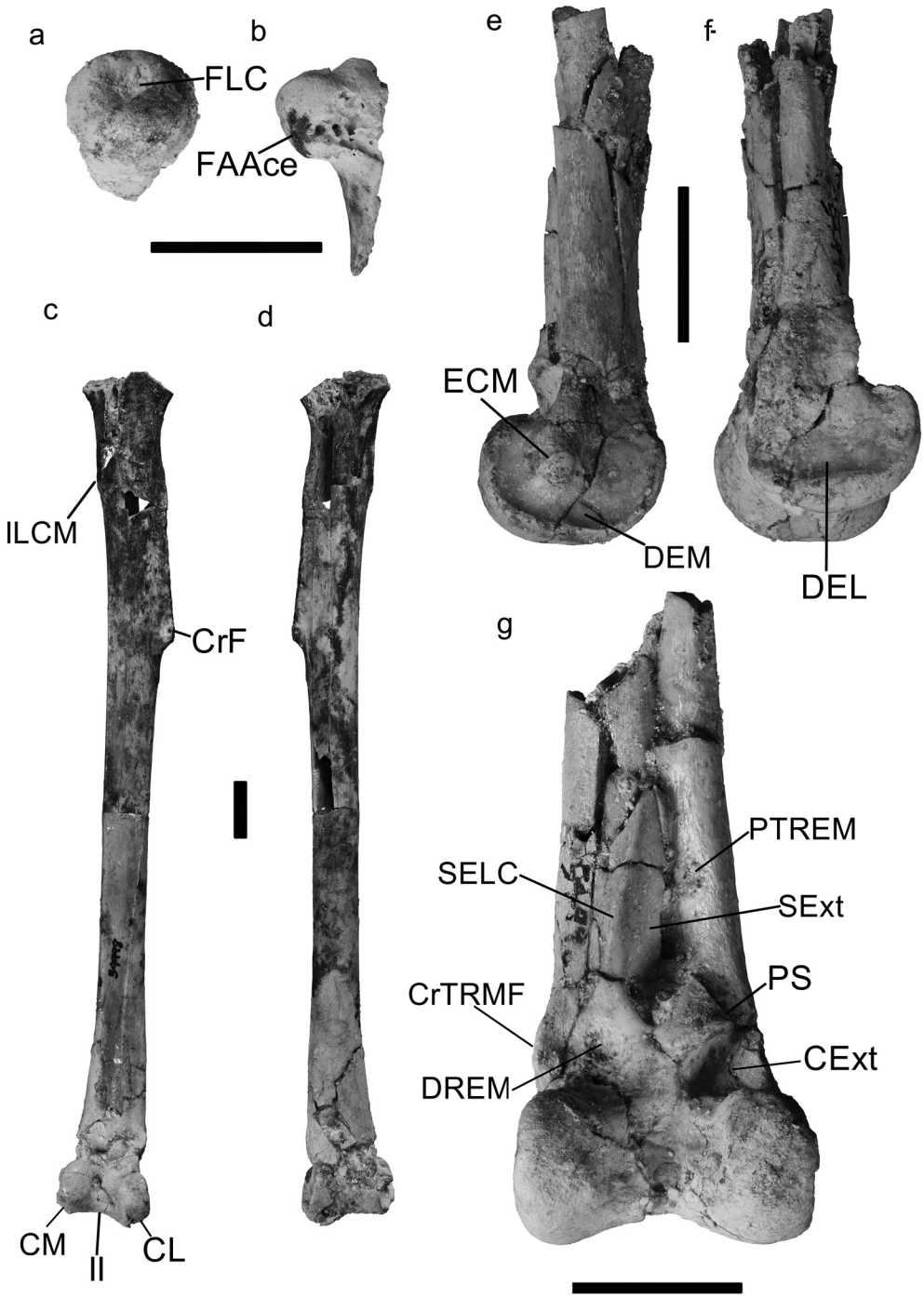

Figure 8. *Archaehierax sylvestris* gen. et. sp. nov. SAMA P.54998 proximal left and right femoral fragments in medial (A) and cranial (B) view, left tibiotarsus in cranial (C) and caudal (D) aspect, and distal right tibiotarsus (E-G) in medial (E) lateral (F) and cranial (G) view. Abbreviations: CExt, canalis extensorius; CrF, crista fibularis; CL, condylus lateralis; CM, condylus medialis; CrTRMF, cranial tuberculum retinaculi musculus fibularis; DEL, depressio epicondylaris lateralis; DEM, depressio epicondylaris medialis; DREM, distal insertion retinaculum extensorium tibiotarsi; ECM, epicondylus medialis; FAAce, facies articularis acetabularis; FLC, fovea ligamenti capitis; II, incisura intercondylaris; ILCM, impressio ligamenti collateralis medialis; PTREM, proximal insertion scar retinaculum extensorium tibiotarsi; PS, pons supratendineus; SExt, sulcus extensorius; SELC, lateral crista beside sulcus extensorius. Scale bars 10 mm.

expands notably with the presence a shallow sulcus extending to the distal end. **(11)** On the dorsal surface, a low ridge is present at the proximal end, with a small but deep fossa set into the caudal side of it. **(12)** A similar fossa is also set into the caudal side of this ridge in proximal view, just distal of the articular facet. **(13)** The ventral face has a deep depression lacking pneumatic foramina just distal of the proximal end.

The manus bones are overall most similar to those of species of Perninae (see SI.2 for more detailed differential comparisons).

Femur (Figure 8(A, B))

In SAMA P.54998, only the caput of both femora has been preserved, preserving the articularis acetabularis face and the fovea ligamenti capitis. The width of the caput is 7.6 mm. The fovea ligament capitis (Figure 8A: FLC) is shallow and set in the proximal margin of the caput. The articularis acetabularis face (Figure 8B: FAAce) is not well defined from the medial face.

Tibiotarsus (Figure 8(C, D, E, F, G))

Both the right and left tibiotarsi are preserved in SAMA P.54998. The left tibiotarsus is almost complete with only the proximal articular surfaces missing. It preserves the base of the cnemial crests and the entire crista fibularis, but damage to the distal end obscures the details of the pons supratendineus, the tuberculum retinaculum m. fibularis, and the distal insertion scar for the retinaculum extensorium tibiotarsi. The right tibiotarsus is missing the entire proximal end, and the distal end could not be reconnected to the shaft but is very well-preserved revealing most features of interest.

As observed on the left element, **(1)** the impressio lig. collateralis medialis (Figure 8C: ILCM) is a slightly elevated tuberculum on the medial face, measuring 4.5 mm wide and 8.9 mm long. **(2)** The crista fibularis (Figure 8C: CrF) is approximately 33.3 mm long, or roughly 24% of the preserved length (135.7 mm). **(3)** The crista fibularis is prominent, maximally projecting 2.4 mm, or approximately 26% of shaft width (9.3 mm) at the same point. **(4)** The width of the crista fibularis is greatest distally. **(5)** The cranial face directly adjacent to the crista fibularis is slightly convex. **(6)** The scar for the ligament that connected to the distal end of the fibula is approximately 34.5 mm long and extends distally along the lateral margin of the shaft, from 38 mm distal to the crista fibularis. **(7)** A distinct linea is visible on the medial margin of the shaft that extends approximately 77.4 mm proximodistally from the distal base of the impressio lig. collateralis medialis. **(8)** The cross-section of the shaft at mid length is roughly circular. **(9)** The sulcus extensorius (Figure 8G: SExt) is medially positioned on the distal third of the shaft and is approximately 5 mm wide at broadest, compared to a shaft width of 10.5 mm at the same section. **(10)** The lateral margin of the sulcus is bordered by a raised crista (Figure 8G: SELC). **(11)** The canalis extensorius (Figure 8G: CExt) is deep, and both openings are quite large. **(12)** The pons supratendineus (Figure 8G: PS) is obliquely angled at roughly 45° to the long axis, and **(13)** is distinctly arched cranially. **(14)** The distomedial margin of the pons supratendineus lies close (1.3 mm) to the medial shaft margin. **(15)** The cranial tuberculum retinaculi m. fibularis (Figure 8G: CrTRMF) is craniolaterally prominent. **(16)** The caudal tuberculum retinaculi m. fibularis is low and barely projecting, but preservation is poor in this region of the bone. **(17)** The proximal scar (tuberositas retinaculum extensoris medialis, Figure 8G: PTREM) is separated proximally from the pons supratendineus by a distance equal to the proximodistal width of the pons. **(18)** The distal/lateral attachment of the extensor retinaculum (Figure 8: DREM) is marked by a deep, round fossa. **(19)** Distal width (17.5 mm) is greater than the maximum distal depth (13.4 mm) by roughly 24% (right element). **(20)** The increase in width from the shaft to the distal end is gradual and symmetrical either side. **(21)** The condyles have roughly equal craniocaudal depth in distal view, **(22)** with a deep incisura intercondylaris roughly 25% of depth of the distal end, **(23)** and the impression in the trochlea cartilaginis tibialis in caudal view forms an inverted v-shape. **(24)** The epicondylus medialis (Figure 8E: ECM) is large and projects well medial to the condylus medialis, being visible in cranial view, and is of moderate robustness. **(25)** The epicondyle is surrounded by a deep depressio medialis (Figure 8E: DEM), which is bordered by a thin but prominent crista on the margins of the condyle. **(26)** The depressio lateralis (Figure 8F: DEL) is shallow, and bordered by a flattened, broad crista on the distal margin of the lateral condyle. The trochlea cartilaginis tibialis is difficult to assess due to breakage, **(27)** but appears largely flat.

Extant accipitrid subfamilies differ as follows:

The medial side of the pons supratendineus is more widely separated from the medial shaft margin **(Trait 14)** in elanines, pernines except *E. forficatus*, gypaetines, aegypiines, circaetines, aquilines, and haliaeetines. **(10)** There is no crista on the lateral margin of the sulcus extensorius in elanines, gypaetines, aegypiines, circaetines, aquilines, haliaeetines, accipitrines or buteonines. **(18)** No species in any subfamily has the lateral/distal retinaculum scar in a deep fossa; it ranges from a shallow fossa (pernines, aegypiines, circaetines, aquilines, haliaeetines), to flat (elanines, some pernines, gypaetines), or slightly elevated rugose surface (accipitrines, buteonines), identifying the deep pit for the distolateral insertion of the retinaculum extensoris medialis as an autapomorphy of the fossil.

The tibiotarsus is overall most similar to that of species of Buteoninae (see SI.2 for more detailed differential comparisons).

Fibula

The proximal ends of the left and right fibulae are preserved in *Archaehierax sylvestris* gen. et. sp. nov. Craniocaudal depth is about 10.2 mm, while width is 3.7 (right) and 4.0 mm (left).

(1) A shallow fossa is present in the cranial half of the proximal lateral face. **(2)** The caudal face has a very shallow depression just distal to the caudal projection. **(3)** The medial face has a broad but shallow sulcus that extends from near the proximal margin down the shaft.

Tarsometatarsus (Figure 9)

The right and left tarsometatarsi are both imperfectly preserved in SAMA P.54998. The left tarsometatarsus preserves the original length of the bone, though the medial half and the proximal end, from mid-length on the medial side to and including the area proximal to the foramen vasculare proximale laterale, has been dorsolaterally twisted approximately 90° relative to the rest of the bone. The lateral half is thus undistorted from just proximal to the foramen vasculare proximale laterale distally. The cotyla lateralis is missing with about half of the eminentia intercotylaris. The foramen vasculare proximale mediale is obscured by the distortion on both the dorsal and plantar side.

The right specimen has the distal half preserved well with all features, but the proximal half is so badly fragmented that nearly all identifying features are lost. Only the crista medialis hypotarsi is recognisable. The specimens reveal the following features:

(1) The length of the tarsometatarsus is about 66–75% of the length of the tibiotarsus (uncertainty allows for the missing proximal end of the tibiotarsus). **(2)** The length to distal width (maximal across trochleae) ratio is approximately 1:6 and shows the tarsometatarsus is moderately elongate among accipitrids. **(3)** The cotyla medialis (Figure 9D: CtM) is deep and with a notably convex dorsal margin.

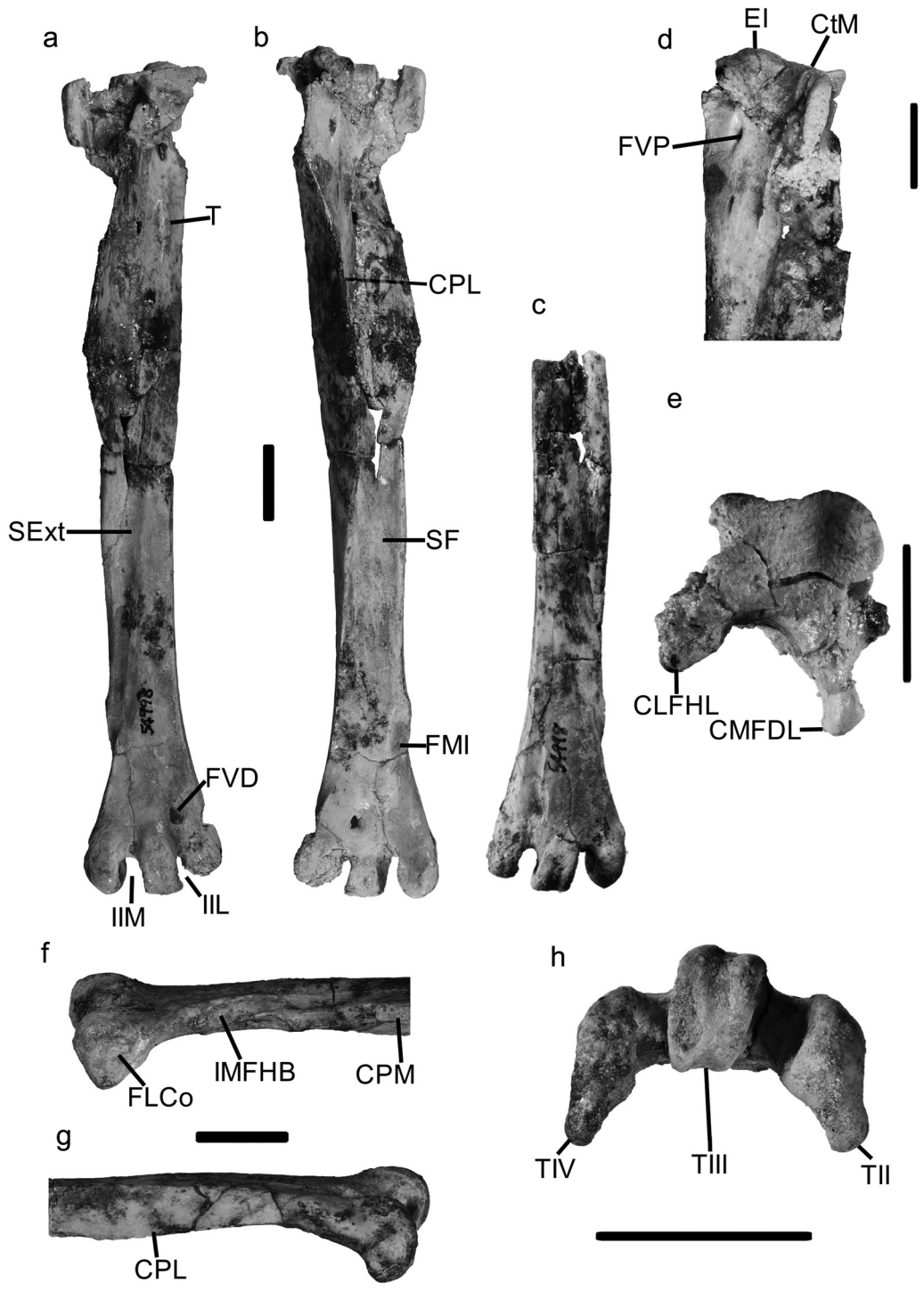

Figure 9. Tarsometatarsi of *Archaehierax sylvestris* gen. et. sp. nov. SAMA P.54998, left in dorsal (A), plantar (B), proximal end plantar (D) and proximal E) view, and distal right in dorsal (C), medial (F), lateral (G), and distal (H) view. Abbreviations: CLFHL, crista lateralis flexoris hallucis longus; CtM, cotyla medialis; CMFDL, crista medialis flexoris digitorum longus; CPL, crista plantares lateralis; CPM, crista plantares medialis; EI, eminentia intercotylaris; FLCo, fovea ligamentosa collateralis; FMI, fossa metatarsi I; FVD, foramen vasculare distale; FVP, foramen vasculare proximale; IIL, incisura intertrochlearis; IIM, incisura intertrochlearis medialis; IMFHB, incisura musculus flexor hallucis brevis; SExt, sulcus extensorius; SF, sulcus flexorius; T, tuberculum; TII, trochlea metatarsi II; TIII, trochlea metatarsi III; TIV, trochlea metatarsi IV. Scale bars 10 mm.

(4) The eminentia intercotylaris (Figure 9D: EI) projects a few millimetres proximally to the rim of the cotyla medialis. **(5)** The crista lateralis flexoris hallucis longus (sensu Mayr 2016) (lateral hypotarsal crista) and the crista medialis flexoris digitorum longus (medial hypotarsal crista) (Figure 9E: CMFDL) are not fused together plantarly, and so form a wide monosulcate hypotarsus. **(6)** The medial hypotarsal crista is distinctly proximodistally longer (8.9 mm from proximal margin to distal hook, 11.4 mm from proximal margin to distal termination point) than the lateral hypotarsal crista (6.0 mm). **(7)** The plantar depth of the lateral hypotarsal crista is 13.6 mm (76%) of

the depth of the medial hypotarsal crista 17.8 mm. **(8)** In medial view, the medial hypotarsal crista has little or no hook distally. **(9)** The sulcus flexorius (Figure 9B: SF) is moderately deep, with the cristae plantares lateralis and medialis quite distinct and projecting plantarly. **(10)** The tuberositas m. cranialis (Figure 9A: T) is positioned towards the lateral side of the shaft, moderately projects dorsally to the adjacent latero-dorsal margin, **(11)** is short and oval shaped, **(12)** and is positioned well distal (5.2 mm) of the lateral foramina vascularia proximalia. **(13)** The impressio retinaculi extensorii, preserved on the dislocated cotyla medialis, are a pair of distinctly projecting cristae, with the retinaculum itself unossified, which is the typical state among the accipitrids. **(14)** The fossa infracotylaris dorsalis is shallow in the undamaged section distal to the eminentia intercotylaris and towards the retinaculi. **(15)** There is a distinct sulcus extensorius (Figure 9A: SExt) at mid-length, which opens to the medial face around two-thirds of the distance distally along the shaft. **(16)** The medial half of the proximal 40% of the shaft is highly compressed as it is in many accipitrids, forming a crista 1.3 mm thick. **(17)** The crista plantaris lateralis (Figure 9G: CPL) is well-developed, extending from the hypotarsus to level with the fossa metatarsi I. **(18)** In lateral aspect the crista plantaris lateralis is markedly projecting plantarly, deepest just proximal to mid-length. **(19)** The foramen vasculare distale (Figure 9A: FVD) has a diameter of about 1.6 mm and is positioned close to the incisura intertrochlearis lateralis. **(20)** The fossa metatarsi I (Figure 9B: FMI) is set largely on the plantar face, though partially faces medially, and measures 6.7 mm long by 3.5 mm wide. **(21)** The incisura m. flexor hallucis brevis (Figure 9F: IMFHB) is very distinct, passing dorsally above and distal to the fossa metatarsi I, to open plantarly between the facet in metatarsi I and trochlea metatarsi II. This state of the incisura was rarely seen in our comparative sample, with a similar but shallower incisura in species of *Haliaeetus* and *Harpia harpyja* (slightly deeper) that ends just proximal to the fossa metatarsi I. **(22)** The fossa supratrochlearis plantaris is very shallow. **(23)** The incisura intertrochlearis medialis (Figure 9A: IIM) and incisura intertrochlearis lateralis (Figure 9A: IIL) are extremely wide compared to in other Accipitridae. **(24)** From distal view, the trochleae are arched dorsally. All trochleae are higher than they are wide (excluding extension from flanges). **(25)** The plantar extent of trochleae metatarsorum II (Figure 9H: TII) and IV are almost identical (9.1 mm and 9.5 mm respectively, measured from right specimen). **(26)** Trochlea metatarsi III (Figure 9H: TIII) is located comparatively much higher dorsally, and while it has a depth of 7.7 mm, the plantar-most point of it is separated from that of trochlea metatarsi IV by about 6.6 mm. **(27)** Trochlea metatarsi II has a robust profile in distal view, with a short, robust plantar projection on its outer margin and a deep fovea ligamentosa collateralis. **(28)** Trochlea metatarsi III has a robust profile in distal view and has a shallow medial groove dorsodistally. **(29)** Trochlea metatarsi III is laterally directed relative to the shaft axis. **(30)** Trochlea metatarsi IV is the narrowest of the trochleae in distal view, with a short, thin plantar projection on the lateral margin. **(31)** The flange on trochlea metatarsi II is moderately projecting plantarly, **(32)** while the flange on trochlea metatarsi IV is quite prominent and plantar oriented. **(33)** The distal extent of the trochleae metatarsorum II and III is roughly equal and surpass distally the distal margin of IV.

Extant accipitrids differ across all subfamilies as follows:

(9) The sulcus flexorius is shallower, with the cristae plantares lateralis and medialis relatively low in elanines, gypaetines, circaetines, haliaeetines, and buteonines. **(21)** The incisura m. flexor hallucis brevis is shallower and shorter ending at or proximal to the fossa metatarsi I in all observed species. **(23)** In all subfamilies, the incisura intertrochleae are relatively narrower and the autapomorphically wide incisura in the fossil is one of its most characteristic features.

The tarsometatarsus is overall most similar to that of species of Elaninae (although more elongate), Aquilinae and Circaetinae (see SI.2 for more detailed differential comparisons).

Digit I (Figure 10A)

The os metatarsale I in SAMA P.54998 is fairly robust, with the proximal end attenuated to a thin point. In dorsal and plantar view, the region immediately proximal to the medial side of the articular surface for I.1 is inflated, creating a > 90° angle just distal of the mid-length point along the 'shaft'. The attachment facet for the tarsometatarsus is quite long, extending to be adjacent with the previously mentioned inflation, but is not prominent in lateral view. The sulcus for a tendon on the distal dorsal face is bordered by a reduced crest that is positioned slightly medial of centre in the metatarsal. The phalanx I.1 is long and moderately robust, with the enlarged proximal end much wider than the corpus. Plantarly, the tubercula flexoria are enlarged, enclosing a broad sulcus that extends as a shallow attachment point to roughly midway on the corpus distally. The lateral side of the face dorsalis of the proximal end is slightly inflated into a ligamental attachment point, forming a modest, rounded mound. The foveae lig. collaterales on the distal end are very deep, and there is only a very shallow indentation set between the two foveae on the dorsal face. The ungual phalanx I.2 (as seen in right side) is slightly larger than the ungual phalanx II.3, with mild curvature along the ungual phalanx. The phalanx I.1 and ungual I.2 exhibit notable hypertrophy in contrast to digits III and IV, a trait that is present in almost all Accipitridae (Fowler et al. 2009).

Digit II (Figure 10B)

Like most accipitrids, there is no fusion of the phalanges II.1 and II.3. The species in Haliaeetinae and *Ictinia* are notable for such fusion (see Jollie 1976). The phalanx II.1 is quite short compared to phalanx II.2, being just under half its length and considerably shortened lengthwise (not compressed lateromedially), which is a common trait in Accipitridae. All phalanges are notably hypertrophied compared to those in digits III and IV.

Digit III (Figure 10C)

Four phalanges are present. The medial face of the ungual phalanx (III.4) lacks the central ridge present in most accipitrids and falconids, though it is possibly that this feature has been poorly preserved.

Digit IV (Figure 10D)

The midshaft width of phalanx IV.4 is 3.2 mm, compared to the 3.8 mm of phalanx I, and the distal end of phalanx IV.4 is distinctly widened, measuring 4.6 mm. This dramatic shift in width along the digit does not appear in the sampled elanine genera (*Elanus, Gampsonyx*), species of *Hieraaetus* (though the section before the articular end is swollen) or *Spizaetus*, but appears to a lesser degree in the pernines, gypaetines, circaetines, aegypiines, species of *Aquila*, and species of *Haliaeetus*.

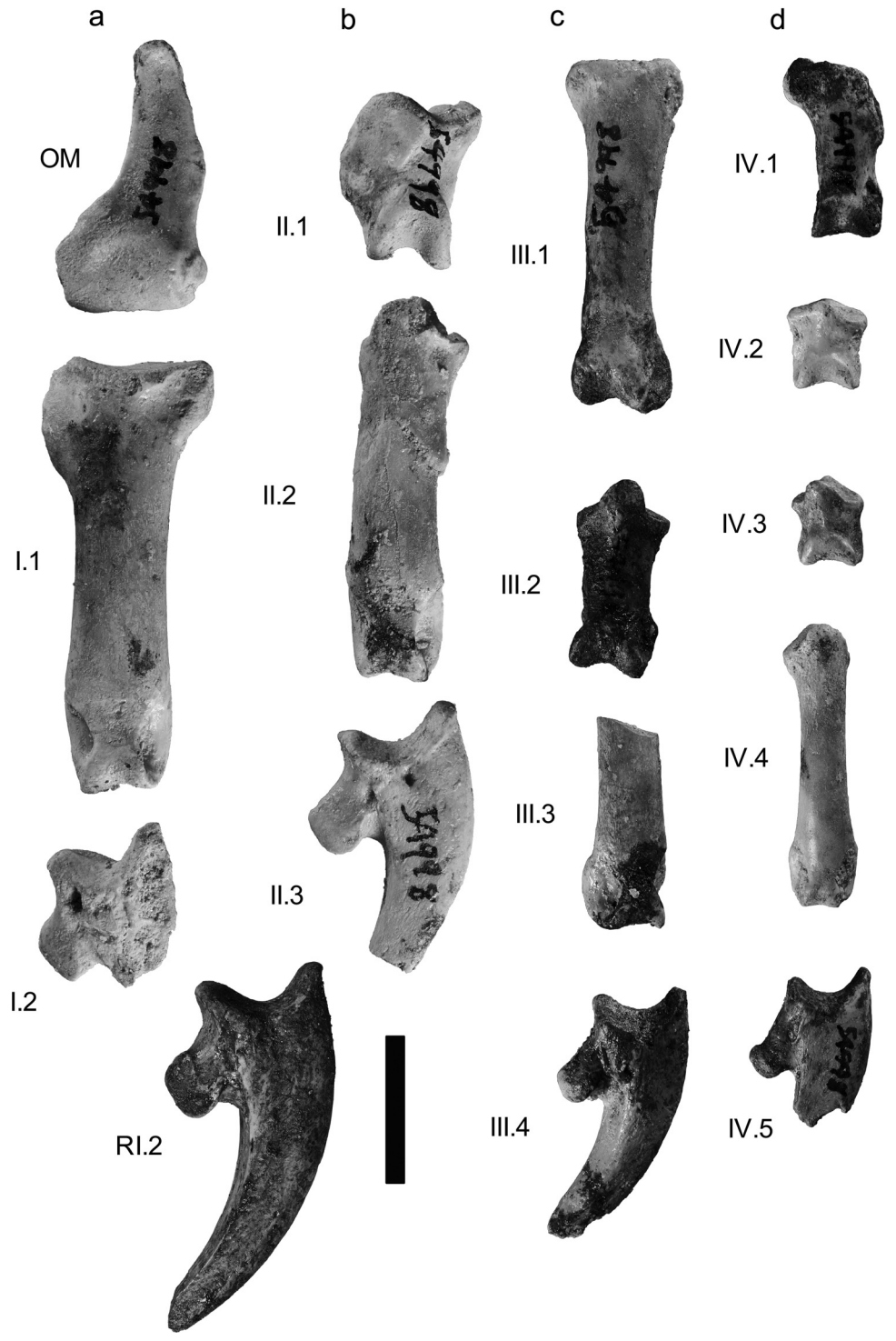

Figure 10. Image showing left pedal phalanges and os metatarsale 1 of *Archaehierax sylvestris* gen. et. sp. nov. SAMA P.54998, digit 1 (A), digit 2 (B), digit 3 (C) and digit 4 (D) with RI.2 added given the left counterpart was broken. Scale bar 10 mm.

Summary

Archaehierax sylvestris shares a mosaic of characters across a broad range of taxa and thus the above comparisons do not reveal clear affinity with any one taxon. Different elements in the fossil skeleton differ markedly as to which subfamilies they most closely resemble: the rostrum maxillare – buteonines; the quadrate – aegypiines; the vertebrae – elanines; the sternum – aegypiines; the coracoid – aegypiines, accipitrines, and buteonines; the scapula – elanines; the humerus – elanines, aegypiines, aquilines, haliaeetines and buteonines; the ulna – circaetines; the os carpi radiale – elanines and buteonines; the os carpi ulnare - elanines, pernines, gypaetines and aquilines; the carpometacarpus - buteonines; the tibiotarsus –

buteonines; and the tarsometatarsus – elanines (fossil is more elongate), aquilines and circaetines. There are several autapomorphies which further differentiate it from all extant subfamilies. Notably these include the sternal basin having a medial bar separating deep pneumatic fossae, humerus with very low proximal projection of the caput, and tarsometatarsus with broad incisurae intertrochleae and the incisura for the m. flexor hallucis brevis tendon extending distal to the fossa metatarsi I. Together, these support differentiation of this taxon with separate subfamilial status, consistent with the phylogenetic results discussed below.

Comparison with fossil accipitrids

Australia has only two described pre-Pleistocene accipitrids. *Pengana robertbolesi* is from Sticky Beak Site in the Riversleigh World Heritage Area, of ? Late Oligocene – Early Miocene age, which is now considered one of the Faunal Zone A sites (Travouillon et al. 2006) that on biochronological grounds are slightly younger than the Pinpa LF (Woodhead et al. 2016). It is represented by a distal tibiotarsus (Boles 1993), and while of similar size, is easily distinguished from *Archaehierax sylvestris* by the following characters: the distal margin of the pons supratendineus is angled less steeply, ~30° relative to the long axis; the condyles have flattened sides in cranial aspect and are not medially and laterally expanded relative to the distal end of the shaft. *Aquila bullockensis* from the mid-Miocene Camfield Beds (12 Ma) of Bullock Creek (Gaff and Boles 2010; Megirian et al. 2010) was described from a distal humerus – which was not preserved in *Archaehierax sylvestris*. However, *A. bullockensis* is very much (>10 Ma) younger than *Archaehierax sylvestris*, much larger, and the morphology of the distal humerus was interpreted to be typical of species of *Aquila*. *Archaehierax sylvestris* has many features on other bone elements that exclude close affinity with both *Aquila* and the Aquilinae, so conspecificity with *A. bullockensis* can be ruled out.

In relation to Oligocene-age fossil accipitrids from elsewhere in the world, the geographic isolation of Australia makes it unlikely that any described species are closely related to *Archaehierax sylvestris*. As reviewed in the Introduction, most late Oligocene and early Miocene accipitrid species are found in North America and Europe. Nearly all of them are described from a single skeletal element, making assessment of relationships with *Archaehierax sylvestris* difficult. The late Oligocene – early Miocene accipitrids from North America, including the relatively complete *Palaeoplancus sternbergi*, are all easily distinguished from *Archaehierax sylvestris* by size, and by morphology of the distal tarsometatarsus; specifically, trochlea metatarsi II is relatively broader and/or the intertrochlear incisions are much narrower.

Four Oligocene fossil accipitrids are described from Europe, all but one of which is based on a single bone:

Aquilavus hypogaea (Milne-Edwards, 1892), from the Quercy fissure fillings, is incomparable as it is based on a femur.

Aquilavus corroyi (Gaillard, 1939), also from Quercy fissure fillings, was described from a tarsometatarsus that resembles *Milvus* according to Mayr (2009). It lacks the wide incisura intertrochleae of *Archaehierax sylvestris*, and the flange on the trochlea metatarsi II is oriented more medially (Gaillard 1939, Figure 1).

Palaeohierax gervaisii (Milne-Edwards, 1863), late Oligocene France, is described from a tarsometatarsus and is larger than *'A.' corroyi*. Compared to *Archaehierax sylvestris*, the incisura intertrochleae are narrow and the flange on trochlea metatarsi II is oriented more medially (Milne-Edwards 1863, Plate 183, Figures 1-10).

Aviraptor longicrus Mayr and Hurum, 2020, of early Oligocene age from Poland, is described from a complete skeleton. It is a very small accipitrid with highly elongate legs like those seen in species of Accipitrinae, which clearly distinguishes it from *Archaehierax sylvestris*.

There are two Middle Oligocene species from Mongolia; *Buteo circoides* Kurochkin, 1968 (distal ulna), and *Venerator* ('*Tutor*') *dementjevi* (Kurochkin, 1968) (distal humerus). Only *B. circoides* can be directly compared to *Archaehierax sylvestris*, with images indicating the tuberculum carpale is less prominent of the ventral condyle, and the ventral condyle has greater distal extent than the dorsal condyle (Kurochkin 1968,Figure 1).

Three fossil accipitrids are known from early Miocene deposits of Europe;

Promilio incertus (Gaillard, 1939) was described from a right tarsometatarsus from Chavroches, France, which lacks the wide incisura of *Archaehierax sylvestris*, the flange on the trochlea metatarsi II is oriented more medially, and the hypotarsal crests are of roughly equal craniocaudal depth (Gaillard 1939, Figure 9).

Aquilavus priscus (Milne-Edwards, 1863), described from a tarsometatarsus, tibiotarsus and carpometacarpus, is from Auvergne, France. It is larger than *P. gervaisii*. Compared to *Archaehierax sylvestris*, the incisura intertrochleae are narrow and the flange on trochlea metatarsi II is oriented more medially (Milne-Edwards 1863, Plate 184, Figures 1-4). On the carpometacarpus, the os metacarpale minus is flat, the processus alularis is less distinct from the distal processus extensorius, and the facies articularis digitalis major has less distal extent than the facies articularis digitalis minor (Milne-Edwards 1863, Plate 184, Figures 14-16). The tibiotarsus seems to lack a distinct scar or rugosity for the distal retinaculum extensorium (Milne-Edwards 1863, Plate 184, Figures 11-13).

Aquilavus depredator (Milne-Edwards, 1871), described from a tarsometatarsus, is from Saint-Gérand le Puy, France. Compared to *Archaehierax sylvestris*, the incisura intertrochleae are narrow and the flange on trochlea metatarsi II is oriented more medially (Milne-Edwards 1871, Plate 183 Figures 11-14; Plate 184, Figures 5-10).

The middle Miocene accipitrids from Asia are all aegypiine vultures (Hou et al. 2000; Zhang et al. 2010, 2012; Li et al. 2016) and so are not closely related (see phylogenetic analysis below).

Family Accipitridae Vigors, 1824
Subfamily indet. Gen. et sp. indet.

Material

Distal right humeral fragment, preserving a relatively unworn distal end and 16.2 mm of shaft, and some associated fragments of the shaft, SAMA P.58917.

Measurements (mm)

Distal width 15.4, least shaft width 8.3, total depth 8.5, condylus dorsalis depth 8.3, condylus dorsalis width 5.2, condylus ventralis depth 5.1, condylus ventralis width 7.3, epicondylus ventralis depth 7.0.

Locality, stratigraphy and age

31° 07.568′ S; 140° 12.737′ E. Site 11, Lake Pinpa, Frome Downs Station, South Australia, Namba Formation, Pinpa LF, late Oligocene. Collected by A. Camens, T. Worthy and W. Handley, 24–26 September 2015.

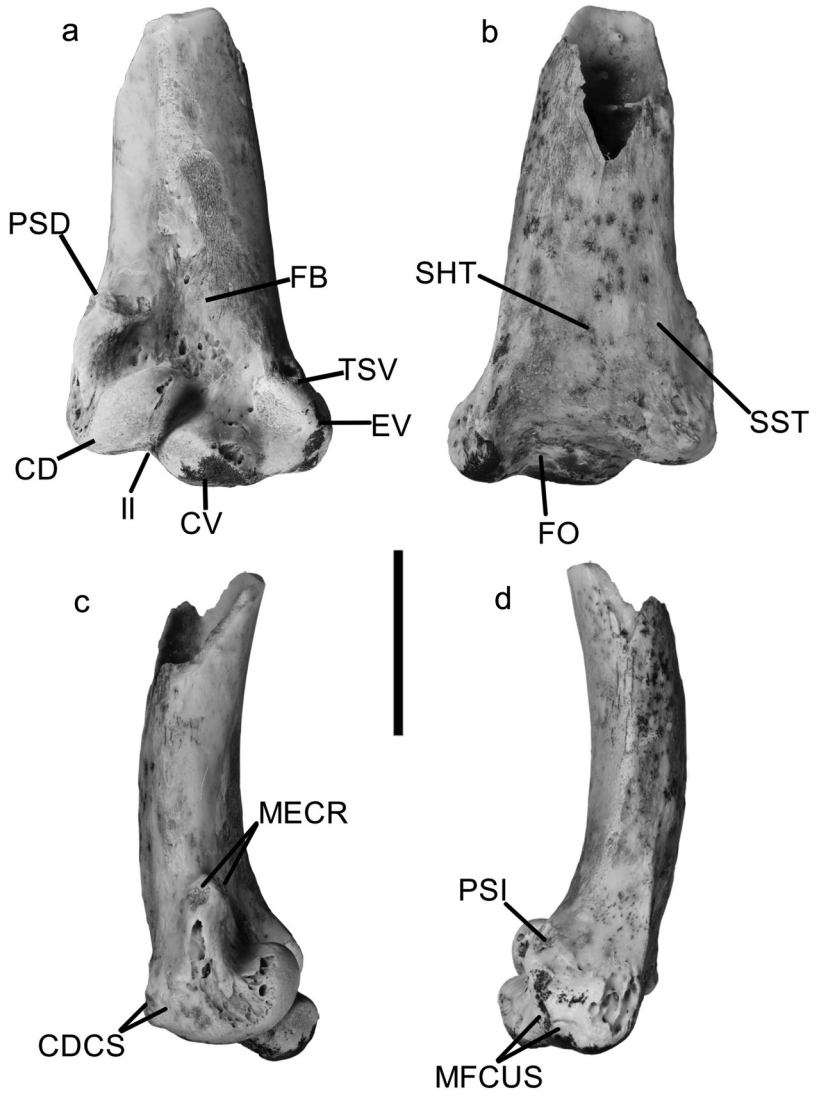

Figure 11. Accipitrid distal right humerus SAMA P.58917 in cranial (A), caudal (B), dorsal (C) and ventral (D) view. Abbreviations: CD, condylus dorsalis; CDCS, condylus dorsalis caudal scars; CV, condylus ventralis; EV, epicondylus ventralis; FB, fossa brachialis; FO, fossa olecrani; II, incisura intercondylaris; MECR, m. extensor carpi radialis insertion scars; MFCUS, musculus flexor carpi ulnaris scars; PF, processus flexorius; PSD, tuberculum supracondylare dorsale; PSI, pronator superficialis insertion; SHT, sulcus humerotricipitalis; SST, sulcus scapulotricipitalis; TSV, tuberculum supracondylare ventrale. Scale bar 10 mm.

Remarks

The fossil can be excluded from other raptor families on the following features:

Falconidae (falconid state in brackets): the condylus dorsalis is thickened and rounded distally (consistently narrow and rectangular); the processus flexorius ends proximal to the condylus ventralis (equidistant).

Pandionidae (state for *Pandion haliaetus* in brackets): a shallow fossa m. brachialis (deep); a flat epicondylus dorsalis (prominently projecting); a flat epicondylus ventralis (prominent); the fossa olecrani is shallow (deep); the sulcus scapulotricipitalis is shallow (deep).

Cathartidae (cathartid state in brackets): a shallow fossa m. brachialis (deep); a lack of pneumatisation in the fossa m. brachialis (present); a flat epicondylus ventralis (prominent).

Sagittariidae (sagittariid state in brackets): the two fossae marking the attachment points for the lig. collaterale dorsale are positioned roughly adjacent to each other (cranial-most fossa slightly proximal to and abutting caudal fossa in sagittariids).

The fossil is broadly similar to accipitrids and displays the following features: **(1)** The tuberculum supracondylare dorsale (Figure 11A: PSD) is located well-proximal to the condylus dorsalis (Figure 11A: CD) and is small, barely projecting dorsally of the shaft, but projects slightly cranially as a proximodistally elongate rugosity; **(2)** the dorsal face/shaft margin between the tuberculum supracondylare dorsale and the epicondylus dorsalis is mildly inflated; Two shallow scars for the m. extensor carpi radialis are present on the tuberculum supracondylare dorsale (Figure 11C: MECR), **(3)** the larger palmar attachment scar on the cranial face adjacent to the dorsal margin is oval **(4)** and the smaller dorsal scar is located on the dorsal face of the processus. **(5)** In caudal view, the processus flexorius (Figure 11: PF) terminates proximal to the condylus ventralis (Figure 11A: CV) but is prominent ventrally. **(6)** The sulcus scapulotricipitalis (Figure 11B: SST) forms a shallow but broad notch roughly 2 mm wide on the caudal face. **(7)** The fossa olecrani (Figure 11B: FO) is moderately deep, defining well the dorsal margin to the processus flexorius but does not create a discontinuity with the sulcus humerotricipitalis. **(8)** The sulcus humerotricipitalis (Figure 11B: SHT) is very shallow, and at 5.3 mm wide extends over half of shaft width of 9.7 mm at the same point. **(9)** The fossa m. brachialis (Figure 11A: FB) is shallow but distinct, with a proximodistal length of 13.8 mm extending well proximal to the tuberculum supracondylare dorsale, and a maximum dorsoventral width of 7.3 mm level with the proximal margin of the

tuberculum supracondylare dorsale. In contrast, the shaft width measures 10.1 mm at the same point. Within the fossa, the impressio m. brachialis is slightly deeper. **(10)** The fossa is well separated (3 mm) from the dorsal margin of the shaft. **(11)** The epicondylus ventralis (Figure 11A: EV) is indistinct from the ventral margin and does not project ventrally past the processus flexorius. **(12)** A single distinct, shallow insertion scar is present on the ventrodistal section of the epicondylus ventralis, with a very faint and shallow second insertion ventrally adjacent to it. These insertions serve as the attachment point for the m. flexor carpi ulnaris. **(13)** The tuberculum supracondylare ventrale (Figure 11A: TSV) projects cranially but not ventrally from the shaft. **(14)** A shallow insertion scar for the pronator superficialis is present just proximal to the tuberculum on the dorsal face. **(15)** The condylus dorsalis (Figure 11A: CD) is 5.9 mm proximodistally long, 4.7 mm dorsoventrally wide and 8.6 mm craniocaudally deep. **(16)** Two small, very shallow insertion scars are present on the caudal section of the dorsal face of the condylus dorsalis by the distal margin (Figure 11C: CDCS), directly craniocaudally adjacent to each other. **(17)** The condylus ventralis is 4.5 mm proximodistally long, 7.3 mm dorsoventrally wide and 5 mm craniocaudally deep. **(18)** The condylus dorsalis is separated by a distinct notch from and set well proximal to the distal margin of the condylus ventralis in cranial view. **(19)** The incisura intercondylaris (Figure 11: II) is narrow, roughly 1.1 mm wide, but distinct. **(20)** The processus flexorius is surpassed distally by the condylus ventralis in caudal view, and strongly projects ventrally in caudal view. **(21)** The ventral margin of the condylus ventralis is not separated by a notch from the processus flexorius in cranial view.

Extant accipitrids differ as follows: **(Trait 1)** The tuberculum supracondylare dorsale projects much further dorsally in all subfamilies and species except *Pernis apivorus* (Perninae), *Polyboroides typus* (Gypaetinae, non-projecting), Aquilinae, Accipitrinae and species of *Buteo* (Buteoninae). **(16)** The insertion scars towards the caudal margin of the condylus dorsalis are both deep in all subfamilies except Elaninae and Accipitrinae, with the latter having the cranial-most insertion being shallow and the caudal-most deep.

The fossil has the most similarities to species from the subfamily Elaninae (see SI.2 for more detailed differential comparisons), but differs markedly in regards to the inflation of the dorsal face between the tuberculum supracondylare dorsale and the epicondylus dorsalis, the size and shape of the palmar and dorsal attachment scars for the m. extensor carpi radialis, the distinct depression in the section of dorsal face caudal to the tuberculum supracondylaris and the epicondylus dorsalis, the sulcus humerotricipitalis width, the fossa m. brachialis length, the configuration of the insertion scars on the distal epicondylus ventralis, the position of the distal margin of the condylus dorsalis relative to that of the condylus ventralis in cranial view, the ventral projection of the processus flexorius, and the connectivity of the condylus ventralis and entepicondyle in cranial view.

As the *Archaehierax sylvestris* specimen SAMA P.54998 lacks a preserved distal humerus, it cannot be compared to SAMA P.58917. However, it is not believed to belong to the same species due to the significantly smaller size of SAMA P.58917 from the humerus size predicted for SAMA P.54998 (see comparative measurements below).

Family Accipitridae Vigors, 1824
Subfamily indet. Gen. et sp. indet.

Material

NMV P.222435, distal left femur preserving intact distal end and 15.5 mm of shaft.

Measurements (mm)

Preserved length 26, DW 13.3, least SW 7.3, preserved condylus medialis depth 9.7, condylus medialis width 5.6, condylus lateralis depth 11.0, condylus lateralis width 6.1.

Locality, stratigraphy and age

31° 11.237'S 140° 13.944'E Ericmas Quarry, Lake Namba, Frome Downs Station, South Australia, Namba Formation, Ericmas LF, late Oligocene. Collected by T. Flannery, 7/4/83.

Remarks

The specimen can be excluded from the Pandionidae and Cathartidae by the presence of a single muscular attachment on the planum popliteum, and from Falconidae and Sagittariidae by the linea intermuscularis caudalis remaining level and visible on the medial margin of the caudal face.

The femur is consistent with accipitrids and has the following morphology.

(Trait 1) The linea intermuscularis caudalis (Figure 12C: LIC) is highly distinct, running along the medial border of the caudal shaft face in a raised line, **(2)** but is not continuous with the tuberculum m. gastrocnemialis medialis, so there is no crista supracondylaris medialis. **(3)** The secondary origin point for the ligamentum collateralis lateralis is very faint and shallow, barely distinct from the surface of the bone. **(4)** The fovea tendineus m. tibialis cranialis is shallow. **(5)** The fossa poplitea (Figure 12B: FPop) is shallow, deepening slightly towards the distal end immediately proximal to the condyles. **(6)** The attachment scar on the planum popliteum (Figure 12B: PPAP) is positioned medially. **(7)** The impressio m. gastrocnemialis lateralis (Figure 12D: IG) is large and shallow. **(8)** The epicondylus lateralis (Figure 12A: EL) is short and very robust but has little projection from the condylus lateralis.

The distal femur NMV P.222435 is from an accipitrid which exhibits the most similarity to those of species in Buteoninae, Aegypiinae, and most of Elaninae (see SI.2 for more detailed differential comparisons). It mainly differs from species in these subfamilies in lacking a prominent crista supracondylaris medialis, the position and shape of the attachment point on the planum popliteum, and the weak projection of the epicondylaris lateralis.

As the distal femur is not a highly diagnostic section of the accipitrid skeleton, and the distal femur is not preserved in *Archaehierax sylvestris* specimen SAMA P.54998, NMV P.222435 is regarded as gen. et. sp. indet. The size difference between NMV P.222435 and the predicted size of the distal femur of SAMA P.54998 is greater than would be predicted from typical sexual dimorphism, which makes it unlikely the two are representatives of the same species (see comparative measurements below).

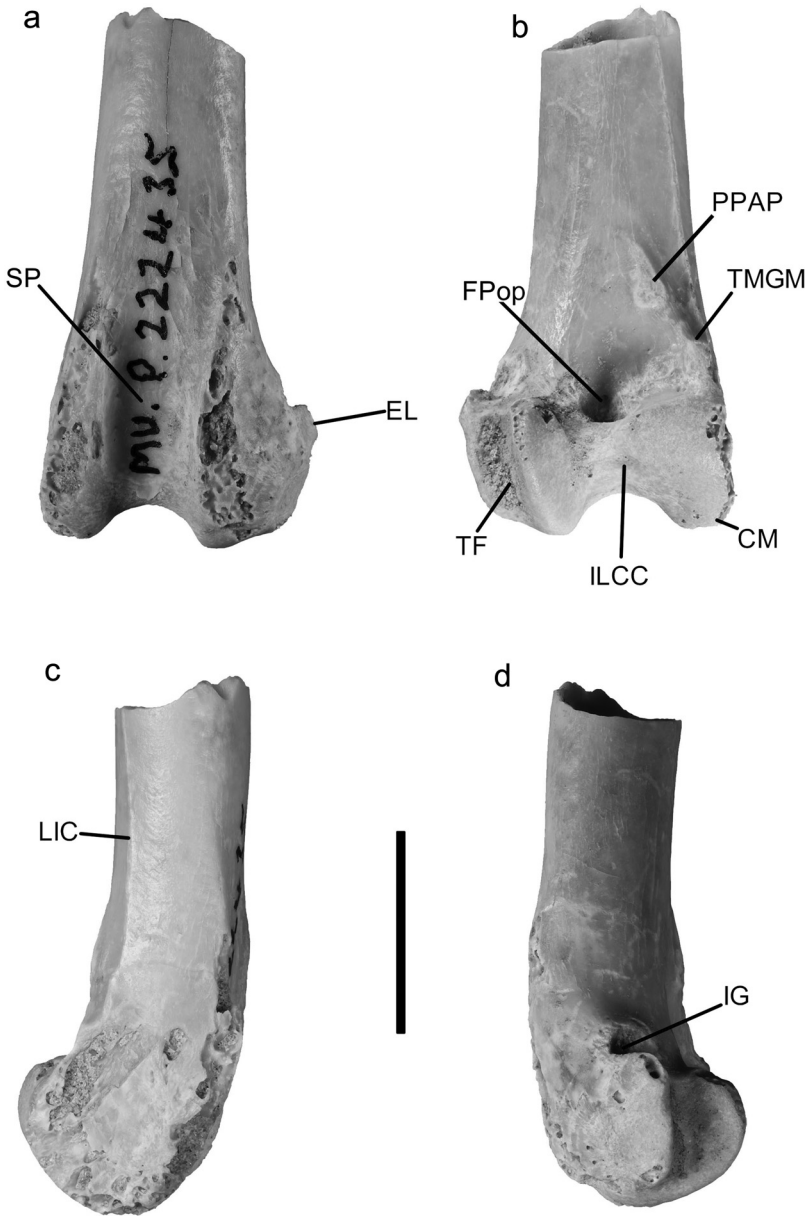

Figure 12. Distal left femur NMV P.222435 depicted in cranial (A), caudal (B), medial (C) and lateral (D) view. Abbreviations: CM, condylus medialis; EL, epicondylus lateralis; FPop, fossa poplitea; IG, impressio m. gastrocnemialis lateralis; ILCC, impressio lig. cruciati cranialis; LIC, linea intermuscularis caudalis; PPAP, planum popliteum attachment point; SP, sulcus patellaris; TF, trochlea fibularis; TMGM, tuberculum muscularis gastrocnemialis medialis. Scale bar 10 mm.

Size comparisons of the three fossils

The width measurements of the proximal humerus, distal humerus, distal tibiotarsus and distal femur of extant taxa were compared (see Appendix 1, Table S2) and showed that the distal width of the humerus was between 80% and 90% of the proximal width of the humerus, while the distal width of the tibiotarsus was between 75% and 110% the distal width of the femur in extant accipitrids. If the bones of *Archaehierax sylvestris* had similar ratios, then it can be predicted that the width of the missing distal humerus should fall in the range 23.4–26.4 mm, while that of the missing distal femur should be between 15.8 and 22.0 mm broad. Based on this, both the isolated distal femur NMV P222435 and the isolated distal humerus SAMA P.58917 are too small to belong to an individual the size of the *A. sylvestris* holotype. However, sexual dimorphism is known to be considerable and common in accipitrids (Brown and Amadon 1968; Marchant and Higgins 1993) and raises the possibility that these isolated fossils may belong to a smaller sex of the one species if they fall within a certain size range. Field et al. (2013) devised multiple algorithms for predicting body mass from skeletal measurements, while Campbell and Marcus (1992) predicted body mass based on the femur and tibiotarsus circumference. Using these, the mass of the bird for the *Archaehierax sylvestris* holotype is estimated as 3.7 kg based on the length of the coracoid facies articularis humeralis, 4.6 kg by the least shaft diameter/width of the tarsometatarsus, and 3.2 kg based on tibiotarsus least shaft circumference. The mass of the bird represented by the distal femur is calculated at 2 kg based on femur shaft width/diameter, or 1.6 kg based on shaft circumference. The mass of the bird represented by the distal humerus is calculated at 1.5 kg based on shaft width/diameter, or 1.6 kg based on circumference. Assuming these predictions are accurate, the femur represents a bird 46–67% smaller than the skeleton specimen, and the humerus one 60–67% smaller. This would be pushing accipitrid sexual dimorphism to its extreme limits, making it unlikely that the fossils represent a single species.

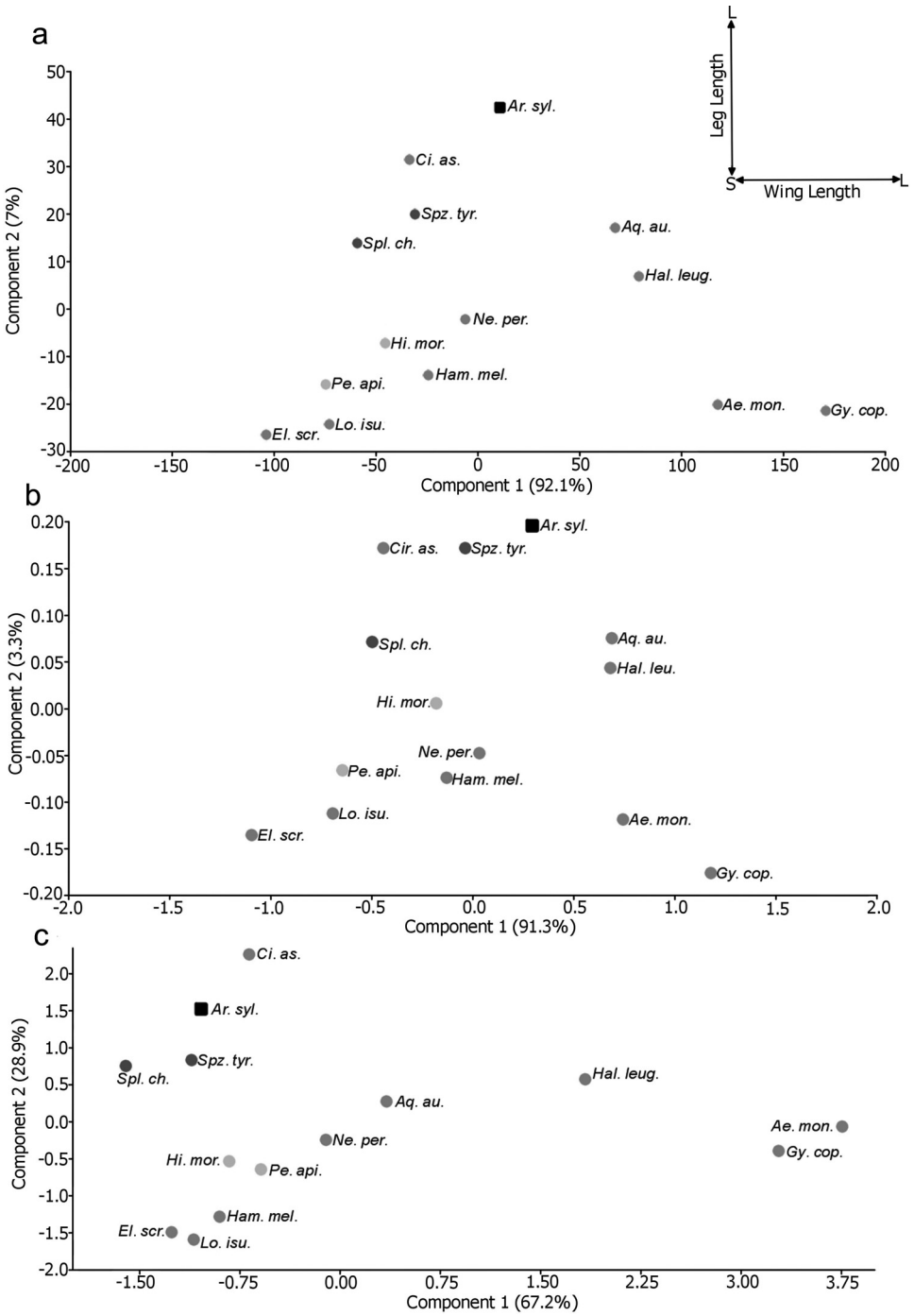

Figure 13. PCA plots using length measurements of the carpometacarpus, ulna, humerus, tibiotarsus, tarsometatarsus, pedal digit 1 and pedal digit 2 treated in three ways. (A) Absolute data, (B) log-transformed data, (C) size standardised data with variables proportional to quadrate height. Directional arrows at top right indicate directionality of limb length (S, short and L, long) along the PC axes. Note: axes in A and B have been scaled for better visualisation, so 2D distances do not represent true 2D distances in PCA space. Abbreviations: *Ae. mon., Aegypius monachus; Ar. syl., Archaehierax sylvestris; Aq. au., Aquila audax; Ci. as., Circus assimilis; El. scr., Elanus scriptus; Gy. cop., Gyps coprotheres; Ham. mel., Hamirostra melanosternon; Hal. leug., Haliaeetus leucogaster; Hi. mor., Hieraaetus morphnoides; Lo. isu., Lophoictinia isura; Ne. per., Neophron percnopterus; Pe. api., Pernis apivorus; Spl. ch., Spilornis cheela; Spz. tyr., Spizaetus tyrannus*. Dark green, forested habitat; light green, woodland/open forest; orange, open habitat (grassland, savannah etc.). Fossil (*Archaehierax*) indicated by black square.

However, these mass predictions use different elements, limiting their comparability. Nevertheless, while considering it likely that at least two accipitrids are represented, we consider it unwise to describe the smaller as a second species when size would be the only distinguishing factor and their congeneric status cannot be assessed.

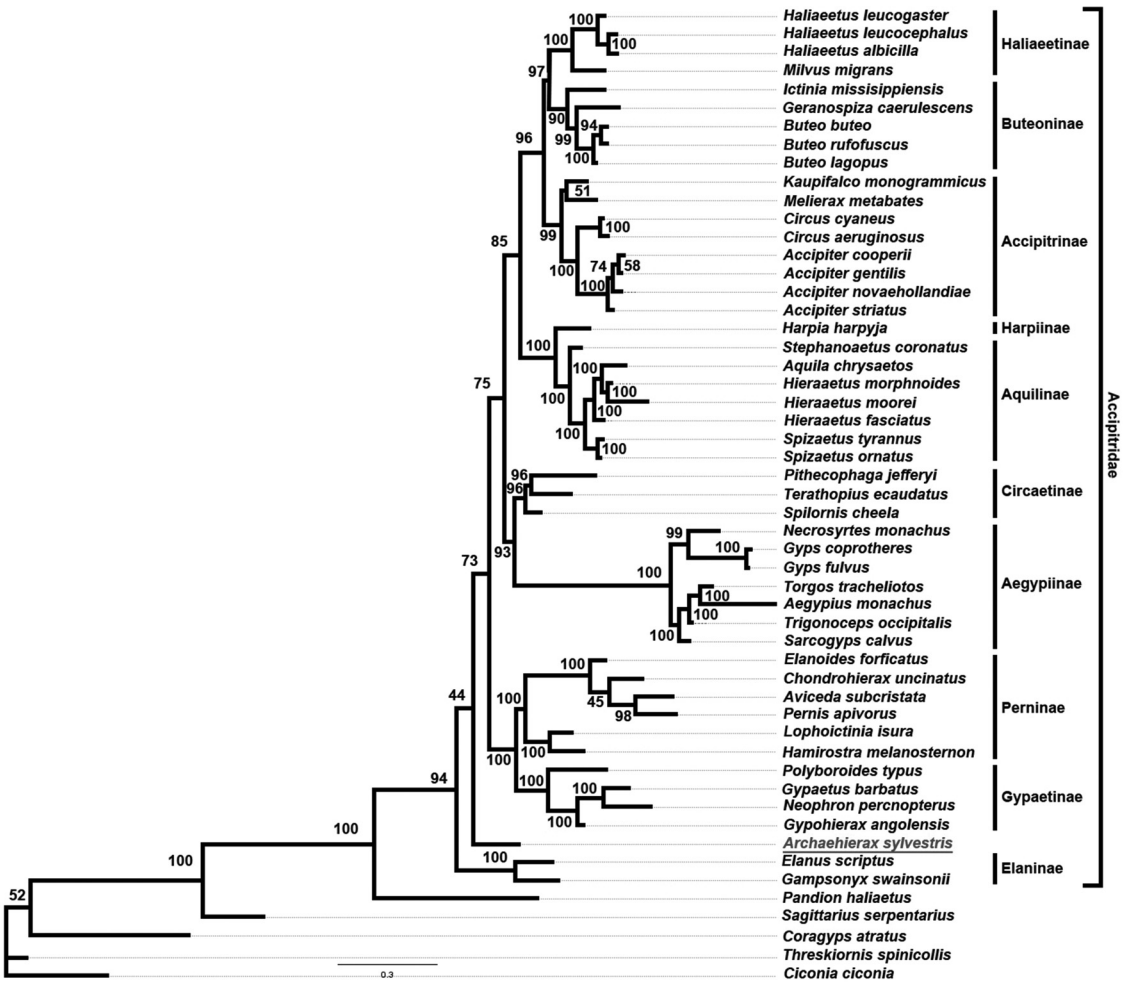

Figure 14. Analysis 4a: combined molecular and morphological data (ordered) analysed with Bayesian methods; molecular and morphological partition branch lengths unlinked. Node values show posterior probability.

PCA analysis of limb measurements

Length data for a range of post cranial measurements were visualised in PCA plots to determine if there was any correlation between them and preferred habitat. All PCAs used a variance-covariance matrix, iterative imputation for missing data (in the case of I.2 length of *Gyps coprotheres*), and 1000 bootstrap replicates. See Appendix 2 for datasets, scree plots, biplots, PCA values.

The first PCA used absolute length measurements of the carpometacarpus, ulna, tibiotarsus, tarsometatarsus, pedal digit 1 and pedal digit 2 (Figure 13A). In the resulting scatterplot PC1 (92.1% variance) was most strongly driven by the ulna, with some influence from the carpometacarpus (wings), the tarsometatarsus and tibiotarsus and PC2 (7% variance) by the tarsometatarsus and tibiotarsus (legs). *Archaehierax sylvestris* was positioned as a long-legged, short-winged taxon, well separated from other species. Both *Spizaetus tyrannus* and *Spilornis cheela* grouped closely together, creating a cluster for forest-habitat accipitrids. *Circus assimilis*, which inhabits grassland and open woodland, was positioned intermediate between *Archaehierax sylvestris* and the forest taxa.

A second PCA was run after log-transforming the measurements. In the resulting scatterplot (Figure 13B) PC1 (91.4% variance), was driven by almost all measurements, with those of the tibiotarsus and tarsometatarsus having slightly more influence than those of the wings and digits, and PC2 (3.3% variance) revealed that species were separated most strongly based on the tarsometatarsus length, with lesser influence from the digit lengths and tibiotarsus length. *Archaehierax sylvestris* grouped with the long-legged and short-winged taxa, but the distribution of the extant taxa changed. *Spizaetus tyrannus* and *Spilornis cheela* were more widely separated, with the open-habitat taxon *Circus assimilis* positioned more closely to *Spizaetus tyrannus*.

As size dominated the first two PCAs, a third PCA was performed with measurements standardised for size, by division of postcranial data by the height of the quadrate, an element which correlates strongly with skull size and therefore body size (Elzanowski et al. 2001). In the resulting scatterplot (Figure 13C), PC1 (67.2%) was most strongly driven by ulna length and to a lesser degree by carpometacarpus length, while PC2 (28.9%) was most strongly driven by tibiotarsus length and tarsometatarsus length. *Archaehierax sylvestris* occupied a more negative position on PC2 relative to *Circus assimilis* as the peak of the long-legged, short-winged taxa, and *Spizaetus* and *Spilornis* clustered together closely once more. *Archaehierax sylvestris* fell intermediate between *Circus assimilis* and the forest accipitrid cluster.

Phylogenetic analyses

We performed phylogenetic analyses of morphological data only, and combined morphological and molecular data, using parsimony and Bayesian methods. We discuss all analyses below, but have most confidence in the analyses combining morphology and molecules, in particular the unlinked Bayesian analyses, for reasons discussed at the end.

Analysis 1: Parsimony, morphology only, unordered characters

The first analysis used only morphological data, with no ordering, constraints or weighting applied to the characters. The resulting 30 most parsimonious trees (hereafter MPTs) had a tree length of 1686 steps (SI.5Figure 1). *Coragyps atratus, Ciconia ciconia, Threskiornis spinicollis*, and *Sagittarius serpentarius* were rooted as the outgroup (PP = 97%), while *Pandion* resolved as sister to Accipitridae with a support value of 97%. This is broadly concordant with independent molecular phylogenetic studies.

Within Accipitridae, the tree is less congruent with DNA trees. The Accipitridae as a family had strong support (87%) with the non-Australian Perninae resolved as the most basal clade, which was strongly supported (87%) but had species left in a polytomy.

The fossil *Archaehierax sylvestris* n. gen. et sp. resolved as a branch between the Circaetinae-Harpiinae-Aquilinae clade and all other subfamilies higher up the tree. However, support for this position was very weak (<50%).

Analysis 2: Parsimony, morphology only, ordered characters

Analysis 2 differed from Analysis 1 by ordering certain multistate characters which formed morphoclines (see SI.1). This generated four MPTs with a tree length of 1720. The resulting strict consensus tree (SI.5Figure 2) is largely the same as for analysis 1, but with the following differences. The Accipitridae resolved with strong support slightly higher than the previous analysis (PP = 88%).

The fossil *Archaehierax sylvestris* was resolved as being between the Elaninae and the Australian endemic Perninae on the phylogenetic tree, though support for this position was very weak (<50%).

Analysis 3: Parsimony, morphology and DNA, ordered characters

As the analyses based on morphology failed to resolve the taxa in a way that reflects strongly supported clades based on comprehensive molecular data, and the primary aim of the analysis was to assess how the fossil related to the well-corroborated clades of modern taxa, molecular data from six genes was added for 47 taxa (see Methods) forming a combined morphology and molecular data matrix used in Analysis 3. Parsimony analysis of this matrix produced three MPTs with a tree length of 1831 (See SI.5Figure 3).

Given the molecular data largely constrains the tree to the relationships dictated by molecular data alone, relationships were mostly the same as those in recent molecular studies (Nagy and Tökölyi 2014; Mindell et al. 2018).

The position of the fossil *Archaehierax sylvestris* varied between the strict consensus tree and the bootstrap majority consensus tree of the same analysis. In the strict consensus tree (SI.5) the fossil resolved as nested within the Circaetinae, sister to *Pithecophaga jefferyi*. However, the bootstrap consensus tree resolved the fossil as its own branch between the Perninae-Gypaetinae and the Circaetinae-Aegypiinae clades with moderate (68%) support.

Analysis 4: Bayesian inference, morphology + DNA, ordered

The Bayesian analysis with molecular and morphological branch lengths unlinked produced a broadly similar tree for living taxa to the bootstrap consensus of the corresponding parsimony analysis, but with overall much stronger supports for higher-level clades (Figure 14). All subfamilies resolved as monophyletic, and the divergence nodes for all subfamilies and major clades were greater than 70% except for one.

The fossil *Archaehierax sylvestris* resolved as a lineage between the Elaninae and the Perninae-Gypaetinae clades (i.e. non-elanine accipitrids). Support for *Archaehierax* plus a clade of all non-Elanine accipitrids was weak (44%), but there was moderate support (73%) for monophyly of all other non-elanine accipitrids excluding *Archaehierax*.

When the branch lengths for the molecular and morphological data were linked (SI.5Figure 4), the position of the fossil changed. *Archaehierax sylvestris* moved up the phylogeny and resolved as an independent branch above the Circaetinae-Aegypiinae clade but below the Harpiinae and relatives. Support for this node was stronger than that of the position resolved by the unlinked analysis, but still weak (56%).

Summary

All phylogenetic analyses resolved *Archaehierax sylvestris* with the Accipitridae, consistent with the conclusions drawn from the morphological descriptions, though its precise position within that family varied. Some analyses found it deeply nested within Accipitridae, closely related to, but outside buteonines, haliaeetines and accipitrines. These analyses include the morphology-only parsimony analyses, morphology+molecular parsimony and morphology+molecular Bayesian analysis with linked branch lengths. However, as discussed below, these deeply nested affinities for *Archaehierax* are problematic, and appear less plausible than the topology retrieved in the Bayesian analysis with branch lengths unlinked – where it was one of the most basal accipitrid lineages, with only Elaninae diverging before it (Figure 14).

A more precise and robust position for *Archaehierax sylvestris* is perhaps prohibited by missing data. Even with the 63 preserved elements, there is still a significant amount of missing data. The mandible and cranium, most of the sternum, the distal ends of the humeri, the pelvis, and most of the femora were not preserved. Thus, only 45% (135/300) of phylogenetic characters could be assessed in SAMA P.54998.

Discussion

Pengana robertbolesi was previously the only accipitrid raptor known from the late Oligocene in Australia (Boles 1993; Worthy and Nguyen 2020), being slightly younger than *Archaehierax sylvestris* at 24–20 Ma (Travouillon et al. 2006; Woodhead et al. 2016), and represented only by a distal tibiotarsus making relationships within Accipitridae difficult to establish. The specimens from the late Oligocene Namba Formation are the oldest accipitrids in Australia and extend the fossil record of the Australian Accipitridae to 26–24 Ma, when Australia was much warmer and heavily forested.

Relationships with fossil and extant Australian Accipitridae

Archaehierax sylvestris is unambiguously an accipitrid based on many skeletal features, but notably the morphology of the tarsometatarsal hypotarsus, the lack of a spina interna on the sternum, and the shortened second and third phalanges of the fourth digit. Unsurprisingly, *Archaehierax sylvestris* has multiple unique features of its skeletal morphology that distinguish it from other accipitrids, such as the low caput humeri (humerus), the two fossae in the pars caudale separated by a pila medialis (sternum), and the wide

incisurae intertrochleares (tarsometatarsus). However, as summarised above, the different elements of *Archaehierax sylvestris* do not reveal a consistent closer relationship to the species in any one subfamily. Some elements, such as the rostrum, carpometacarpus and tibiotarsus, show much similarity to species in more derived subfamilies like the Buteoninae, while others, such as the quadrate, vertebrae, and sternum resemble those of more basal subfamilies like Elaninae and Aegypiinae. Other elements, like the humerus, ossa carpalia and the tarsometatarsus, share features with multiple subfamilies. The scapula, ulna, radius, carpometacarpus, carpal phalanges, fibula and pedal phalanges do not align well with the species of any one subfamily. The morphology of the os carpi radiale also excludes the fossil from an accipitrid clade comprising Harpiinae, Aquilinae, Haliaeetinae, Buteoninae and Accipitrinae (see Mayr 2014). This mix of affinities among characters contributes to understanding why the fossil does not group robustly in any subfamily in the phylogenetic analyses. This typifies many Palaeogene fossil bird species across multiple families (see Mayr 2009) and, along with the phylogenetic results, supports the idea that *Archaehierax* does not belong to an extant subfamily. Missing data probably exacerbates the problem as about 55% of characters could not be coded.

In our parsimony analysis using combined morphological and molecular data SI.5, *Archaehierax sylvestris* resolved either deeply nested within Circaetinae as sister to *Pithecophaga jefferyi* (strict consensus tree) or as a stem lineage situated between the clade Gypaetinae-Perninae and Aegypiinae-Circaetinae (bootstrap consensus tree). The Bayesian analysis of combined morphological and molecular data with morphology and molecular branch lengths linked had *A. sylvestris* resolved as above the Aegypiinae-Circaetinae clade but lower than the Harpiinae and Aquilinae. In contrast, the Bayesian analysis of combined morphological and molecular data, with unlinked molecular and morphological branch lengths, resolved *Archaehierax sylvestris* near the base of the Accipitridae, immediately above the Elaninae. The topology of the unlinked molecular and morphology branch lengths tree (Figure 14, analysis 4a) is preferred for several reasons; firstly, given the age of the fossil, a more basal position on the accipitrid phylogenetic tree is more plausible. Dated molecular phylogenies imply that most of the extant accipitrid subfamilies had not diverged by the late Oligocene, with only the Elaninae, which diverged at 33.7 Ma (Mindell et al. 2018), likely present, as the Perninae +Gypaetinae clade diverged at 23.8 Ma from remaining accipitrids (Mindell et al. 2018). Other lineages emerged during or after the middle Miocene (Nagy and Tökölyi 2014; Oatley et al. 2015; Prum et al. 2015; Mindell et al. 2018). Secondly, while many analyses of combined morphological and molecular datasets link branch lengths between these data types (e.g. Ronquist et al. 2012), this might be justifiable only under certain circumstances. Duchéne et al. (2020) compared the effects of linking branch lengths of gene loci trees and demonstrated that partitioning and linking loci to create proportionate branch lengths gave the strongest support, while analyses that had unlinked loci, or loci that were linked to produce identical branch lengths, received weaker support. Goloboff et al. (2019) explored the question of whether assuming a common mechanism of evolution to both all genetrees and morphological data was warranted and concluded that morphological data was generally not compatible with the common clock assumption used when linking branch lengths, producing low levels of branch length correlation. Similarly, Barba-Montoya et al. (2021) found a poor linear relationship between branch lengths for morphological and molecular data, consistent with the idea that the morphological traits were evolving at much more variable rates compared to the molecular ones. Based on this, the results estimated by linking morphological and molecular branch lengths (SI. 5) should be regarded with caution.

The molecular-based divergence dates for Aquilinae (Nagy and Tökölyi 2014; Mindell et al. 2018) suggest that *Aquila bullockensis*, at 14–12 Ma (Woodhead et al. 2016), pre-dates the inferred age of the *Aquila* genus by at least 5 Ma. Morphologically the holotype distal humerus has several distinct differences from *Aquila audax*, including a reduced distal projection of the processus flexorius, a tuberculum supracondylare ventrale with less cranial projection and no proximal narrowing, little to no convexity between the processus supracondylare dorsale and epicondylus dorsalis, and the dorsal insertion for the m. extensor radii is positioned offset from the processus supracondylare dorsale. This does not necessarily mean that *A. bullockensis* is not an aquiline, but rather that it is unlikely to be a member of the crown *Aquila* or any other extant aquiline genus, and that the initial comparative descriptions were too limited to support referral of the species to *Aquila*. Since the description of the holotype, more fossil material that likely belongs to *A. bullockensis* has been discovered and is awaiting description, which may change interpretations of the relationship of *A. bullockensis* to the extant Aquilinae.

In relation to size, it is clear that *Archaehierax sylvestris* was a large accipitrid, smaller than the wedge-tailed eagle *Aquila audax* and the white-bellied sea eagle *Haliaeetus leucogaster* but larger than the black-breasted buzzard *Hamirostra melanosternon* among the extant Australian fauna. It is tempting to assume from this that it must belong to a lineage of large accipitrids. However, while size is sometimes useful in diagnosing clade membership, there are notable exceptions. Haast's eagle *Hieraaetus moorei*, one of the largest eagles ever known at an estimated 15 kg (Worthy and Holdaway 2002), is most closely related to the little eagle *Hieraaetus morphnoides* (Bunce et al. 2005; Knapp et al. 2019), which weighs under 1 kg, the two diverging from a common ancestor approximately 1 million years ago (Knapp et al. 2019). Another example is seen among extant species; the Philippine eagle *Pithecophaga jeffreyi* is morphologically convergent on the Harpiinae in terms of large body size, prey preference, and preferred habitat, but groups molecularly with the Circaetinae, most of which are medium-sized reptile specialists.

Regardless of its closest extant relative, *Archaehierax sylvestris* demonstrates the presence of Accipitridae in Australia since the late Oligocene and that there were at least two divergent clades (*A. sylvestris* and *Pengana robertbolesi*) in Australia around the Oligo-Miocene boundary. All well-sampled Australian faunas from the late Oligocene onwards are now known to have contained accipitrids (Baird et al. 1991; Boles 1993; Gaff and Boles 2010; Rich and van Tets 1982; Louys and Price 2015; Worthy and Yates 2018). However, the geographic origin of these austral accipitrids is difficult to infer, given the presence of accipitrids across multiple continents at this time and a lack of phylogenetic analyses of them with fossils elsewhere.

Conspecificity of the isolated distal humerus and femur specimens from other sites in the Namba Formation with *Archaehierax sylvestris* could not be excluded based on morphology given the holotype lacks these elements, although their much smaller size makes this unlikely, exceeding differences attributable to sexual dimorphism. However, in the absence of overlapping skeletal elements, establishing whether they are congeneric or not is impossible, so we refrain from describing them as a new species.

Palaeobiology

Archaehierax sylvestris is inferred to have inhabited forested areas, based on the pollen records from the Namba Formation (Martin 1990) and the associated fauna in the Pinpa LF, which contains many arboreal taxa such as koalas (phascolarctids), and members of four families of possums and kin (phalangeriforms) (see above; Rich et al. 1991). Our principal component analyses show the fossil taxon grouped most closely to species with relatively shorter wings and longer legs. This body form is observed in forest dwelling eagles and hawks, such as species of *Spizaetus, Spilornis, Harpia harpyja* and *Pithecophaga jeffreyi*, which are adapted to flying through more constricted spaces among the trees and vegetation (Brown and Amadon 1968; Holdaway 1991 unpublished thesis). However, it is also present in the spotted harrier *Circus assimilis*, which *Archaehierax sylvestris* was also closely associated with in PCA plots, which favours open grassland and lightly wooded areas for its habitat (Brown and Amadon 1968; Marchant and Higgins 1993; Debus 1998). In the case of *Circus assimilis*, however, wingspan to leg length proportion is less the result of the wings being shortened, but more the product of the legs being hyper-elongate compared to other accipitrids, especially in the tarsometatarsus, to facilitate a specialised hunting strategy. *Circus assimilis* is known to forage by slowly flying less than five metres above vegetation (Aumann 2001) and has been documented pursuing small prey such as lizards on foot (Buij 2014). It is likely that the high ratio between the wing and leg length in *C. assimilis* is therefore being driven by a need to reach into grass cover to quickly grab small vertebrates before they can escape. As *Archaehierax sylvestris* does not exhibit the extreme elongate tarsometatarsus morphology observed in *C. assimilis*, and more closely resembles that of the crested serpent-eagle *Spilornis cheela* and the black hawk-eagle *Spizaetus tyrannus*, it can be inferred that the ecology of *Archaehierax sylvestris* was more akin to the latter species.

With its shorter wings allowing manoeuvrability, *Archaehierax* would not have been a particularly fast flier, but would have been capable of more agile twists and turns in flight than an accipitrid of its size with a typical wingspan. If we use extant forest eagle species such as those in *Spizaetus* as a morphological analogue, it can be assumed that *Archaehierax sylvestris* was likely an ambush hunter, waiting on a perch within forest cover until prey came into range, and then attacking with a quick burst of speed (Whitacre and Jenny 2013).

The potential diet of *Archaehierax* can be inferred based on that of living analogues, such as species in *Spizaetus*. A female ornate hawk-eagle *Spizaetus ornatus* was recorded feeding on the remains of an estimated 3.2 kg Central American agouti (*Dasyprocta punctata*) and later, on a great curassow (*Crax rubra*), which can weigh between 3.1 and 4.8 kg (though it was not directly observed killing these animals). Whitacre and Jenny (2013) recorded a male with an adult great tinamou (*Tinamus major*) around 1 kg in weight, which is also the average weight for male *Spizaetus ornatus. Archaehierax sylvestris* is notably larger than the species of *Spizaetus* observed in this project (*Spizaetus ornatus, Spizaetus tyrannus*), and assuming similar prey hunting abilities, would have been quite capable of preying on many of the mammals and birds known from the Pinpa Local Fauna.

Based on its larger physical size, phylogenetic position, and the proportions of the tibiotarsus to the tarsometatarsus, it is unlikely that *Archaehierax sylvestris* was restricted to preying on large invertebrates and small vertebrates as seen in the elanines and some of the pernines. The extant Australian elanines, the letter-winged kite *Elanus scriptus* and the black-shouldered kite *Elanus axillaris*, primarily feed upon small mammals (typically mouse-sized), lizards, and large insects such as beetles, grasshoppers and locusts (Brown and Amadon 1968; Marchant and Higgins 1993). The pernine kite *Hamirostra melanosternon* feeds upon small mammals (rabbit-sized at largest), reptiles, and birds, and has been observed to break open eggs of large ground-dwelling birds using either stones or its beak (Brown and Amadon 1968; Marchant and Higgins 1993). The square-tailed kite *Lophoictinia isura* preys on a wide array of small birds, reptiles, large insects, and even bird eggs from nests (Brown and Amadon 1968; Marchant and Higgins 1993).

However, *Archaehierax sylvestris* also lacks the robustness of legs seen in the species of aquilines and harpiines that feed on larger birds and small to medium mammals. The morphology and tibiotarsus-tarsometatarsus ratio of the fossil are also slenderer compared to the fish eagles/haliaeetines, which require the sturdiness to strike through water and the grip to maintain a hold on struggling prey, so despite living near a lake this bird likely did not fish like these species. *Aquila audax* feeds on mammals ranging in size from rabbits to small wallabies, and is also a frequent scavenger of roadkill, while *Haliaeetus leucogaster* near exclusively preys on large fish and sea-snakes (Brown and Amadon 1968; Marchant and Higgins 1993). *Hieraaetus morphnoides*, a smaller bird that is closely related to *Aquila*, preys upon small rabbits and other mammals of a similar size, as well as small ground birds (Brown and Amadon 1968; Marchant and Higgins 1993). *Archaehierax* is larger than *H. morphnoides*, but its more gracile morphology may have restricted it to prey of a similar size to that preferred by this species.

The reduced size of the flange on trochlea metatarsi II in *Archaehierax sylvestris*, as well as its strongly plantar orientation, differs greatly from most Accipitridae. As this marks the point where the musculature for digit II connects to the tarsometatarsus, this could indicate a reduced ability to manoeuvre this digit in the plantar-medial direction, which is the orientation present in most accipitrids. However, the wider spacing of the trochleae could indicate a greater foot span when the toes are extended for prey capture, which might compensate for the loss of potential manoeuvrability.

The Pinpa Local Fauna contains a diverse array of animals (see above), some of which would have been potential prey for *Archaehierax sylvestris*. If a diet of small to medium birds and mammals ranging in habitat from arboreal, terrestrial and littoral is inferred, prey species may have included *Wilaru tedfordi* (a presbyornithid), *Ngawupodius minya* (a dwarf megapode), smaller individuals and juveniles of *Madakoala devisi* (an early koala), a huge diversity of possums and many of the waterbirds that appear in abundance in the Local Fauna.

Acknowledgments

We would like to thank Phillipa Horton, Maya Penck and Mary-Anne Binnie (SAMA), Judith White and Joanne Cooper (NHMUK), Chris Milensky (Smithsonian), Mark Robbins (KU), Tim Ziegler and Karen Roberts (NMV), and Leo Joseph and Alex Drew (ANWC) for allowing access to collections and loans of specimens, without which this project could not have been done. We would also like to thank Warren Handley for his input regarding mass allometry, Elizabeth Scharsachs and her family for providing accommodation in Tring, and the PhD students of Flinders Palaeontology for their support and willingness to talk over thoughts and concerns.

We thank the Mark Mitchell Foundation for a grant to T. H. Worthy, A. B. Camens that funded some of the fieldwork component. For assistance in the field, we thank Amy Tschirn and Warren Handley. We acknowledge the support of Andrew Black (Blackie), manager, for access to Frome Downs Station that allowed this work.

We also thank Gerald Mayr, Nikita Zelenkov, and an anonymous reviewer for looking over the manuscript before publication and providing valuable feedback and corrections.

Authors contributions

EKM and THW designed the study. EKM collected all data, compiled the morphological matrix and performed all analyses. MSYL assisted with analysis of the molecular data and the combined analyses of morphological and molecular data. THW and MSYL contributed to data interpretation. EKM wrote the manuscript, and all authors edited the manuscript. THW and ABC collected the fossil material of *Archaehierax sylvestris* while on field work.

Disclosure statement

No potential conflict of interest was reported by the author(s).

Funding

This work was supported by the Sir Mark Mitchell Research Foundation [NA].

ORCID

Ellen K. Mather http://orcid.org/0000-0001-9437-1395
Michael S. Y. Lee http://orcid.org/0000-0002-3905-0887
Aaron B. Camens http://orcid.org/0000-0003-0464-0665
Trevor H. Worthy http://orcid.org/0000-0001-7047-4680

References

Alley NF. 1998. Cainozoic stratigraphy, palaeoenvironments and geological evolution of the Lake Eyre Basin. Palaeogeogr Palaeoclimatol Palaeoecol. 144(3–4):239–263. doi:10.1016/S0031-0182(98)00120-5.

Amadon D. 1964. Taxonomic notes on birds of prey. Am Mus Novit. 2166:1–24.

Archer M, Tedford RH, Rich TH. 1987. The Pilkipildridae, a new family and four species of ?petauroid possums (Marsupialia: Phalangerida) from the Australian Miocene. In: Possums and opossums: studies in evolution. M Archer editor. Surrey Beatty & Sons Pty Ltd and The Royal Zoological Society of New South Wales, Sydney, Australia; p. 607–627

Aumann T. 2001. Habitat use, temporal activity patterns and foraging behaviour of raptors in the south-west of the Northern Territory, Australia. Wildl Res. 28:365–378. doi:10.1071/WR99091.

Baird RF. 1991. Avian fossils from the Quaternary of Australia. In: Vickers-Rich P, Monaghan JM, Baird RF, Rich TH, editors. Vertebrate palaeontology of Australasia. Melbourne: Pioneer Design Studio Ltd, Lilydale, & Monash University Publications Committee; p. 809–849.

Baird RF, Rich PV, Van Tets GF. 1991. Localities yielding avian assemblages of Quaternary age in Australia. In: Vickers-Rich P, Monaghan JM, Baird RF, Rich TH, editors. Vertebrate palaeontology of Australasia. Melbourne: Pioneer Design Studio Ltd, Lilydale, & Monash University Publications Committee; p. 850–870.

Barba-Montoya J, Tao Q, Kumar S. 2021. Molecular and morphological clocks for estimating evolutionary divergence times. BMC Ecol Evol, 21(1): 1–15.

Baumel JJ, Witmer LM (1993) Osteologia. In: Handbook of avian anatomy: nomina anatomica avium. JJ Baumel, AS King, JE Breazile, HE Evans and JC Vanden Berge editors. Publications of the Nuttall Ornithological Club 23. Nuttall Ornithological Club, Cambridge, Massachusetts; p. 45–132.

Beck RMD, Louys J, Brewer P, Archer M, Black KH, Tedford RH. 2020. A new family of diprotodontian marsupials from the latest Oligocene of Australia and the evolution of wombats, koalas, and their relatives (Vombatiformes). Sci Rep. 10:9741. doi:10.1038/s41598-020-66425-8

Boles WE. 1993. *Pengana robertbolesi*, a peculiar bird of prey from the Tertiary of Riversleigh, northwestern Queensland, Australia. Alcheringa. 17:19–25. doi:10.1080/03115519308619485.

Boles WE, Finch MA, Hofheins RH, Vickers-Rich P, Walters M, Rich TH. 2013. A fossil stone-curlew (Aves: Burhinidae) from the Late Oligocene/Early Miocene of South Australia. In: International meeting of the Society-for-Avian -Paleontology-and-Evolution 2012. Naturhistorisches Museum Wien, Vienna, Austria; p. 43–62.

Boles WE, Ivison TJ. 1999. A new genus of dwarf megapode (Galliformes: Megapodiidae) from the Late Oligocene of central Australia. Smithson Cont Paleobiol. 89:199–206.

Brodkorb P. 1964. Catalogue of fossil birds: part 2 (Anseriformes through Galliformes). Bull Flo Mus Nat Hist. 8(3):195–335.

Brown L, Amadon D. eds. 1968. Eagles, hawks and falcons of the world. Michelin House, London, England.

Buij R. 2014. Spotted Harrier hunting lizards on foot. Aust Field Ornithol. 31 (2):107–112.

Bunce M, Szulkin M, Lerner HRL, Barnes I, Shapiro B, Cooper A, Holdaway RN, Penny D. 2005. Ancient DNA provides new insights into the evolutionary history of New Zealand's extinct giant eagle. PLoS Biol. 3(1):e9. doi:10.1371/journal.pbio.0030009.

Burleigh JG, Kimball RT, Braun EL. 2015. Building the avian tree of life using a large-scale, sparse supermatrix. Mol Phylogenet Evol. 84:53–63. doi:10.1016/j.ympev.2014.12.003.

Callen RA. 1977. Late Cainozoic environments of part of Northeastern South Australia. J Geol Soc Aust. 24(3–4):151–169. doi:10.1080/00167617708728976.

Callen RA, Tedford RH. 1976. New late Cainozoic rock units and depositional environments, Lake Frome area, South Australia. Trans R Soc S Aust. 100 (3):125–167.

Campbell KE, Marcus L. 1992. The relationship of hindlimb bone dimensions to body weight in birds. In: Papers in avian paleontology honoring Pierce Brodkorb. KE Campbell editor. Natural History Museum of Los Angeles County Science Series, 36, Los Angeles, California; p. 395–412

Campbell V, Lapointe FJ. 2009. The use and validity of composite taxa in phylogenetic analysis. Syst Biol. 58(6):560–572. doi:10.1093/sysbio/syp056.

Christidis L, Boles W. 2008. Systematics and taxonomy of Australian birds. Melbourne, Australia: CSIRO Publishing.

De Pietri V, Scofield RP, Zelenkov N, Boles WE, Worthy TH. 2016. The unexpected survival of an ancient lineage of anseriform birds into the Neogene of Australia: the youngest record of Presbyornithidae. Roy Soc Open Sci. 3:150635. doi:10.1098/rsos.150635

Debus SJS. 1998. The birds of prey of Australia: a field guide. Melbourne, Australia: Oxford University Press.

Dickinson EC, Remsen JV Jr, Eds. 2013. The Howard & Moore Complete Checklist of Birds of the World. 4th ed. Vol. 1. Eastbourne (UK): Aves Press.

Drexel JF, Preiss WV. 1995. The Geology of South Australia: the Phanerozoic. Vol 2. Geol. Surv. S. Aust. Bull. 54.

Duchéne DA, Jun Tong K, Foster CSP, Duchéne S, Lanfear R, Ho SYW, Kosakovsky Pond S. 2020. Linking branch lengths across sets of loci provides the highest statistical support for phylogenetic inference. Mol Biol Evol. 37(4):1202–1210. doi:10.1093/molbev/msz291.

Elzanowski A, Paul GS, Stidham TA. 2001. An avian quadrate from the Late Cretaceous Lance Formation of Wyoming. J Vert Paleo. 20(4):712–719. doi:10.1671/0272-4634(2000)020[0712:AAQFTL]2.0.CO;2.

Elzanowski A, Stidham TA. 2010. Morphology of the quadrate in the Eocene anseriform *Presbyornis* and extant galloanserine birds. J Morphol. 271:305–323.

Elzanowski A, Zelenkov NV. 2015. A primitive heron (Aves: Ardeidae) from the Miocene of Central Asia. J Ornithol. 156:837–846. doi:10.1007/s10336-015-1164-y.

Eyton TC. 1867. Osteologia Avium; or, A Sketch of the Osteology of Birds. Vol 2. Hobson R, Wellington, Salop/Shropshire, England

Feldmann R. 1989. Whitening fossils for photographic purposes. Paleontoll Soc SpecPubl. 4:342–346. doi:10.1017/S2475262200005323.

Ferguson-Lees J, Christie DA. 2001. Raptors of the World. London: Christopher Helm Publishers; p. 992. eds

Field DJ, Lynner C, Brown C, Darroch SAF, Iwaniuk A. 2013. Skeletal correlates for body mass estimation in modern and fossil flying birds. PLoS One. 8(11): e82000. doi:10.1371/journal.pone.0082000.

Fordyce RE. 1983. Rhabdosteid dolphins (Mammalia: Cetacea) from the Middle Miocene, Lake Frome area, South Australia. Alcheringa: An Australasian Journal of Palaeontology. 7(1):27–40. doi:10.1080/03115518308619631.

Fowler DW, Freedman EA, Scannella JB, Pizzari T. 2009. Predatory functional morphology in raptors: interdigital variation in talon size is related to prey restraint and immobilisation technique. PloS One. 4:e7999. doi:10.1371/journal.pone.0007999.

Gadow H. 1891. Anatomischer Theil. Dr HG Bronn's Klassen und Ordnungen des Thier-Reichs. Leipzig: wissenschaftlich dargestelit in Wort und Bild. CF Winter'sche Verlagshandlung. *Vögel*. Vol. 6. pt 4, p.1008.

Gaff P, Boles WE. 2010. A new eagle (Aves: Accipitridae) from the Mid Miocene Bullock Creek Fauna of northern Australia. Rec Aust Mus. 62:71–76. doi:10.3853/j.0067-1975.62.2010.1557.

Gaillard C. 1939. Contribution à l'étude des oiseaux fossils. Arch Mus Hist Nat Lyon. 15:1–100.

Gill, B. J., Bell, B. D., Chambers, G. K., Medway, D. G., Palma, R. L., Scofield, R. P., Tennyson, A. J. D. & Worthy, T. H. (2010) Checklist of the Birds of New Zealand, Norfolk and Macquarie Islands, and the Ross Dependency, Antarctica. B. J. Bell (Ed). Te Papa Press, Wellington

Gill F, Donsker D, Rasmussen P (Eds). 2020. IOC World Bird List (v10.2). doi: 10.14344/IOC.ML.10.2.

Goloboff PA, Pittman M, Pol D, Xu X. 2019. Morphological data sets fit a common mechanism much more poorly than DNA sequences and call into question the Mkv model. Syst Biol. 68(3):494–504.

Griffiths CS, Barrowclough GF, Groth JG, Mertz LA. 2007. Phylogeny, diversity, and classification of the Accipitridae based on DNA sequences of the RAG-1 exon. J Avian Biol. 38:587–602. doi:10.1111/j.0908-8857.2007.03971.x.

Hackett SJ, Kimball RT, Reddy S, Bowie RC, Braun EL, Braun MJ, Chojnowski JL, Cox WA, Han K-L, Harshman J, et al. 2008. A phylogenomic study of birds reveals their evolutionary history. Science. 320:1763–1768. doi:10.1126/science.1157704.

Holdaway RN 1991. Systematics and palaeobiology of Haast's eagle (*Harpagornis moorei* Haast, 1872) (Aves: Accipitridae). Unpublished PhD thesis. Department of Zoology, University of Canterbury, Christchurch (New Zealand). 472 p.

Holdaway RN. 1994. An exploratory phylogenetic analysis of the genera of the Accipitridae, with notes on the biogeography of the family. In: Meyburn B-U, Chancellor RD, editors. Raptor conservation today. London (UK): World Working Group on Birds of Prey and Owls; p. 601–649.

Hou L. 1984. The Aragonian vertebrate fauna of Xiacaswan, Jiangsu 2. Aegypinae (Falcaniformes [sic], Aves). Vert PalAs. 22(1):14–22.

Hou L, Zhou Z, Zhang F, Li J. 2000. A new vulture from the Miocene of Shandong, eastern China. Vert PalAs. 38(2):108–112.

Jollie M. 1976. A contribution to the morphology and phylogeny of the Falconiformes. *Evolutionary Theory*, 1: 285–298.

Knapp M, Thomas JE, Haile J, Prost S, Ho SYW, Dussex N, Cameron-Christie S, Kardailsky O, Barnett R, Bunce M, et al. 2019. Mitogenomic evidence of close relationships between New Zealand's extinct giant raptors and small-sized Australian sister-taxa. Mol Phylogenet Evol. 134:122–128. doi:10.1016/j.ympev.2019.01.026.

Kurochkin EN. 1968. Fossil remains of birds from Mongolia. Ornitologiya. 9:323–330.

Kurochkin EN. 1976. A survey of the Paleogene birds of Asia. Smithson Cont Paleobiol. 27:75–86.

Lanfear R, Frandsen PB, Wright AM, Senfeld T, Calcott B. 2016. PartitionFinder 2: new methods for selecting partitioned models of evolution for molecular and morphological phylogenetic analyses. Mol Biol Evol. msw260. doi:10.1093/molbev/msw260

Lerner HRL, Mindell DP. 2005. Phylogeny of eagles, Old World vultures, and other Accipitridae based on nuclear and mitochondrial DNA. Mol Phylogenet Evol. 37:327–346. doi:10.1016/j.ympev.2005.04.010.

Li Z, Clarke JA, Zhou Z, Deng T. 2016. A new Old World vulture from the late Miocene of China sheds light on Neogene shifts in the past diversity and distribution of the Gypaetinae. Auk. 133:615–625. doi:10.1642/AUK-15-240.1.

Lindsay JM. 1987. Age and habitat of a monospecific foraminiferal fauna from near-type Etadunna Formation, Lake Palankarinna, Lake Eyre Basin. South Aust Department Mines Rep. 87:93.

Linnaeus C. 1758. Systema Naturae per Regna Tria Naturae, 10th Edition, revised, Vol 1: Regnum Animale. Salvii, L. Holmiae, Stockholm, Sweden, iv + 824 pp.

Livezey BC, Zusi RL. 2007. Higher-order phylogeny of modern birds (Theropoda, Aves: neornithines) based on comparative anatomy. II. Analysis and discussion. Zool J Linn Soc-Lond. 149:1–95.

Louys J, Price GJ. 2015. The Chinchilla Local Fauna: an exceptionally rich and well-preserved Pliocene vertebrate assemblage from fluviatile deposits of south-eastern Queensland, Australia. Acta Palaeontologica Polonica. 60 (3):551–572.

Marchant S, Higgins PJ. 1993. Handbook of Australian, New Zealand and Antarctic Birds. Vol. 2: Raptors to Lapwings. Melbourne (Victoria): Oxford University Press.

Martin HA. 1990. The palynology of the Namba Formation in the Wooltana-1 bore, Callabonna Basin (Lake Frome), South Australia, and its relevance to Miocene grasslands in central Australia. Alcheringa. 14(3):247–255. doi:10.1080/03115519008619058.

Mayr G. 2006a. The post-cranial osteology and phylogenetic position of the Middle Eocene *Messelastur gratulator* Peters, 1994 – a morphological link between owls (Strigiformes) and falconiform birds? J Vert Palaeontol. 25 (3):635–645. doi:10.1671/0272-4634(2005)025[0635:TPOAPP]2.0.CO;2.

Mayr G. 2006b. A new raptorial bird from the Middle Eocene of Messel, Germany. Hist Biol. 18(2):99–106. doi:10.1080/08912960600640762.

Mayr G. 2009. A well-preserved skull of the "falconiform" bird *Masillaraptor* from the middle Eocene of Messel (Germany). Palaeodiversity. 2:315–320.

Mayr G. 2011. Well-preserved new skeleton of the Middle Eocene *Messelastur* substantiates sister group relationship between Messelasturidae and Halcyornithidae (Aves, ?Pan-Psittaciformes). J Syst Palaeontol. 9:159–171. doi:10.1080/14772019.2010.505252.

Mayr G. 2014. Comparative morphology of the radial carpal bone of neornithine birds and the phylogenetic significance of character variation. Zoomorphology. 133:425–434. doi:10.1007/s00435-014-0236-5.

Mayr G. 2016. Variations in the hypotarsus morphology of birds, and their evolutionary significance. Acta Zool. 97(2):196–210. doi:10.1111/azo.12117.

Mayr G. 2017. Avian Evolution. Chichester (West Sussex): John Wiley and Sons.

Mayr G. 2018. Size and number of the hypoglossal nerve foramina in the avian skull and their potential neuroanatomical significance. J Morphol. 279 (2):274–285. doi:10.1002/jmor.20770.

Mayr G, Hurum JH. 2020. A tiny, long-legged raptor from the early Oligocene of Poland may be the earliest bird-eating diurnal bird of prey. Sci Nat. 107(48). doi:10.1007/s00114-020-01703-z.

Mayr G, Perner T. 2020. A new species of diurnal birds of prey from the late Eocene of Wyoming (USA) – one of the earliest New World records of the Accipitridae (hawks, eagles and allies). Neues Jahrb Geol Paläontol-Abh. 297 (2):205–215. doi:10.1127/njgpa/2020/0921.

Megirian D, Prideaux GJ, Murray PF, Smit N. 2010. An Australian land mammal biochronological scheme. Paleobiology. 36(4):658–671. doi:10.1666/09047.1.

Migotto R (2013) Phylogeny of Accipitridae (Aves: Accipitriformes) based on osteological characters. PhD Dissertation, Universidade de São Paulo, Insituto de Biociências, Departmento de Zoologia.

Miller AH. 1966. The fossil pelicans of Australia. Mem Qld Mus. 14(5):181–190.

Miller MA, Pfeiffer W, Schwartz T 2010. Creating the CIPRES Science Gateway for inference of large phylogenetic trees. In: *Proceedings of the Gateway Computing Environments Workshop* (*GCE*), New Orleans, LA; p. 1–8.

Milne-Edwards A. 1863. Mémoire sur la distribution géologique des oiseaux fossils et description de quelques espèces nouvelles. Ann Sci Nat Zool. 4 (20):133–176.

Milne-Edwards A. 1871. Des caracteres ostéologiques des oiseaux de proie diurnes. In: Recherches anatomiques et paléontologiques pour servir a l'histoire des oiseaux fossils de la France. Victor Masson et Fils, Paris, France; p. 406–473.

Milne-Edwards A. 1892. Sur les oiseaux fossiles des dépots Eocenes de Phosphate de Chaux du sud de la France. *Comptes Rendus duSecond Congrés Ornithologique International, Budapest*. p. 60–80.

Mindell DP, Fuchs J, Johnson JA. 2018. Phylogeny, taxonomy and geographic diversity of diurnal raptors: Falconiformes, Accipitriformes and Cathartiformes. In: Sarasola JH, Grande J, Negro J, editors. Birds of Prey: biology and conservation in the XXI century. Springer, Cham, Switzerland; p. 3–32.

Mlíkovský J. 2002. Cenozoic birds of the world part 1: Europe. Ninox Press, Praha, Czech Republic.

Mourer-Chauviré C. 1991. The Horusornithidae nov. fam., Accipitriformes (Aves) with a hyperflexible intertarsal joint from the Eocene of Quercy. Geobios. 13:183–192. doi:10.1016/S0016-6995(66)80023-2.

Nagy J, Tökölyi J. 2014. Phylogeny, historical biogeography and the evolution of migration in accipitrid birds of prey (Aves: Accipitriformes). Ornis Hungarica. 22:15–35. doi:10.2478/orhu-2014-0008.

Norrish K, Pickering JG. 1983. Clay Minerals. In: Soils: an Australianviewpoint. CSIRO Division of Soils, editors. Melbourne: CSIRO/Academic Press; p. 281–308.

Oatley G, Simmons RE, Fuchs J. 2015. A molecular phylogeny of the harriers (*Circus*, Accipitridae) indicate the role of long distance dispersal and migration in diversification. Mol Phylogenet Evol. 85:150–160. doi:10.1016/j.ympev.2015.01.013.

Olson SL. 1985. The fossil record of birds. In: Farmer DS, King JR, Parkes KC, editors. Avian Biology (Vol. 8). New York: Academic Press; p. 79–252.

Peters JL. 1934. Check-list of the birds of the world: vol. 1. Cambridge: Harvard University Press.

Pledge NS. 2003. A new species of *Muramura* Pledge (Wynyardiidae: Marsupialia) from the Middle Tertiary of the Callabonna Basin, Northeastern South Australia. Bull Am Mus Nat Hist. 279:541–555. doi:10.1206/0003-0090(2003)279<0541:C>2.0.CO;2.

Pledge NS. 2016. New specimens of ektopodontids (Marsupialia: Ektopodontidae) from South Australia. Mem Mus Vic. 74:173–187. doi:10.24199/j.mmv.2016.74.15.

Prum RO, Berv JS, Dornburg A, Field DJ, Townsend JP, Lemmon EM, Lemmon AR. 2015. A comprehensive phylogeny of birds (Aves) using targeted next-generation DNA sequencing. Nature. 526(7574):569–573. doi:10.1038/nature15697.

Rasmussen DT, Olsen SL, Simons EL. 1987. Fossil birds from the Oligocene Jebel Qatrani Formation, Fayum Province, Egypt. Smithson Cont Paleobiol. 62:1–19.

Rich P, van Tets J. 1982. Fossil birds of Australia and New Guinea: their biogeographic, phylogenetic and biostratigraphic input. In: The Fossil Vertebrate Record of Australasia. PV Rich and EM Thompson editors. Monash University Offset Printing Unit, Clayton, Victoria; p. 235–384.

Rich TH, Archer M, Hand SJ, Godthelp H, Muirhead J, Pledge NS, Flannery TF, Woodburne MO, Case JA, Tedford RH, et al. 1991. Australian Mesozoic and Tertiary terrestrial mammal localities. In: Vickers-Rich P, Monaghan JM, Baird RF, Rich TH, editors. Vertebrate palaeontology of Australasia. Melbourne: Pioneer Design Studio Ltd, Lilydale, & Monash University Publications Committee; p. 1005–1057.

Rich TH, Archer M, Tedford RH. 1978. *Raemeotherium yatkolai*, gen. et. sp. nov., a primitive diprotodontid from the medial Miocene of South Australia. Mem Mus Vic. 39:85–91. doi:10.24199/j.mmv.1978.39.06.

Rich THV, Archer M. 1979. *Namilamadeta snideri*, a new diprotodontan (Marsupialia, Vombatoidea) from the medial Miocene of South Australia. Alcheringa. 3(3):197–208. doi:10.1080/03115517908527793.

Ridgway R. 1874. Catalogue of the ornithological collection of the Boston Society of Natural History Part II: Falconidae. Proc Boston Soc Nat. 16:43–72.

Ronquist F, Klopfstein S, Vilhelmsen L, Schulmeister S, Murray DL, Rasnitsyn AP. 2012. A total-evidence approach to dating with fossils, applied to the early radiation of the Hymenoptera. Syst Biol. 61(6):973–999. doi:10.1093/sysbio/sys058.

Sharpe RB. 1874. *Catalogue of the Accipitres, or diurnal birds of prey, in the collection of the British Museum* (*Volume 1*). UK (London): Order of the Trustees.

Sibley CG, Ahlquist JE. 1990. Phylogeny and classification of birds: a study in molecular evolution. New Haven, Connecticut: Yale University Press.

Stirton RA, Tedford RH, Miller AH. 1961. Cenozoic stratigraphy and vertebrate palaeontology of the Tirari Desert, South Australia. Rec South Aust Mus. 14:19–61.

Stresemann E, Amadon D. 1979. Order Falconiformes. In: Mayr E, Cottrell G, editors. *Check-list of the birds of the world, Volume I, 2nd edition; revision of the work of James L. Peters*. Museum of Comparative Zoology, Cambridge, Massachusets. p. 271–425.

Sushkin PP. 1905. Zur Morphologie des Vogelskelets: vergleichende Osteologie der normalen Tagraubvögel (Accipitres) und die Fragen der Classification: mit IV Taf. Nouv MémSoc Imp Naturalistes Moscou. 16:164–247.

Tedford RH, Woodburne MO. 1987. The Ilariidae, a new family of vombatiform marsupials from Miocene strata of South Australia and an evaluation of the homology of molar cusps in the Diprotodontia. In: Archer M, editor. Possums and opossums: studies in evolution (Vol. 2). New South Wales: Surrey Beatty and Sons, Chipping Norton; p. 401–418.

Tedford RH, Archer M, Bartholomai A, Plane M, Pledge NS, Rich T, Rich P, Wells RT. 1977. The discovery of Miocene vertebrates, Lake Frome area, South Australia. BMR J Aust Geol Geop. 2:53–57.

Thorn KM, Hutchinson MN, Lee MSY, Brown NJ, Camens AB, Worthy TH. 2021. A new species of *Proegernia* from the Namba Formation in South Australia and the early evolution and environment of Australian egerniine skinks. Roy Soc Open Sci. 8:201686. doi:10.1098/rsos.201686.

Travouillon KJ, Archer M, Hand SJ, Godthelp H. 2006. Multivariate analyses of Cenozoic mammalian faunas from Riversleigh, north-western Queensland. *Alcheringa: an Australasian journal of Palaeontology,*30(S1): 323–349.

Vickers-Rich P. 1991. The Mesozoic and Tertiary history of birds on the Australian plate. In: Vickers-Rich P, Monaghan JM, Baird RF, Rich TH, editors. Vertebrate palaeontology of Australasia. Melbourne: Pioneer Design Studio Ltd, Lilydale, & Monash University Publications Committee; p. 721–809.

Vieillot LJP. 1816. Analyse d'une nouvelle ornithology elementaire. D'eterville, Paris, 70 pp.

Vigors NA. 1824. Sketches in ornithology; or, observations on the leading affinities of some of the more extensive groups of birds. On the groups of Falconidae. Zoological Journal, 308–346

Walker CA, Dyke GJ. 2006. New records of fossil birds of prey from the Miocene of Kenya. Hist Biol. 18(2):95–98. doi:10.1080/08912960600639434.

Wetmore A. 1933. An Oligocene eagle from Wyoming. Smith Misc Collect. 87 (19):1–9.

Whitacre D, Jenny JP. 2013. Neotropical birds of prey: biology and ecology of a forest raptor community. Ithaca: Cornell University Press, Sage House.

Willis PMA. 1997. Review of fossil crocodiles from Australasia. Aust Zool. 30 (3):287–298. doi:10.7882/AZ.1997.004.

Willis PMA, Molnar RE. 1991. A new middle Tertiary crocodile from Lake Palankarinna, South Australia. Rec South Aust Mus. 25(1):39–55.

Wink M. 1995. Phylogeny of Old and New World vultures (Aves: Accipitridae and Cathartidae) inferred from nucleotide sequences of the mitochondrial cytochrome b gene. Z Naturforsch C. 50:868–882. doi:10.1515/znc-1995-11-1220.

Wink M, Sauer-Gürth H. 2004. Phylogenetic relationships in diurnal raptors based on nucleotide sequences of mitochondrial and nuclear marker genes. In: Chancellor RD, Meyburg B-U, editors. Raptors Worldwide. Budapest: World Working Group on Birds of Prey and Owls, MME/Birdlife Hungary; p. 483–498.

Woodburne MO, Tedford RH, Archer M, Pledge NS. 1987a. *Madakoala*, a new genus and two species of Miocene koalas (Marsupialia: Phascolarctidae) from South Australia and a new species of *Perikoala*. In: Archer M, editor. Possums and opossums: studies in evolution (Vol. 1). New South Wales: Surrey Beatty and Sons, Chipping Norton; p. 293–317.

Woodburne MO, Tedford RH, Archer M. 1987b. New Miocene pseudocheirids (Pseudocheiridae: Marsupalia) from South Australia. In: Archer M, editor. Possums and opossums: studies in evolution (Vol. 2). New South Wales: Surrey Beatty and Sons, Chipping Norton; p. 639–679.

Woodburne MO, MacFadden BJ, Case JA, Springer MS, Pledge NS, Power JD, Woodburne JM, Springer KB. 1994. Land mammal biostratigraphy and magnetostratigraphy of the Etadunna Formation (Late Oligocene) of South Australia. J Vert Paleontol. 13(4):483–515. doi:10.1080/02724634.1994.10011527.

Woodburne MO, Tedford RH. 1975. The first Tertiary monotreme from Australia. Am Mus Novit. 2588:1–11.

Woodburne MO, Tedford RH, Archer M, Turnbull WD, Plane MD, Lundelius EL. 1985. Biochronology of the continental mammal record of Australia and New Guinea. Spec Pub South Aus Department Mines Energy. 5:347–363.

Woodhead J, Hand SJ, Archer M, Graham I, Sniderman K, Arena DA, Black KH, Godthelp H, Creaser P, Price E. 2016. Developing a radiometrically-dated chronologic sequence for Neogene biotic change in Australia, from the Riversleigh World Heritage Area of Queensland. Gondwana Res. 29 (1):153–167. doi:10.1016/j.gr.2014.10.004.

Worthy TH. 2009. Descriptions and phylogenetic relationships of two new genera and four new species of Oligo-Miocene waterfowl (Aves: Anatidae) from Australia. Zool J Linn Soc-Lond. 156:411–454. doi:10.1111/j.1096-3642.2008.00483.x.

Worthy TH. 2011. Descriptions and phylogenetic relationships of a new genus and two species of Oligo-Miocene cormorants (Aves: Phalacrocoracidae) from Australia. Zool J Linn Soc-Lond. 163(1):277–314. doi:10.1111/j.1096-3642.2011.00693.x.

Worthy TH, Holdaway RN. 2002. The lost world of the moa: prehistoric life of New Zealand. Bloomington, Indiana: Indiana University Press.

Worthy TH, Mitri M, Handley WD, Lee MS, Anderson A, Sand C, Evans AR. 2016. Osteology supports a stem-gallifo rm affinity for the giant extinct flightless bird *Sylviornis neocaledoniae* (Sylviornithidae, Galloanseres). PLOS ONE. 11(3):e0150871. doi:10.1371/journal.pone.0150871.

Worthy TH, Nguyen JMT. 2020. An annotated checklist of the fossil birds of Australia. Trans R Soc S Aust. 144(1):66–108.

Worthy TH, Yates A. 2018. A review of the smaller birds from the late Miocene Alcoota local faunas of Australia with a description of a new anatids species. Contribuciones del MACN. 7:221–252.

Zhang Z, Feduccia A, James HF, Iwaniuk A. 2012. A Late Miocene accipitrid (Aves: Accipitriformes) from Nebraska and its implications for the divergence of Old World vultures. PLOS ONE. 7(11):e48842. doi:10.1371/journal.pone.0048842.

Zhang Z, Zheng X, Zheng G, Hou L. 2010. A new Old World vulture (Falconiformes: Accipitridae) from the Miocene of Gansu Province, northwest China. J Ornithol. 151:401–408. doi:10.1007/s10336-009-0468-1.